SEISMIC RESPONSE OF A VISCOELASTIC LAYER

A THESIS

Submitted in partial fulfilment of the requirements for the award of the degree of

DOCTOR OF PHILOSOPHY

in

EARTH SCIENCES

by

SUMANA BASU

DEPARTMENT OF EARTH SCIENCES
INDIAN INSTITUTE OF TECHNOLOGY ROORKEE
ROORKEE - 247 667 (INDIA)

DECEMBER, 2008

INDIAN INSTITUTE OF TECHNOLOGY ROORKEE
ROORKEE

CANDIDATE'S DECLARATION

I hereby certify that the work which is being presented in this thesis entitled **SEISMIC RESPONSE OF A VISCOELASTIC LAYER** in partial fulfilment of the requirements for the award of the Degree of Doctor of Philosophy and submitted in the Department of Earth Sciences, Indian Institute of Technology Roorkee, Roorkee is an authentic record of my own work, carried out during a period from July 2004 to December 2008 under the supervision of Dr. V.N. Singh and Dr. S. Mukhopadhyay, Professor, Department of Earth Sciences, Indian Institute of Technology Roorkee, Roorkee.

The matter presented in this thesis has not been submitted by me for the award of any other degree of this or any other University/Institute.

Sumana Basu
(SUMANA BASU)

This is to certify that the above statement made by the candidate is correct to the best of our knowledge.

Saparika
(S. Mukhopadhyay)
Supervisor

V.N. Singh
(V.N. Singh)
Supervisor

Date:

The Ph.D. Viva-Voce Examination of **Ms. Sumana Basu**, Research Scholar, has been held on May 27, 2009.

V.N. Singh Saparika
Signature of Supervisors

Signature of External Examiner

ABSTRACT

In seismic prospecting, the reflected seismic wavelets yield valuable information about the reflector and properties of the path traversed by seismic waves. Their arrival times give information about its location of the reflector in the earth and their amplitudes provide an estimate of the acoustic impedance contrast at the reflector. Shape of a seismic wavelet is also its very important attribute. It is the result of frequency dependent attenuation and dispersion of seismic waves, which in turn are caused by anelasticity of the propagating medium and solid – fluid interaction in the fluid saturated porous medium. A careful analysis of shape of wavelets should yield important information about the pore fluids. For this purpose, important factors affecting the shape of wavelets need to be identified and a quantitative estimate of their influence on the shape of wavelets obtained. In the present work, an attempt has been made to achieve this objective.

Plane wave synthetic seismograms have been generated at a number of offsets at the surface of a three layered earth model. These seismograms simulate a CMP (Common Mid Point) gather just before AVO (Amplitude Variation with Offset) analysis. A 50 Hz Ricker pulse has been used as the source wavelet. The second layer of the three layered earth model is porous and viscoelastic; the other two layers are elastic. Standard Linear Solid (SLS) model has been used to represent the visoelastic behaviour of the solid matrix of the second layer. Biot's theory has been used to compute complex and frequency dependent velocities of P- and S-waves in the porous viscoelastic layer saturated with gas and water or oil and water or only water. In all computations the frequency range is 1 – 100 Hz, the most commonly accepted frequency range in seismic prospecting Equations similar to Zoeppritz equations have been derived to compute complex and frequency dependent reflection coefficients. Vertical component of displacement of reflected P waves at the surface of the earth model have been computed including transmission losses and

free surface effect accounted for. The synthetically generated reflected seismic wavelets have been analyzed to quantify the effect of viscoelasticity and type and amount of pore fluids on the shape of seismic wavelets.

The results obtained in this work indicate that porosity, type and amount of the pore fluids and solid – fluid interaction in the porous viscoelastic layer influence the frequency dependence of seismic wave velocities, quality factor, attenuation coefficients and reflection coefficients. Seismic wave velocities are influenced by variations of porosity to a greater extent than to variations in water saturation. Variation of peak amplitude of seismic wavelets with offset is dominated by the type of pore fluid. The shapes of seismic wavelets show a marked variation with porosity, becoming broader at high porosity and also undergoing change of polarity. Greater changes are observed with gas in the pores. Distinguishing different fluids on the basis of wavelet shapes becomes more noticeable at larger offsets. AVO analysis carried on synthetic data indicates that attributes A and B are also sensitive to porosity and water saturation.

ACKNOWLEDGEMENT

This thesis arose in part out of years of research that has been done since I came to IIT Roorkee. By that time, I have worked with a great number of people whose contribution in assorted ways to the research and the making of this thesis deserved special mention. It is a pleasure to convey my gratitude to them all in my humble acknowledgment.

In the first place, I would like to express my gratitude to Prof. V.N. Singh for his invaluable supervision, advice, and guidance from the very early stage of this research as well as giving me extraordinary experiences throughout the work. Above all and the most needed, he provided me unflinching encouragement and support in various ways. His truly scientist intuition has made him as a constant oasis of ideas and passions in science, which exceptionally inspire and enrich my growth as a student, a researcher and a scientist want to be.

I convey my heartfelt gratitude to Dr. S. Mukhopadhyay, Associate Professor, for providing me with an opportunity to undertake this doctoral research work through her ever-valuable suggestions, advices, ideas and criticisms at all stages of the work. Her indelible presence in all my decisions in formulating the research plan has incredibly helped me in outlining the presentation of my thesis work.

Deepest gratitude to the Head of the Department Prof. R. P. Gupta and members of the DRC, Prof. A. K. Pachauri and Prof. P. K. Gupta, Department of Earth Sciences and Dr. D. Shanker, Assistant Professor, Department of Earthquake Engineering for their valuable suggestions throughout the research program.

I owe my gratitude to Ministry of HRD, Govt. of India for providing me a constant fellowship for four years with contingent grant utilized in the research work.

My special thanks to Nair ji and Rakesh ji for their indispensable help dealing with travel funds, administration and bureaucratic matters during my stay at IIT Roorkee.

It is a pleasure to express my gratitude wholeheartedly to my seniors, Dr. Suman Kumar Mandal, Arundhati Biswas, Aniket Chakraborty and Dr. Jyoti Shah for their encouragement and moral support during the course of research.

Collective and individual acknowledgments are also owed to my colleagues whose presence somehow perpetually refreshed, helpful, and memorable. Many thanks go in particular to Purushothaman, for his constant support and advice.

I would like to thank my friends Susmita Ghosh, Sushmita Bhattachariya, Aparajita, Putul, Anwesha, Sugandha, Sonia, Priyanka and all my juniors for their unflinching support, encouragement, advice and giving me such a pleasant time in Roorkee.

Where would I be without my family? I would like to thank all my family members for their encouragements and support since my childhood. My parents deserve special mention for their inseparable support and blessings. My parents and my grandmother, in the first place are the persons who put the fundament of my learning character, showing me the joy of intellectual pursuit ever since I was a child and sincerely raised me with theirs caring and gentle love. Thanks to my brother for being supportive and caring siblings.

I owe a special thanks to my husband, Dr. Debabrata Dutta, for his valuable guidance, support and caring to materialize this thesis.

Finally, I would like to thank everybody who was important to the successful realization of this thesis, as well as expressing my apology that I could not mention personally one by one.

(SUMANA BASU)

CONTENTS

LIST OF FIGURES

LIST OF TABLES

CHAPTER – 1
INTRODUCTION

1.1 MOTIVATION

Delineation of geological conditions suitable for accumulation of oil or gas has been one of the main objectives of seismic reflection prospecting. With continuous advancement in techniques of acquisition, processing and interpretation of seismic reflection data, it is now possible, for example, to determine, the nature and geologic history of a sedimentary basin and its depositional environment from seismic sections (seismic stratigraphy), delineating gas sands through AVO analysis, and characterization and surveillance of oil reservoirs through 3D seismics. Another interesting application of seismic reflection data is the possibility of analyzing shapes of recorded wavelets. Potsma (1958) recognized the importance of the change of shape of seismic wavelets as a source of information about the properties of the medium in which the waves propagate. There are several well-known factors that determine the shape of a seismic wavelet emitted by a point source. Some of these factors are: (i) distance from the source, (ii) presence of interfaces, (iii) presence of inhomogeneities that give rise to scattering, and (iv) roughness of the reflectors. The anelasticity of the medium through which the waves propagate and interaction between the solid and fluid phases during wave propagation are also important factors that influences the shape of wavelets. The contributions of the above factors have to be carefully analyzed and quantified before shapes of seismic wavelets can be used for fluid characterization.

The interpretation of seismic reflection data depends not only on the type of data used for inversion (travel times, amplitudes or some other attributes of the recorded seismic wavelets) but also on the simplicity or complexity of model used for representing the subsurface. The seismic wavelet is a very short duration pulse when it is generated by an explosive source. This short duration pulse, the so called source wavelet, undergoes a

number of changes during its travel downward and back to the surface after reflection. The recorded seismic wavelets that correspond to primary reflections contain information about the properties of earth materials encountered during its propagation and the reflectors. Through the processing and analysis of an ensemble of recorded seismic wavelets that represent primary reflections, the correct disposition of the reflectors is sought to be determined in the subsurface thus yielding important information about the existence of structural traps. This is constrained by the model of the earth used in the interpretation of seismic data.

Traditionally, the travel times of seismic reflection wavelets are interpreted on the assumption that the earth consists of discrete layers that are homogeneous, isotropic and perfectly elastic or simply elastic. The last property, in its strictest sense, implies that subsurface rocks are non-attenuating and non-porous. In reality, no rock in the top 10 km of the earth's crust comes anywhere near these ideals: homogeneity, isotropy and perfect elasticity. In reality, the seismic waves get attenuated and dispersed while propagating through the real earth making the recorded seismic wavelet deficient in high frequencies and spread out in time. This degrades resolution. Various deconvolution procedures during processing seek to compensate for this effect.

Amplitudes of seismic waves decay as distance from the source increases. Part of this decay is due to the phenomenon of spherical spreading that is simply a function of distance from the source and affects all waves irrespective of their frequency and nature of the intervening medium. Rest of the decay of amplitude is governed by the attenuating properties of the medium through which waves travel and is frequency dependent, with energy associated with higher frequency components of the wavelet disappearing and converted into heat. This leads to changes in the frequency content of the wavelet with its spectral bandwidth becoming narrower and narrower as the distance from the source increases. The end result of these spectral modifications is the change in the shape of the

wavelet which becomes extended in time. These frequency dependent changes cannot be explained if the rock layers are considered elastic. Since attenuation of seismic waves is always observed, the behavior of the medium of propagation is essentially anelastic. It is to be expected that porosity, nature and amount of different fluids (e.g., water, oil and/or gas) in the reservoir rock in the pore spaces along with anelastic nature of the solid phase of the medium will govern the changes in the shape of the recorded seismic wavelets.

The changes in the shapes of seismic wavelets that result due to wave propagation in porous viscoelastic media containing one or more fluids can yield important information on the fluids in the reservoir. The main objective of the work in this thesis is to carry out a systematic study of the shapes of reflected seismic wavelets in the seismic frequency range (1-100 Hz) and to quantify the effect of anelasticity of the solid phase of the medium of propagation and nature and amount of fluids present in the pore spaces in modifying this shape. The earth model considered here is assumed to be made up of homogeneous and isotropic media. The porosity when present is random in nature in such a way that macroscopically the porous medium is essentially homogenous and isotropic.

1.2 ANELASTICITY

As mentioned above the anelastic behavior of the medium leads to attenuation and dispersion of the seismic waves propagating through it that leads to changes in the shape of recorded wavelets. The consequences of anelasticity of the medium are that its elastic modulii, and hence the velocities of seismic waves, are complex. Since the stresses induced by the passage of seismic waves are periodic in nature, the elastic modulii and wave velocities are also frequency dependent. The real part of these complex and frequency dependent velocities contributes to the propagation of the waves whereas their imaginary part leads to their attenuation. Because of frequency dependence of wave velocities,

dispersion also occurs. The end result is the modification of the spectral bandwidth of the propagating wavelet giving rise to changes in reflected wavelets' shape.

The attenuation of seismic waves due to the anelasticity of the medium is usually described with the help a frequency dependent attenuation parameter, $a(\omega)$, defined by

$$a(\omega) = \frac{\pi\omega}{2cQ} \qquad \text{.....(1.1)}$$

where c is wave velocity and Q is quality factor of the medium. In general, both c and Q are frequency dependent.

Anelastic behavior of a medium can be modeled through a linear relationship between stress and strain and their time derivatives. This kind of linear anelastic behavior is known as viscoelasticity. Some aspects of viscoelasticity are presented in the following paragraphs.

In Appendix D (Part I) stress – strain behavior of elastic, viscoelastic and viscoelastic materials under cyclic loading has been given.

1.3 VISCOELASTICITY

Unlike purely elastic substances, a viscoelastic substance has an elastic component and a viscous component. An elastic substance, on being subjected to stress, develops an instantaneous elastic strain and returns to its unstrained state quickly and completely when the stress is removed. Under constant stress, the strain in an elastic substance remains constant with time. A viscoelastic substance, on the other hand, when subjected to stress, develops an instantaneous elastic strain. If the stress is not removed, the strain increases with time. When the stress is removed, the elastic part of the strain disappears instantaneously and the remaining strain disappears over a period of time. At the atomic level, elasticity is usually the result of bond stretching along crystallographic planes in an ordered solid whereas viscoelasticity is the result of an amorphous material. The viscous

component of a viscoelastic substance is characterized by a proportionality between stress and time rate of strain and the coefficient of proportionality is called viscosity. A viscoelastic material has the following properties:

1) Hysteresis is seen in the stress-strain curve (Figure 1.1b).

2) Stress relaxation occurs: step constant strain causes decreasing stress.

3) Creep occurs: step constant stress causes increasing strain.

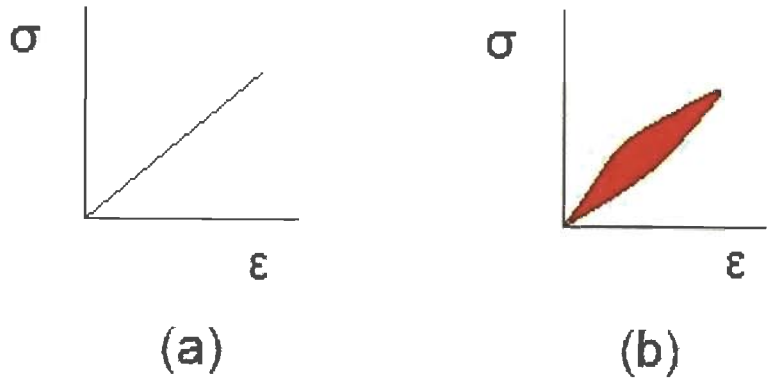

Figure 1.1: ***Stress-strain curves for (a) a purely elastic material and (b) a viscoelastic material. The red area is a hysteresis loop and shows the amount of energy lost (as heat) in a loading and unloading cycle; σ denotes the stress and ε, the strain.***

Purely elastic materials do not dissipate energy (in form of heat) when a load is applied and then removed. However, a viscoelastic substance loses enegy when a load is applied and then removed. Hysterisis is observed in the stress-strain curve with the area of the loop representing the energy lost during the loading cycle.

1.3.1 Viscoelastic Creep

When subjected to a step constant stress, viscoelastic material experiences a time-dependent increase in strain. This phenomenon is known as viscoelastic creep (Figure 1.2). At a time $t = t_o$, a viscoelastic material is subjected to a constant stress that is maintained for a sufficiently long time period. The material responds to the stress with a strain that increases until the material ultimately fails. When the stress is maintained for a shorter

time period, the material undergoes an initial strain which increases until a time $t = t_1$, after which the strain immediately decreases and then gradually decreases for times $t > t_1$ to a residual strain (relaxation).

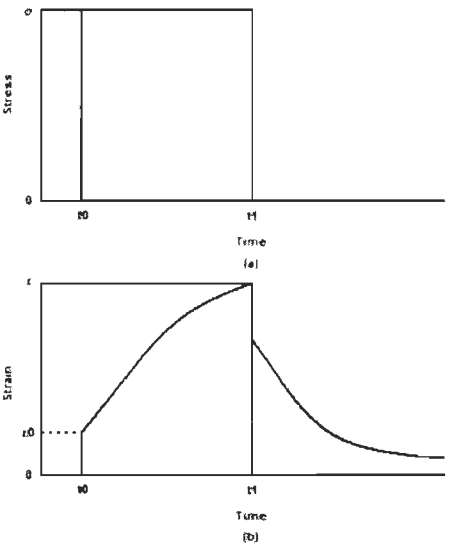

Figure 1.2: ***(a) Applied stress and (b) induced strain as functions of time for a viscoelastic material.***

A short description has been given in Appendix D (Part II) about the relaxation mechanism in a viscoelastic material.

1.3.2 Viscoelatic Materials

There are two types of viscoelastic material:

1) Linear Viscoelastic material
2) Non-linear viscoelastic material

In the present work only linear viscoelatic materials have been taken into consideration. Therefore, the main features of only this type of materials have been described in the following section. A short note on non-linear viscoelasticity has been given in Appendix D (Part III).

Linear viscoelasticity is applicable to small strains. The different models of linear viscoelasticity include the Maxwell model, the Kelvin-Voigt model, and the Standard Linear Solid model. These models have been proposed to predict a viscoelastic material's response under different loading conditions. Viscoelastic behavior is comprised of elastic and viscous components modeled as linear combinations of springs and dashpots, respectively. Each model differs in the arrangement of these elements and all of these viscoelastic models can be equivalently modeled as electrical circuits. The elastic modulus of a spring is analogous to a circuit's resistance and the viscosity of a dashpot to its capacitance.

The growth of current in an RC circuit resembles the build-up of strain in a viscoelastic material. In Appendix D (Part IV) the growth of current in such a circuit has been shown that models build-up of strain in a Kelvin –Viogt solid.

The elastic component, as previously mentioned, can be modeled as a spring, defined by the relation

$$\sigma = E\varepsilon \qquad \text{.....(1.2)}$$

where σ is the stress, E is the elastic modulus of the material and ε is the strain, similar to Hooke's Law. Physically this represents the behavior of a Hookean solid with E representing the rigidity.

The viscous components can be modeled as a dashpot such that the stress-strain rate relationship defined by,

$$\sigma = \eta \frac{d\varepsilon}{dt} \qquad \text{.....(1.3)}$$

where η is the viscosity of the material. Physically this represents the behavior of a Newtonian fluid.

The relationship between stress and strain can be simplified for specific stress rates. For high stress states/short time periods, the time derivative components of the stress-strain

relationship dominate. A dashpot resists changes in length, and in a high stress state it can be approximated as a rigid rod. Since a rigid rod cannot be stretched past its original length, no strain is added to the system.

Conversely, for low stress states/longer time periods, the time derivative components are negligible and a dashpot can be effectively removed from the system - an "open" circuit. As a result, only the spring connected in parallel to the dashpot will contribute to the total strain in the system.

In the next section, the characteristics of the three models, i.e., Maxwell model, Kelvin-Voigt model and Standard Linear Solid model (SLS), of linear viscoelasticity have been described.

1.3.2.1 *Maxwell Model*

The Maxwell model can be represented by a dashpot and a spring connected in series (Figure 1.3a). This model represents a liquid (able to have irreversible deformations) with some additional reversible (elastic) deformations. If put under a constant strain, the stresses gradually relax. When a material is put under a constant stress, the strain has two components. First, an elastic component occurs instantaneously, corresponding to the spring, and relaxes immediately upon release of the stress. The second is the viscous component that grows with time as long as the stress is applied. The Maxwell model predicts that stress decays exponentially with time, which is accurate for most polymers. A limitation of the model is that it is unable to predict creep in materials based on a simple dashpot and spring connected in series. The Maxwell model for creep or constant-stress conditions postulates that strain will increase linearly with time. However, viscoelastic materials mostly show the strain rate to be decreasing with time.

(a)

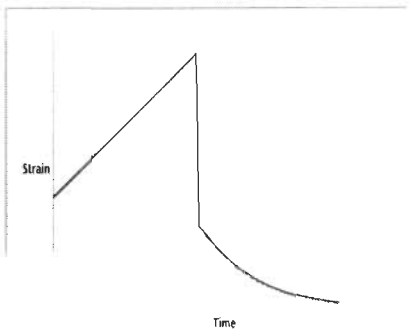

(b)

Figure 1.3: ***Maxwell Model; (a) Schematic representation (b) Behavior under application and removal of constant stress.***

1.3.2.2 *Kelvin-Voigt Model*

The Kelvin-Voigt model, also known as the Voigt model, consists of a dashpot and a spring connected in parallel (Figure 1.4). It is used to explain the stress relaxation behaviors of a viscoelastic material.

This model represents a solid undergoing reversible, viscoelastic strain. Upon application of a constant stress, the material deforms at a decreasing rate, asymptotically approaching the steady-state strain. When the stress is released, the material gradually relaxes to its undeformed state. At constant stress (creep), the model is quite realistic as it predicts strain to tend to σ/E as time continues to infinity. Similar to the Maxwell model, the Kelvin-Voigt Model also has limitations. The model is extremely good for modeling creep in materials, but with regards to relaxation the model is much less accurate.

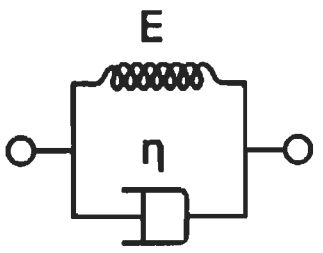

(a)

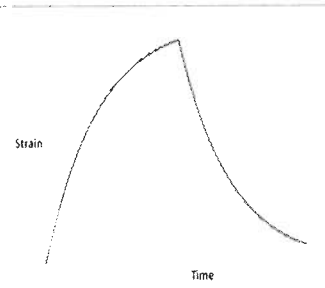

(b)

Figure 1.4: ***Kelvin-Voigt model; (a) Schematic representation (b) Behaviour under application and removal of a constant stress.***

1.3.2.3 *Standard Linear Solid Model*

The Standard Linear Solid Model effectively combines the Maxwell Model and a Hookean spring in parallel (Figure 1.5(a)). A viscous material is modeled as a spring and a dashpot in series with each other, both of which are in parallel with a lone spring. Under a constant stress, the modeled material will instantaneously deform to some strain, which is the elastic portion of the strain, and after that it will continue to deform and asymptotically approach a steady-state strain (Figure 1.5(b)). This last portion is the viscous part of the strain.

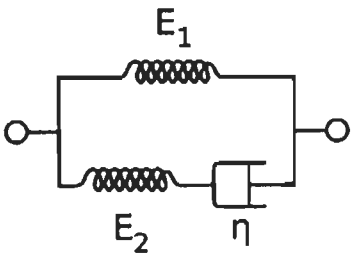

(a)

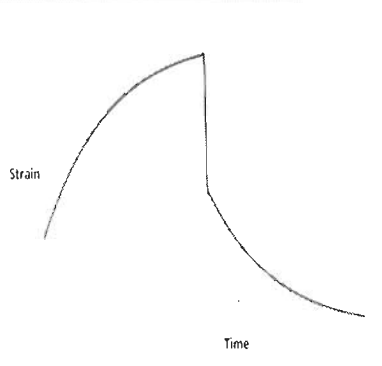

(b)

Figure 1.5: ***Standard Linear Solid model; (a) Schematic representation (b) Behaviour under application and removal of a constant stress.***

In the present work Standard Linear Solid model has been chosen to represent the anelastic layer of the earth model. Its behavior under constant stress represents quite closely the response of earth materials under similar conditions. For cyclic loads to which a medium is presented during wave propagation, the behavior of this model leads to complex and frequency dependent elastic modulii and hence wave velocities. This model as shown in Figure 1.5(a) is also characterized by a pair of relaxation times, τ_σ and τ_ε, corresponding to behavior under constant stress and constant strain. These lead to a frequency dependent Q and attenuation coefficient $a(\omega)$. This is known as a single mechanism model. The observed constant Q behavior in the seismic frequency band has been sought to be represented by models composed of a parallel arrangement of elements like those shown in Figure 1.5(a) corresponding to a number of τ_σ - τ_ε pairs.

This Standatrd Linear Solid is a more satisfactory model for the behavior of the Earth's crust and mantle under stresses and strains associated with seismic vibrations (Ben-Menahem and Singh, 1981).

The frequency dependence of wave velocities and Q of a single mechanism model as described above ensures that the computed waveforms of seismic wavelets obey principles of causality in the manner suggested by Aki and Richards (2002). In the present work synthetic seismograms have been generated and shapes of seismic wavelets are analyzed to quantify the effect of viscoelasticity; The adherence to the principle of causality has been ensured through the use of Standard Linear Model to represent the behavior of anelastic layer.

1.4 POROUS MEDIA

The upper 6 to 7 kilometers of earth that are of interest in seismic prospecting for hydrocarbon exploration are not only anelastic but also porous. Porosity varies from rock to rock, but a certain amount of porosity, even if very small, is always present. The pore

space of the rock may be occupied by oil and water or gas and water or only water as is the case with a reservoir rock. The presence of porosity lowers the bulk and the shear modulii of the rock and hence the wave velocities. Porosity also lowers density of the rock. In a simple manner the velocity and density of a porous and fluid saturated rock can be represented by the following relations:

$$\frac{1}{V_B} = \frac{1-\phi}{V_M} + \frac{\phi S_W}{V_W} + \frac{\phi(1-S_W)}{V_H} \qquad \text{.....(1.4)}$$

$$\rho_B = (1-\phi)\rho_m + \phi S_W \rho_W + \phi(1-S_W)\rho_H \qquad \text{.....(1.5)}$$

where ϕ is the porosity, ρ, the density, V, the velocity of P-waves and S_W, the water saturation. The subscripts B, M, W and H stand for bulk, matrix, water and hydrocarbons. The relationship for velocity is the well known time average equation, first proposed by Wyllie(1956, 1958) and is one of several empirical relationships. Gassmann (1951) and Hashin-Shtrikman(1963) considered the problem of predicting elastic modulii of porous rocks from theoretical viewpoint.

Biot (1956) considered the propagation of elastic waves in a porous elastic solid saturated with viscous fluid. It accounts for the motion of fluids in the interconnected voids of an isotropic, homogeneous, and porous solid assuming Poiseuille fluid flow. Biot predicted the existence of two dilatational waves i.e. a fast P-wave, a slow P -wave and an S-wave propagating through a porous medium. In the present work, this Biot's theory has been used to compute seismic wave velocities in a viscoelastic porous medium with appropriate modifications.

1.5 PRESENT WORK

Since Biot's theory was put forward, the solutions of the boundary value problem of seismic wave propagation in porous media have been investigated (Deresiewicz 1960, 1961, Deresiewicz and Rice 1962, Dutta & Ode 1983, Sharma 1981). This involved setting

up of appropriate boundary conditions at the interface between two porous media or between a porous and a non-porous media. In the present work, a three-layered model has been considered. The second layer of this layer is porous and viscoelastic whereas the first and third layers are elastic. A boundary value problem has been solved to obtain the plane wave reflection and transmission coefficients at the two interfaces. Synthetic seismograms have been generated at the surface of the three layered earth model for a number of offsets simulating an AVO situation. A Ricker pulse has been assumed to represent the source wavelet. The changes in the shapes of reflected seismic wavelets at different offsets have been studied for different porosities and water saturations of the second layer. The variations of velocities (fast and slow P-waves as well as S-wave), quality factor (Q) and attenuation coefficients with frequency have been studied for different porosities and water saturations of the second layer.

1.6 IMPORTANCE OF THE WORK

The work presented in this thesis has aimed at quantifying the effect of viscoelasticity, porosity and type and amount of interstitial fluids in determining the changes in the shapes of reflected seismic wavelets. It has been found that porosity and fluid content have significant effect on the shapes of seismic wavelets. The processing and interpretation of seismic reflection data broadly relies on the theory of seismic wave propagation in elastic media. The effect of porosity and pore fluids is taken into account on the basis of empirical relations or Gassmann's relations. However, these ignore the anelastic nature of the propagating medium and solid-fluid interaction during wave propagation. Moreover, more than one fluid is nearly always present in the reservoir rock. The empirical relations assume the presence of single fluid only. In the present work, these restrictions have been relaxed and a more general treatment of the theory of seismic wave propagation in viscoelastic porous media has been used. Presence of more than one fluid in the pore

spaces has been allowed. The results obtained indicate a significant change in the shape of seismic wavelets with change in porosity, type and amount of fluid. Based on the method presented in this work, new and improved techniques of seismic data processing can be developed that can take into account the effect of anelasticity of the propagating medium and presence of one or two pore fluids.

1.7 PLAN OF THESIS

In the **Chapter 2**, a review of pertinent literature has been presented.

In **Chapter 3**, the theoretical basis of the work presented in this dissertation has been provided. The details of equations of motion in viscoelastic porous media and their solutions have been discussed. Some theoretical details of the Standard Linear Solid model have also been provided along with the boundary value problem for computing reflection coefficients and equations used for generating synthetic seismograms.

Chapter 4 provides the details of the selection of models parameters. The model parameters used in this work have been listed. Some details of the computational procedure have been provided and the special and novel aspects of the procedure emphasized.

In the **Chapter 5**, the results arrived at in the present study have been presented and discussed.

Finally, a summary and some of the important conclusions of the present study have been given in **Chapter 6**.

CHAPTER – 2

REVIEW OF LITERATURE

2.1 INTRODUCTION

Potsma (1958) recognized the importance of the change of shape of seismic wavelets as a source of information on the properties of the medium in which the waves propagate. He listed several well-known factors that determine the shape of a seismic wavelet emitted by a point source. Some of these factors are distance from the source, presence of interfaces, presence of inhomogeneities that give rise to scattering and roughness of the reflectors. He also mentioned the deviations from elastic behavior as a factor that influences the shape of wavelets. He presented a theory of anelasticity in which linear relations between stress and strain and their time derivatives take the place of Hooke's law. This kind of linear anelastic behavior was termed viscoelasticity. This type of viscoelastic solid can be represented by a parallel arrangement of "Maxwell elements" where a Maxwell element consists of a spring and dashpot in series and is characterized by a spring constant (μ), a "viscosity coefficient" (η) and a relaxation time (η/μ). The need of a parallel arrangement of a number of Maxwell's elements arises from the recognition that there are a number of mechanisms, which are capable of storing potential energy and dissipating this energy. If the stress and strain in such a viscoelastic solid are assumed to be harmonically varying in time, a generalized modulus of elasticity M (ω) is defined that is complex and frequency dependent. As a result, the velocities of propagation of seismic waves in such a solid also become complex and frequency dependent, leading to attenuation and dispersion of waves. Another possibility to account for attenuation and dispersion in viscoelastic solids was also pointed out: the coupling between different types of waves. This is important in a porous medium containing fluid where dissipation of energy occurs due to the relative motion between solid matrix and fluid. In such a condition, there is a wave in solid matrix

modified by the presence of fluid in the pores, and a wave in the pore fluid modified by the solid matrix. Thus, all the essential features of the propagation of seismic waves in porous elastic media were outlined.

The problem of predicting shape of seismic wavelets and study of its variation with the properties of the medium and type and amount of pore fluids has many aspects. Some of these are:

(i) Properties of seismic waves that exist in the presence of pore fluids

(ii) Predicting velocities of seismic waves in porous media containing one or more fluids in the pores

(iii) Propagation of seismic waves in a porous anelastic medium

(iv) Reflection and transmission of seismic waves, propagating in porous anelastic media

(v) Synthetic seismograms when seismic waves propagate in two or more layered earth when some of the layers may be anelastic.

(vi) Effect of anelasticity and pore fluids on AVO analysis.

An attempt has been made to review the work that has been carried out and covers the above aspects.

2.2 SEISMIC WAVES IN FLUID FILLED POROUS SOLIDS

Biot (1956) developed a theory for the propagation of seismic waves in a porous elastic solid containing a compressible viscous fluid. The emphasis was on materials where fluid and solid are of comparable densities, for instance, in the case of water-saturated rock, and was restricted to the lower frequency range where the assumption of Poiseuille flow is valid. The existence of two compressional and one shear wave was predicted. The properties of the waves when the fluid is frictionless (i.e. non-viscous) and when it is dissipative (i.e. viscous) were discussed. When the fluid is viscous, the two dilatational

waves are denoted as waves of the first and second kind. The waves of the first kind are true waves. Their dispersion is practically negligible with a phase velocity increasing or decreasing with frequency depending on a mechanical parameter. The absorption coefficient is proportional to the square of the frequency. The waves of the second kind are highly attenuated. They are in the nature of a diffusion process and the propagation is closely analogous to heat conduction. The phase velocity of shear waves increases slightly with frequency while the absorption coefficient is proportional to the square of the frequency. The concept of a characteristic frequency was also introduced. This frequency is governed by the kinematic viscosity of the pore fluid and diameter of the pores. For a porous material, it is assumed that Poiseuille flow breaks down when this quarter wavelength is of the order of the diameter of the pores. It happens when the frequency of waves exceeds the characteristic frequency.

Biot (1962) reformulated the theory of propagation of acoustic waves in porous media with special emphasis on viscoelastic properties and relaxation effects. Equations governing the propagation of acoustic waves in viscoelastic media were presented and some particular solutions were obtained and discussed. The theory for elastic media was also extended to anisotropic media.

2.3 SEISMIC VELOCITIES IN POROUS MEDIA

Gassmann (1951) derived elastic constants for porous rocks by a straightforward application of static elasticity, obtaining speeds, which agree with Biot's low-frequency values. Gassmann'a relations describe the bulk and shear modulii of saturated rocks at very low frequencies. They are important for predicting how P- and S-wave velocities depend on the fluid modulus at low frequencies, that is, at seismic and possibly well logging frequencies (Nolen-Hoeksema, 2000). The relations are sum of two parts: the modulus of the framework (the frame modulus, K_{fram} and μ_{frame}) and the modulus of the fluid-filled

pores (the pore modulii, K_{pore} and μ_{pore}). The shear modulus is not affected by fluid saturation.

Dvorkin et al. (1995) estimated the velocity/frequency dispersion and attenuation in fully saturated rocks by employing the squirt-flow mechanism of solid/fluid interaction. They considered a fully saturated isotropic, macroscopically homogeneous rock with a pore space that has compliant (soft) and stiff portions. Stiff portions of the pore space have relatively small variations of pore pressure when the rock is loaded by a passing wave. Soft portions of the pore space tend to transfer more of the stress to the fluid, which results in high variations of induced pore pressure. At low frequencies, these pressures are assumed to equilibrate leading to Gassmann's formula for the bulk modulus of saturated rock. At higher frequencies, intensive cross-flow between the soft and the stiff parts persists resulting in wave-energy dissipation and thus velocity/frequency dispersion. At very high frequencies, the fluid is unrelaxed and blocked in the compliant pores. Attenuation approaches zero and both *P*- and S-wave velocities approach their high-frequency limits. They derived theoretical formulas for relating compressional and shear-wave velocities and attenuation in fully saturated rocks to frequency, based on the squirt-flow mechanism with the squirting flow occurring between thin compliant pores and stiff pores. They showed that in water-saturated samples, the transition from low-frequency velocity values to high-frequency velocity values occurs at frequencies higher than 0.1 MHz that are much above the range used in seismic prospecting

Nolen-Hoeksema (2000) incorporated specific modulus – porosity relations in the Gassmann relations through the frame modulii; for example, $K_{frame} = K_{solid} \cdot f_K(\varphi)$ and $\mu_{frame} = \mu_{solid} \cdot f_\mu(\varphi)$ where φ is porosity, and $f_K(\varphi)$ and $f_\mu(\varphi)$ provide the functional dependence of the frame moduli on porosity. The subscript "solid" refers to the solid grain (mineral) material. He calculated K_{pore} and Biot coefficients α_K and α_μ. These coefficients vary from 0 to 1 and describe the frame modulii relative to the solid grain modulii. The coefficient,

α_K, was introduced by Biot (1941) and is equivalent to (1 - K_{frame} / K_{solid}). Specifying a particular frame modulus porosity relationship has implications for both α_K and α_μ. The term α_K in turn affects K_{pore} which responds to changes in pore fluid. The effect of different modulus – porosity models on α_k, α_μ and K_{pore} were examined. This is important when estimating the effect of pore fluid on seismic body waves.

Johnson (2001) presented a theory of frequency dependent acoustics in patchy saturated porous media. Biot – Gassmann - Woods theory, applicable at low frequencies (upto 1000 Hz), predicts an abrupt change in compressional modulus and hence the compressional wave speed, when only a very small gas saturation is introduced. Essentially the compressional modulus is either the dry value or the fully saturated value and it is very unlikely to lie in between the two limits. The acoustic logging data, as presented by Brie et al. (1995), showed that there is a continuum of measured speeds ranging from the dry to the saturated values. The alternative is to consider the patchy saturated situation when a rock sample is 100% saturated with water in some regions (''patches''), and 100% saturated with gas in others. For such a situation, the Biot- Gassmann – Hill theory, applicable at high frequencies (>1000 Hz), predicts that the effective bulk modulus is much more smoothly varying as a function of gas saturation than is predicted by the Biot – Gassmann - Woods theory. The properties of crossover from the Biot–Gassmann–Woods result at low frequencies to the Biot–Gassmann–Hill result at high frequencies have been described. Exact results for the approach to the low and the high frequency limits have been derived. A simple closed-form analytic model based on these exact results has been presented. Comparison against the exact solution in simple geometries for the case of a gas and water saturated rock demonstrates that the analytic theory is extremely accurate over the entire frequency range. The model has two geometrical parameters, one of which is the specific surface area of the patches. In the special case, that one of the fluids is a gas, the second parameter is a different, but also simple, measure of the patch size of the stiff fluid.

Batzle et al. (2001) presented experimental evidence to indicate that fluid motion and pressure control rock velocity changes and seismic sensitivity to pore fluid types. One obvious factor controlling the fluid motion is viscosity. The effect of viscosity is different for Poiseuille and squirt flow mechanism. For the dry sample compressional and shear wave velocities show little frequency influence which shows that the primary dispersive effects are dependent on pore fluids. When saturated with glycerine, strong frequency dependence was found. Shear velocity is not independent of the fluid but increases with increasing fluid viscosity, indicating a viscosity contribution to the shear modulus. The compressional wave velocity is also found to increase with viscosity. The dispersion behavior in these investigations is consistent with the model of squirt flow. A second factor influencing the fluid flow is permeability. It is expected that lower permeabilities should require longer times, or lower frequencies, for saturated rocks to relax. In extreme unrelaxed cases (such as for low permeability), the seismic frequency band will be in the high-frequency regime. To be in the low-frequency range, higher permeabilities, perhaps above a few tens of millidarcies, more typical of sands, are required.

Batzle et al. (2006) presented the results of experimental measurements of the influence of fluid mobility on seismic velocity dispersion. The measurements were made from seismic to ultrasonic frequencies. The ratio of rock permeability to fluid viscosity is defined as fluid mobility that largely controls pore-fluid motion and pore pressure in a porous medium. The measurements suggest that high fluid mobility permits pore-pressure equilibrium and results in a low-frequency domain where Gassmann's equations are valid. Only those rocks with high permeability (porous sands and carbonates) will remain in the low-frequency domain in the seismic or sonic band. Most sedimentary rocks — shale, siltstones, tight sandstones and carbonates, heavy oil sands, and evaporates have very low permeability and thus low fluid mobility. These rocks thus fall in the high-frequency

regime, even in typical seismic exploration frequencies. This is even the case for permeable rock saturated with viscous oil.

Cacrcione and Picotti (2006) considered a periodically stratified medium and investigated the amount of attenuation and velocity dispersion caused by different types of heterogeneities in the rock properties, namely, porosity, grain and frame moduli, permeability, and fluid properties. They found that most effective loss mechanisms result from porosity variations and partial saturation, where one of the fluids is very stiff and the other is very compliant, such as, a highly permeable sandstone at shallow depths, saturated with small amounts of gas with around 10% saturation and water. Grain and frame-moduli variations are the next cause of attenuation. The relaxation peak moves towards low frequencies as the background permeability decreases and the viscosity and thickness of the layers increase.

2.4 PROPAGATION OF SEISMIC WAVES IN A POROUS ANELASTIC MEDIUM

White (1965) extended Gassmann's approach to calculate the effect of fluid flow on shear wave attenuation, obtaining the same expression as Biot's low frequency attenuation. White (1975) further applied the low frequency analysis to show how pressure differences at a boundary may cause substantial fluid flow and how the shifting fluid couples back into the seismic wave to a significant degree. When a compressional wave travels through a porous rock, pressure gradients in the fluid cause some flow relative to the rock skeleton and hence some loss of energy. Within a single homogeneous rock, these gradients are small and attenuation due to fluid flow is negligible at seismic frequencies. If the rock has mixed saturation, with segregated pockets of gas, for instance, then pressure gradients are high near the inhomogeneities and fluid flow will also be high. The loss of energy at these local spots when averaged over the total volume can lead to a large attenuation for the compressional wave. White investigated this loss mechanism mathematically by assuming

an ideal geometry. He considered a model wherein spherical gas pockets are located at the corners of a cubic array (Figure 2.1). The skeleton is assumed to be uniform with the pockets having a spherical volume saturated with gas in a rock which is elsewhere saturated with liquid. At low frequencies, an elementary cube with its enclosed sphere of gas is a typical volume, with average properties, which are the same as the average properties of the composite medium. Even for computing average bulk modulus, however, the combination of a cube and a sphere is complicated. Hence, the typical volume is considered to be equivalent to the concentric spheres shown in the lower part of the figure, where the volume of the outer sphere is the same as the volume of the original cube. White (1978) calculated the speeds of compressional waves for a particular model in which the inhomogeneities, whose dimensions are small compared to the wavelength of the seismic wave but much larger than the grains, are gas-filled spherical regions in an otherwise brine-filled rock. He found that a compressional wave passing through such a composite medium can induce a rather large fluid flow near the inhomogeneities, resulting in a substantial loss of energy (due to viscosity of the denser fluid).

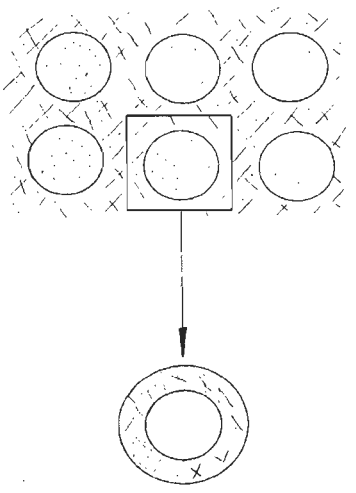

Figure 2.1: ***Model of porous rock with mixed saturation-spherical pockets saturated with gas, intervening volume saturated with liquid. The typical volume considered is the pair of concentric spheres shown in the lower part of the figure (White. 1975).***

Buchen (1971) investigated the problem of propagation of a class of plane inhomogeneous waves in linear viscoelastic media. It was shown that the energy in such an inhomogeneous wave does not propagate normal to the wave fronts. The direction in which the wave suffers maximum attenuation is different from that in which phase changes most rapidly.

Dutta and Ode (1979a, b) carried out investigations to eliminate some of the questioned approximations in White's treatment (White, 1975) of the spherical model by using a more rigorous and systematic approach based on Biot's (1962) field equations. They described the coupled motion of the solid and fluid phases of a saturated porous rock. In the White's model the fluid in the inner sphere was taken to be gas, while that in the outer shell was brine. They showed that White's model can be solved as a boundary value problem using Biot's theory and that the dissipation mechanism proposed by White for partially gas-saturated porous rock is due to Biot's type II (or the diffusion) wave. They also found that an anomalously large absorption at the exploration seismic frequency band was predicted by this model for young, unconsolidated sandstones. For a given size of the gas pockets and their spacing, the attenuation coefficient increases almost linearly with frequency (f) to a maximum value and then decreases approximately as $1/f$. A sizable velocity dispersion was also predicted by this model. A low gas saturation (4-6 percent) was found to yield high absorption and dispersion.

Dutta and Seriff (1979) suggested modifications of formulas for bulk modulus and quality factor as given by White (1975), for case of gas-filled spheres, to bring the results into good agreement with the more exact calculations of Dutta and Ode (1979 a, b). The modified formulas give the expected Gassmann-Wood velocity at very low frequencies. They also showed that inclusion of the finite gas compressibility in numerical calculations for gas-filled spheres shows an interesting maximum of the attenuation at low gas saturations that is not seen if the gas is ignored. They also compared the attenuation

calculated for the same rock and fluids but for three different geometries of the gas-filled regions and found that the configuration of the gas-filled zones does not have an important effect on the magnitude of the attenuation.

Berryman (1988) investigated the following phenomenon: Biot's theory (Biot, 1956) predicts that the attenuation coefficient of fast P-waves and S-waves are proportional to the fluid permeability. Although the observed attenuation is generally in qualitative agreement with the theory, the magnitude of the observed attenuation coefficient in rocks is an order of magnitude higher than expected. He concluded that the high degree of local heterogeneity in rock properties causes different parts of the rock to play the leading roles in the processes of wave attenuation and fluid flow. The regions of high permeability produce the majority of the attenuation while the regions of low permeability tend to dominate the fluid flow.

Ursin and Toverud (2002) described eight different mathematical models for the complex elastic modulus or propagation velocity. These models include Kolsky – Futterman (KF) model (Kolsy 1956, Futterman 1962), the constant Q model of Kjartansson (1979), the Cole-Cole model (Cole and Cole, 1941), and Standard Linear Solid (SLS) model (Ben-Menahem and Singh (1981). These models were compared to find similarities and differences between them. For this purpose, they considered plane wave propagation in a homogeneous viscoelastic medium. They computed the attenuation, phase velocity in the seismic frequency band and then compared the propagation of a Ricker wavelet, using the KF model as a reference. They found that all models except the SLS model behave similarly to the KF model

Toverud and Ursin (2005) inverted a zero offset vertical seismic profiling (VSP) data set with respect to attenuation parameters. Eight different attenuation models were successively applied in the inversion scheme providing eight sets of parameters. The models used had been used earlier in Ursin and Toverud (2002). It was found that the

Kolsky-Futterman model performed slightly better than the other models where the SLS model came off as somewhat better. These results support the widespread use of these two models in seismic processing.

Carcione (2006) showed that waves in dispersive media exhibit elliptical polarization. The direction of the major axis of the ellipse deviates from the propagation direction. In addition, the Snell's law does not give the ray path, since the propagation direction does not coincide with the energy flow direction.

2.5 REFLECTION AND TRANSMISSION OF WAVES PROPAGATING IN POROUS ANELASTIC MEDIA

Borcherdt (1982) investigated the problem of the reflection and refraction of general P and SV waves in elastic and anelastic solids. The waves are incident on welded boundaries and the free surface. The detailed treatment of this problem predicted that contrasts in intrinsic absorption at boundaries in general give rise to inhomogeneous P and SV waves with velocities and attenuations respectively less than and greater than those for homogeneous waves, elliptical particle motions, maximum energy flow in directions different from phase propagation and physical characteristics dependent on angle of incidence.

Sharma et al. (1990) considered the problem of reflection and refraction of P – and SV- waves at an interface separating the linear viscoelastic solid and liquid saturated porous solid half spaces. They used Biot's formulation of wave propagation in the liquid saturated porous medium. In addition, the theory of Borcherdt (1973) for plane waves in a linear homogeneous viscoelastic medium was used. They plotted the amplitude and energy ratios of the reflected P- and SV- waves and incident P-waves with angles of incidence for the case when the porous medium is a sandstone saturated with kerosene.

Sharma and Gogna (1991) considered the problem of propagation of seismic waves in a linear viscoelastic porous solid saturated by a viscous liquid and reflection of P- and

SV-waves at the free surface of such a solid. They derived analytic expressions for reflection coefficients. They plotted the modulus of reflection coefficients with angle of incidence for the case when the porous medium is water saturated sandstone.

Samec and Blangy (1992) studied the effects of both attenuation and anisotropy on synthetic Amplitude versus Offset (AVO) trends. They found that contrasts in viscoelasticity do not appear to control the variation of reflection coefficients with angles of incidence for small angles but are a controlling factor of amplitudes. They also found that viscoelastic anisotropy could severely affect the variation of the reflection coefficients with angles of incidence. Propagation effects, which continuously alter the signal during propagation because of attenuation and dispersion, have an important influence on interpretation of AVO trends.

Carcione (1997) considered the problem of reflection and transmission of elastic waves in two viscoelastic transversely isotropic media in contact. It was shown that for an incident homogeneous wave, the reflected wave is of the same type while the other waves are inhomogeneous. If the transmission medium is elastic, the refracted waves are inhomogenous of the elastic type, i.e., attenuation vectors are perpendicular to the direction in which energy propagates. On the other hand, if the incident medium is elastic and the transmission medium is anelastic, the attenuation vectors of the transmitted waves are perpendicular to the interface.

Ursin and Stovas (2002) investigated the reflection and transmission responses of a layered viscoelastic medium. They derived the first-order approximations of the PP and SS transmission responses. These consist of a phase shift and attenuation term from direct transmission through the layers and two attenuation terms from back scattered P and S waves. It was suggested that the average of these responses might be used for overburden corrections in AVO analysis.

Cerveny (2004) investigated the laws of reflection and transmission of plain waves at a planar interface between two homogeneous anisotropic viscoelastic half spaces. He presented algorithms for determining the slowness vectors of reflected and transmitted plane waves from the known slowness vectors of the incident waves. In visoelastic media, slowness vectors are complex-valued, the real part being the propagation vector and the imaginary part, the attenuation vector. When these two vectors are parallel, the waves are known as plane waves and when these are non-parallel, inhomogeneous waves exist. For unrestricted anisotropy and viscoelasticity, the algorithms require solution of an algebraic equation of sixth degree in each half space.

Stine (2004) investigated the sensitivity of AVO reflectivity to fluid properties in porous media. He calculated reflection and transmission coefficients using Biot theory. The models considered by him consist of sandstone over sandstone (fluid boundary) and shale over sandstone. The properties of one of the layers are allowed to vary while that of the other are held constant. In the first kind of models, different fluids (gas, oil and water) occupy the two sandstones. The reflection coefficients showed small differences from those calculated using Zoeppritz equations. He also examined the sensitivity of the reflection coefficients to different physical parameters (permeability, porosity and viscosity) by a graphical approach. The sensitivity analysis has also been complemented by calculating partial derivatives of the reflection coefficients with respect to individual parameters. It was found that the Biot slow wave has the most significant sensitivity to fluid properties. However, this wave is not directly observable in normal data. This wave, however, may remove energy from the reflected P-wave as part of energy partitioning during reflection. There is small sensitivity of reflection coefficients to permeability but significant sensitivity to porosity. It was found that there is a significant amount of sensitivity to viscosity at the gas-liquid boundary in a homogenous reservoir sand, but very little in the shale over sand boundaries. The two gas-water contact models and the constant

gas sand over varied oil sand model have the greatest sensitivity to changes in the viscosity. For those three models, the reflection coefficients in Biot theory are up to three times more sensitive to changes in the fluid viscosity as they are to permeability changes.

2.6 SYNTHETIC SEISMOGRAMS

Krebes and Hron (1980) generated ray-synthetic synthetic seismograms for SH-wave body waves for a plane layered crustal model in both the elastic and anelastic cases taking into account anelastic reflection and transmission coefficients and the geometrical spreading factor. The seismograms for the anelastic cases exhibited amplitude attenuation and waveform spreading. The amplitudes and phases of the arrivals were also seen to depend significantly on the direction of maximum attenuation of the initial ray segment.

Carcione et al. (1988) presented a formulation for wave propagation in an anelastic medium. They considered wave propagation in a general inhomogeneous anelastic medium within the framework of the theory of linear viscoelasticity. The concept of a spectrum of relaxation mechanisms is used to define the constitutive relations. The proposed method has been used to describe elastic waves propagation though porous media. Simulations displayed a strong velocity dispersion for both P- and S-waves, viscoelastic wavefield arriving earlier than the elastic one, faster shear mode then the dilatational mode and comparable amplitudes of the shear and dilatational modes.

Borcherdt and Glassmoyer (1989) investigated the free surface reflection of anelastic inhomogeneous wavefields. They presented numerical modeling results based on exact closed-form solutions for the problems of incident inomogeneous P and SV waves (Borcherdt, 1982). They obtained numerical results for a model of Pierre shale (McDonal *et al.,* 1958) and describe the dependence of particle motion amplitudes on wave field inhomogeneity, angle of incidence, and intrinsic material absorption. They defined and

calculated anelastic, free surface, and reflection coefficients for inhomogeneous wave fields for energy, displacement amplitude, volumetric strain, and phase.

Quiroga-Goode et al. (1994) compared two methods of computing ray synthetic seismograms in anelastic media (stationary ray method and conventional ray method) with the finite difference approach. These methods were applied to generate SH synthetic seismograms in a model wherein an anelastic layer is sandwiched between two half spaces; the upper half-space is elastic and the lower, anelastic. By making direct comparisons between synthetic seismograms obtained with the stationary ray method, conventional ray method, and finite differences, they found that the stationary ray method agreed with the finite-difference solution better than the conventional ray method.

Carcione (1993) presented two-dimensional (2-D) and three-dimensional (3-D) forward modeling in linear viscoelastic media. Simulations on a model separating an elastic medium from a viscoelastic medium with similar elastic moduli but different attenuations shows that the interface generates appreciable reflected energy. In another simulation, the response of a single interface in the presence of highly dissipative sandstone lenses is computed, properly simulating the anelasticity of direct and converted P- and S-waves. Simulation of a commonshot reflection survey over a gas cap reservoir indicates that attenuation significantly affects the bright spot response.

2.7 OBJECTIVES

The above review of pertinent literature has revealed that there are still some gaps in our knowledge about the influence of viscoelasticity and solid – fluid interaction on different aspects of the problem of seismic wave propagation in porous viscoelastic solids saturated with gas and water, oil and water or only water. Frequency dependent attenuation of seismic waves in real earth is well established and means that the anelascity of the propagating medium must be taken into account. Viscoelastic models of the solid matrix of

the propagating medium require that the seismic wave velocities, quality factor and attenuation coefficients become complex and frequency dependent. The aim of the present work, then, is to carry out a systematic investigation of the influence of porosity, type of pore fluids and water saturation on (i) frequency dependence of seismic wave velocities, quality factor, attenuation coefficients and reflection coefficients; (ii) dependence amplitude of reflected wave lets on offset; (iii) shape of wavelets at different offsets; and (iv) quantification of the influence of viscoelasticity and solid – fluid interaction on the attenuation and shape of wavelets.

CHAPTER – 3

THEORETICAL BACKGROUND

3.1 INTRODUCTION

Real earth media are composed of materials that are anelastic. Waves that propagate in such media are attenuated and dispersed. However, materials in the earth have traditionally been modeled as elastic media without any attenuation and dispersion. To solve the wave propagation problems in porous anelastic media saturated with viscous fluids and generate synthetic seismograms, a boundary values problem involving equations of motion in such media has to be formulated and solved. In this chapter, some essential aspects of this problem have been presented. At first, some aspects of modeling of anelastic materials have been discussed.

Elastic media are composed of materials that exhibit elastic behavior. Such media are essentially nonporous and follow Hooke's law of linear elasticity, i.e., direct proportionality between stress and strain for small strains such as those that are induced by seismic waves. Under a constant stress, an elastic strain appears that remains unchanged with time. When the load is removed, the elastic strain disappears completely. Solution of wave propagation problems in elastic media is quite well known and has been briefly given in Appendix A. When the media are anelastic, they exhibit anelastic behavior, i.e., time dependent strain. Under constant load, the initially induced elastic strain increases rapidly at first and then gradually. When the load is removed, there is a sudden drop in strain followed by gradual return to condition of no strain. In such media, stress is also proportional to time derivative of strain.

3.2 ANELASTIC MEDIA

As mentioned earlier, real earth media are anelastic. In such media seismic waves undergo attenuation as a result of a variety of processes, which can be summarized macroscopically as "internal friction" (Aki and Richards, 2002). The gross effect of internal friction is represented by the non-dimensional quantity Q, the quality factor. It is a property of the anelastic medium through which the wave propagates.

A plane wave propagating with speed c along the x-direction in a perfectly elastic medium retains its shape exactly and all frequency components travel coherently with the same velocity. In an anelastic medium its amplitude, $A(x)$ at a distance x, can be written as

$$A(x) = A_0 \exp[-a(\omega)x] \qquad \text{.....(3.1)}$$

where $\alpha(\omega)$ is the attenuation coefficient, defined as

$$a(\omega) = \frac{\omega}{2cQ} \qquad \text{.....(3.2)}$$

Knopoff (1964) concluded, on the basis of experimental measurements, that Q is frequency dependent and that $Q(\omega) \propto \omega^{-1}$ for a variety of fluids, but that Q is approximately constant for the frequency range of observation in solids. However, for frequency independent Q and c, it has been shown by Aki and Richards(2002) that the shape of wavelets observed at a distance x does not follow the principle of causality, i.e., the wavelet is found to have appreciable amplitude even before $t = x/c$, its geometrical time of arrival. It has been shown that in order that amplitude of the wavelet is zero for $t \le x/c_\infty$, both Q and c should be frequency dependent and the following relation must be satisfied:

$$\frac{\omega}{c(\omega)} = \frac{\omega}{c_\infty} + H[a(\omega)] \qquad \text{.....(3.3)}$$

where c_∞ is the limit of $c(\omega)$ as ω goes to infinity and $H[a(\omega)]$ is the Hilbert transform of the attenuation coefficient. Because of frequency dependence of c, attenuation of the wave is accompanied by dispersion.

According to Liu et al. (1976), attenuation is due to a superposition of different relaxation phenomena, each one of which would be represented by the stress-strain relation

$$\sigma + \tau_\sigma \frac{d\sigma}{dt} = M_R\left(\varepsilon + \tau_\varepsilon \frac{d\varepsilon}{dt}\right) \qquad \text{.....(3.4)}$$

where σ represents the stress and ε, the strain. The quantity τ_ε is the characteristic relaxation time of strain under an applied step in stress and τ_σ, the relaxation time for the stress corresponding to a step in strain. M_R is called the relaxed elastic modulus since it gives the ratio of stress to strain in the limit as t goes to infinity. It is defied as

$$M_R = M_U\left(\frac{\tau_\varepsilon}{\tau_\sigma}\right) \qquad \text{.....(3.5)}$$

where M_U is the unrelaxed elastic modulus in the sense that it gives the ratio of stress to strain as soon as the stress has been applied, before the material has started to relax (via creep) to some new configuration (Aki and Richards, 2002).

The stress strain relation (Eq. 3.4) applies to a Standard Linear Solid (SLS). It is a mechanical model of an anelastic material that consists of springs and dashpots. The spring represents a model of linear elasticity with the property that the extension is proportional to the applied force and that it exhibits instantaneous elasticity and instantaneous recovery. This behavior is also a characteristic of elastic solids. The energy stored in the spring is $\sigma^2/2\mu$. The dashpot, on the other hand, is the mechanical model of a viscous fluid. It is used to represent Stokes' linear viscosity (Ben-Menahem and Singh, 1981). It has the property that its rate of extension (velocity of piston) is proportional to the applied force. Therefore, when subjected to a step of constant stress, it will deform continuously at a constant rate. The rate of energy dissipation is the dashpot is $\sigma^2/2\eta$, where η is the viscosity.

A mechanical model of an anelastic material that consists of springs and dashpots is known as the viscoelastic model. The simplest of such models is the Maxwell model that consists of a spring in series (Figure 1.3). Another simple model is the Kelvin – Voigt

model that consists of a spring and dashpot in parallel (Figure 1.4). None of these models, however, truly represents the behavior, under constant load, of earth materials. Rocks build up an instantaneous strain upon sudden application of stress which then increases, rapidly at first and then at decreasing rate. This behavior is closely reproduced by a standard linear solid that consists of a spring in parallel with a Maxwell model (Figure 3.1).

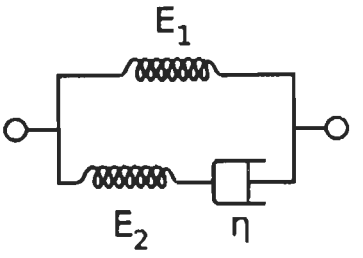

Figure 3.1: ***Schematic representation of the Standard Linear Solid model.***

The parameters M_R, τ_ε and τ_σ appearing in (Eq. 3.4) are defined in terms of E_1, E_2 and η as follows:

$$M_R = \frac{E_1 E_2}{E_1 + E_2}, \qquad \tau_\varepsilon = \frac{\eta}{E_1}, \qquad \tau_\sigma = \frac{\eta}{E_1 + E_2} \qquad \text{.....(3.6)}$$

The response of the Standard Linear Solid to a step of constant stress, $\sigma_0 H(t)$, is given by

$$\varepsilon(t) = \left(\frac{\sigma_0}{M_R}\right)\left[1 - \left(1 - \left(\frac{\tau_\sigma}{\tau_\varepsilon}\right)\exp\left(\frac{-t}{\tau_\varepsilon}\right)\right)\right]H(t) \qquad \text{.....(3.7)}$$

For a step of constant strain, $\varepsilon_0 H(t)$, the response is given by

$$\sigma(t) = M_R \varepsilon_0 \left[1 + \left(\frac{\tau_\varepsilon}{\tau_\sigma}\right)\exp\left(\frac{-t}{\tau_\sigma}\right)\right]H(t) \qquad \text{.....(3.8)}$$

The quantity τ_σ is called the stress relaxation time under constant strain, and τ_ε, the strain relaxation time under constant stress.

For harmonic stress cycle, represented by $\sigma = S\exp(-i\omega t)$ and corresponding strain cycle, $\varepsilon = E\exp(-i\omega t)$, the response is (Ben Menahem and Singh, 1981)

$$M(\omega) = \frac{S}{E} = M_R \left[\frac{(1 - i\omega\tau_\varepsilon)}{(1 - i\omega\tau_\sigma)} \right] \qquad \text{.....(3.9)}$$

where $M(\omega)$ is the frequency dependent elastic modulus. Thus for cyclic loading which occurs in the presence of a seismic wave, the elastic modulus is complex and frequency dependent. Since the standard linear solid follows the linear stress-strain relation given by (Eq. 3.4), it is a linear viscoelastic model.

The Standard Linear Solid described above is characterized by one set of values of relaxation times τ_σ and τ_ε, and thus it is a solid with a single relaxation mechanism. It is characterized by a frequency dependent quality factor, $Q(\omega)$, given by (Aki and Richards, 2002)

$$\frac{1}{Q(\omega)} = \omega \frac{(\tau_\varepsilon - \tau_\sigma)}{(1 + \omega^2 \tau_\varepsilon \tau_\sigma)} \qquad \text{.....(3.10)}$$

and frequency dependent velocity, $c(\omega)$, given by

$$[c(\omega)]^2 = \left(\frac{M_U}{\rho} \right) \left[1 + \left(\frac{M_U}{M_R} - 1 \right) \left\{ \frac{1}{(1 + \omega^2 \tau^2 \varepsilon)} \right\} \right]^{-1} \qquad \text{.....(3.11)}$$

These two quantities are shown in Figure 3.2 and Figure 3.3 (a) and (b).

It has been remarked earlier that Knopoff (1964) observed that Q is approximately constant for the frequency range of observation in solids. In order to reproduce such a constant Q values, Liu et al. (1976) superposed twelve relaxation peaks of the type shown in Figure 3.2, all sharing the same relaxed modulus M_R and found that over the frequency range 0.0001 – 10 Hz, Q^{-1} is effectively constant and phase velocity has a linear dependence on ln ω. They arrived at the same conclusion when they considered a continuous superposition of relaxations, specified by a density function. Liu et al. (1976) used a uniform distribution for the density function.

In the present work a single mechanism model has been used. The appropriate values of relaxation times, τ_σ and τ_ε have been obtained from Carcione (2003). Frequency dependent wave velocities have been obtained from

$$c(\omega) = \sqrt{\frac{M(\omega)}{\rho}} \qquad \text{.....(3.12)}$$

and $Q(\omega)$ has been obtained from

$$Q(\omega) = -\left\{\frac{\mathrm{Re}\{M(\omega)\}}{\mathrm{Im}\{M(\omega)\}}\right\} \qquad \text{.....(3.13)}$$

In the above relations, $c = \alpha$ or β, the P or S-wave velocity. $M(\omega) = \lambda(\omega) + 2\mu(\omega)$ for P-waves and $M(\omega) = \mu(\omega)$ for S-waves. Values of τ_σ and τ_ε are different for P and S waves and are given in Table 4.4.

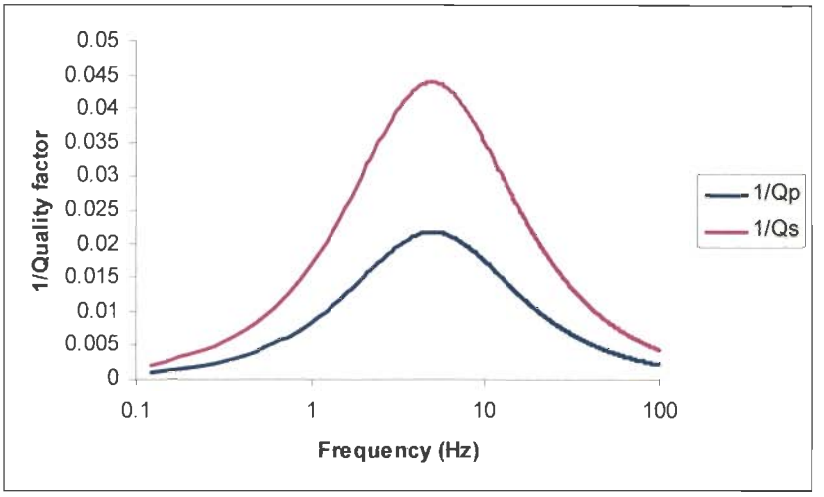

Figure 3.2: ***Variation of quality factors with the frequency. The frequency range considered for the present work is 0-100Hz. Q_p and Q_s stand for quality factor for P-wave and S-wave respectively.***

The frequency dependence of Q for Maxwell and Kelvin-Voigt models are shown in Appendix D (Part V).

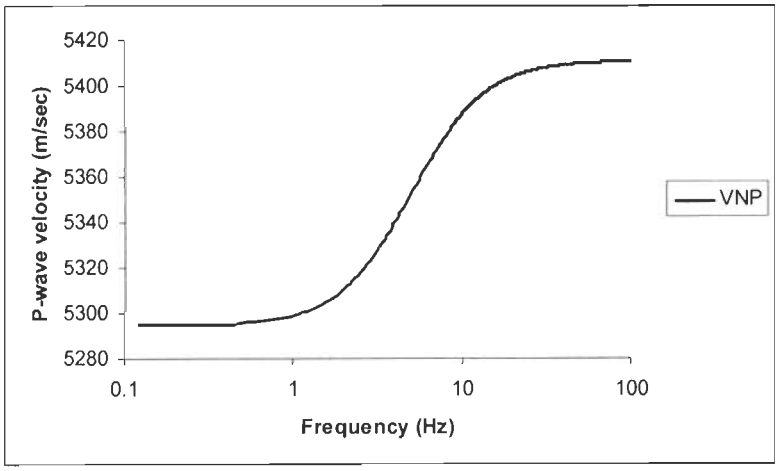

(a)

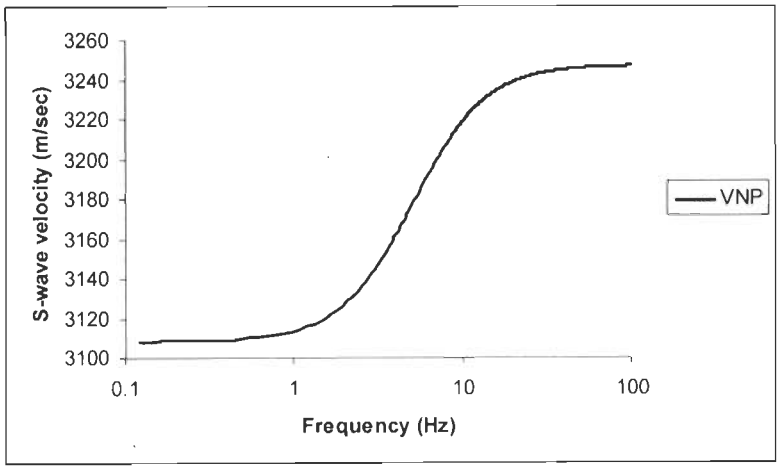

(b)

Figure 3.3: ***Variation of (a) P-wave, and (b) S-wave velocity with frequency. The frequency range is from 0 to 100 Hz. VNP stands for viscoelastic non-porous.***

For one dimensional wave propagation in an anelastic medium, the propagating wave is described by $\exp[-a(\omega)x]\exp[i\omega\left(\frac{x}{c(\omega)}-t\right)]$. The direction of maximum attenuation is also the direction of increasing phase delay. For plane waves in two dimensions, these two directions are different. Solutions to following equation are considered:

$$\ddot{\psi} + K^2\psi = 0 \qquad \text{.....(3.14)}$$

where $K = \omega/c(\omega)$ is complex because $c(\omega)$ is now complex. Plane wave solution to (Eq. 3.14) is the following

$$\psi = S\exp(-\omega\vec{A}\cdot\hat{x})\exp[i\omega(\vec{P}\cdot\hat{x}-t)] \qquad \text{.....(3.15)}$$

where $\vec{A}$ and $\vec{P}$ are vectors with real Cartesian components (Aki and Richards, 2002). $\vec{A}$ is the direction of maximum attenuation and $\vec{P}$ is the direction of wave propagation. From (Eq. 3.14) and (Eq. 3.15) the following relations are obtained:

$$P^2 - A^2 = \mathrm{Re}\{K^2\} \qquad \text{.....(3.16)}$$

and

$$PA\cos\gamma = \frac{1}{2}\mathrm{Im}\{K^2\} \qquad \text{.....(3.17)}$$

where γ is the angle between $\vec{P}$ and $\vec{A}$. The wave is said to be homogeneous or inhomogeneous according to whether $\gamma = 0$ or $\gamma \neq 0$. For elastic media, since K is always real, it follows (from Eq. 3.17) that either $A = 0$ or $\gamma = \pi/2$. But for anelastic media, neither A can be zero nor γ can be $\pi/2$. For one dimensional case, when $A \neq 0$, $\gamma = 0$ which corresponds to a homogeneous wave. However, when anelastic half spaces are involved, the propagating waves are necessarily inhomogeneous and $0 < \gamma < \pi/2$. The case of wave propagation involving two half spaces, one of which is elastic and the other is anelastic, is discussed below.

The complex vector, $\vec{K}$, can be written as $\omega(\vec{P} + \mathrm{i}\,\vec{A})$. The solution of (Eq. 3.14) can be written as

$$\begin{aligned}\psi &= S\exp[i\omega(\vec{K}\cdot\hat{x}-t)] \\ &= S\exp[i\omega(K_x x + K_z z) - t]\end{aligned} \qquad \text{.....(3.18)}$$

where K_x and K_z are x- and z-components of $\vec{K}$. Obviously,

$$K_x = p \text{ and } K_z = \sqrt{(c^{-2} - p^2)} \qquad \text{.....(3.19)}$$

In anelastic media, p (= sin i / $c(\omega)$) will be complex and so will be K_z. Let $P_z = d_r + id_i$. and $p = p_r + ip_i$. Then

$$K_x x + K_z z = (p_r x + d_r z) + i(p_i x + d_i z) = \vec{P} \cdot \hat{x} + i\vec{A} \cdot \hat{x} \qquad \text{.....(3.20)}$$

and

$$\begin{aligned} \psi &= S \exp[-\omega(p_i x + d_i z)] \exp[i\omega(p_r x + d_r z) - t] \\ &= S \exp[-\omega(\vec{A} \cdot \hat{x})] \exp[i\omega(\vec{P} \cdot \hat{x} - t)] \end{aligned} \qquad \text{.....(3.21)}$$

The attenuation and propagation vectors are given by

$$\vec{A} = p_i \hat{i} + d_i \hat{k} \text{ and } \vec{P} = p_r \hat{i} + d_r \hat{k} \qquad \text{.....(3.22)}$$

The attenuation of the wave is governed by the attenuation coefficient, given by

$$a(\omega) = \frac{\omega}{2c(\omega)Q(\omega)} \qquad \text{.....(3.23)}$$

Now consider the case of P-waves incident at the interface separating an elastic half space from an anelastic half space. The elastic half space occupies the region $z < 0$, and anelastic half space, $z > 0$. The P-waves are incident from the side of the elastic half space. The displacements in the elastic half space are given by equations A-2 and A-3. In the viscoelastic half space, the displacements are

$$u_x^2 = P_2^d(\alpha_2 p) \exp\{i\omega(px + \xi_2 z - t)\} + S_2^d(\beta_2 \eta_2) \exp\{i\omega(px + \eta_2 z - t)\} \qquad \text{.....(3.24)}$$

$$u_2^z = P_2^d(\alpha_2 \xi_2) \exp\{i\omega(px + \xi_2 z - t)\} - S_2^d(\beta_2 p) \exp\{i\omega(px + \eta_2 z - t)\} \qquad \text{.....(3.25)}$$

where

i_2 : angle made by down going transmitted P-ray with normal

j_2 : angle made by down going transmitted S-ray with normal

ξ_2 : $\dfrac{\cos i_2}{\alpha_2} = \sqrt{(\alpha_2^{-2} - p^2)}$

η_2 : $\dfrac{\cos j_2}{\beta_2} = \sqrt{(\beta_2^{-2} - p^2)}$

P_2^d : displacement amplitude of transmitted P-wave

S_2^d: displacement amplitude of transmitted S-wave

α_2, β_2 : complex and frequency dependent P- and S-wave velocities, respectively.

It has been assumed here that all angles are real, i.e., following form of Snell's law is used:

$$\frac{\sin i_1}{\alpha_1} = \frac{\sin j_1}{\beta_1} = \frac{\sin i_2}{\mathrm{Re}(\alpha_2)} = \frac{\sin j_2}{\mathrm{Re}(\beta_2)} \qquad \text{.....(3.26)}$$

The boundary conditions at $z = 0$ are similar to those for the elastic case (Appendix A). The relations (Eq. A-10 to A-13) apply to this case also, except that the quantities corresponding to the lower anelastic half space will be differently defined. The reflection coefficients can thus be computed using relations similar to (Eq. A-22).

3.3 VELOCITIES IN POROUS MEDIA

A basic requirement in porous media is to be able to compute their seismic wave velocities. A number of empirical relations exist, e.g., those proposed by Wyllie (1958) and Raymer (1980) that yield seismic wave velocities in porous media saturated with fluids. However, these lack any physical basis and ignore solid-fluid interaction at the time of passage of seismic waves. Gassmann's relations (Gassmann, 1951) provide an alternate method for achieving the same. A brief account, based on Nolen-Hoeksema (2000) is given in Appendix B.

3.4 POROUS VISCOELASTIC MEDIA

In porous viscoelastic media, the solid material behaves anelastically. Following Sharma and Gogna (1991) the differential equations governing the displacement $\vec{u}$ of solid matrix and $\vec{U}$ of interstitial fluid in a homogeneous isotropic porous solid, saturated by a viscous fluid, are given by

$$\mu^* \nabla^2 \vec{u} + (\lambda^* + \mu^* + \alpha^{*2} M^*) \nabla(\nabla \cdot \vec{u}) + \alpha^* M^* \nabla(\nabla \cdot \vec{w}) = \frac{\partial^2}{\partial t^2}(\rho_b \vec{u} + \rho_f \vec{w}) \qquad \text{.....(3.27)}$$

$$\nabla(\alpha^* M^* (\nabla \cdot \vec{u}) + M^* (\nabla \cdot \vec{w})) = \frac{\partial^2}{\partial t^2}(\rho_f \vec{u} + m\vec{w}) + \frac{\eta_b}{\chi}\frac{\partial \vec{w}}{\partial t} \qquad \text{.....(3.28)}$$

where

$$\vec{w} = \varphi(\vec{U} - \vec{u})$$

and λ^* and μ^* are complex Lame's constants of the solid matrix, m is Biot's parameter which depends on porosity φ and bulk density of fluid ρ_f, η_b is viscosity and χ is permeability (ρ_f *and* η_b have been defined below). The vector $\vec{w}$ represents the flow of liquid relative to the solid measured in terms of volume per unit area of the bulk medium. The quantities α^* and M^* are the complex elastic coefficients defined by

$$\alpha^* = 1 - \delta^* K_b^* \qquad \text{.....(3.29)}$$

$$M^* = 1/(\gamma^* + \delta^* - \delta^{*2} K_b^*) \qquad \text{.....(3.30)}$$

$$\gamma^* = \varphi\left(\left(\frac{1}{K_f}\right) - \left(\frac{1}{K_d^*}\right)\right) \qquad \text{.....(3.31)}$$

$$\delta^* = \frac{1}{K_d^*} \qquad \text{.....(3.32)}$$

Here γ^* is complex coefficient of fluid content, δ^* is complex unjacketed compressibility (Biot, 1957) and K_b^* (= λ^* +2/3 μ^*) is complex jacketed incompressibility. K_b^* is the bulk modulus of a saturated porous medium calculated using Gassmann's theory (Appendix B). K^*_d is the bulk modulus of dry frame (Eq. B-5). K_f is the bulk modulus of fluid has been defined below.

The viscous fluid (oil or gas) when present in the pore spaces is always accompanied with some water. The water saturation in such cases rarely falls below 10% and this minimum value is called irreducible water saturation. Therefore, the properties of individual fluid have to be combined properly so that the porous medium can be considered to be saturated with a single fluid. Therefore, the properties of the fluids are combined using following relations:

Density $\qquad \rho_f = S_w \varphi \rho_w + (1 - S_w)\varphi \rho_o \qquad$ .....(3.33)

Viscosity $\qquad \eta_b = S_w \eta_w + (1 - S_w)\eta_o \qquad$ .....(3.34)

Bulk modulus $$K_f = \frac{1}{\left(\frac{S_w}{K_w}\right) + \left(\frac{1 - S_w}{K_{fl}}\right)} \qquad \text{.....(3.35)}$$

where S_w is water saturation, ρ_w and ρ_{fl} stand for density of water and the fluid present in the pores, respectively, η_w and η_{fl} stand for viscosity of water and the fluid present in the pores, respectively, and K_w and K_{fl} stand for bulk modulus of water and fluid present in the pores, respectively.

The bulk density (ρ_b) of the porous medium when more than one fluid is present is given by

$$\rho_b = (1 - \varphi)\rho_s + S_w \varphi \rho_w + (1 - S_w)\varphi \rho_{fl} \qquad \text{.....(3.36)}$$

The stress strain relations are

$$\tau_{ij} = 2\mu^* e_{ij} + \left[\left(\lambda^* + \alpha^{*2} M^*\right)e + \alpha^* M^* \xi\right]\delta_{ij} \qquad \text{.....(3.37)}$$

$$P_f = -\alpha^* M^* e - M^* \xi \qquad \text{.....(3.38)}$$

where τ_{ij} and e_{ij} are strain and stress tensors, e is cubical dilatation and $\xi = div\, \vec{w}$. P_f denotes fluid pressure.

Equations (3.27 and 3.28) are valid in the low frequnecy range where the flow in the pores is of Poiseuille type. The Poiseuille flow breaks down if frequency f exceeds a certain value f_l, given by

$$f_l = \frac{\pi \eta_b}{4 \rho_f d^2} \qquad \text{.....(3.39)}$$

where d is diameter of the pores. The seismic frequency range (1-100 Hz) falls well below f_l for the parameters of the model used here. The pore diameter is aasumed to be 0.00003 m.

The displacement vectors $\vec{u}$ and $\vec{w}$ can be represented in terms of displacement potentials ϕ_j and $\vec{\psi}_j$ (j = 1,2) as

$$\vec{u} = \nabla\phi_1 + \nabla\times\vec{\psi}_1 \qquad \text{.....(3.40)}$$

$$\vec{w} = \nabla\phi_2 + \nabla\times\vec{\psi}_2 \qquad \text{.....(3.41)}$$

where the displacements and hence the potentials, are assumed to be time harmonic (~ $e^{i\omega t}$). On substituting in (Eq. 3.40 and 3.41), the following relations are obtained:

$$\phi_1 = \phi_{11} + \phi_{12} \qquad \text{.....(3.42)}$$

$$\phi_2 = \mu_1\phi_{11} + \mu_2\phi_{12} \qquad \text{.....(3.43)}$$

$$\vec{\psi}_2 = \alpha_0\vec{\psi}_1 \qquad \text{.....(3.44)}$$

where

$$\mu_j = \frac{\rho_f\alpha^* - \rho_b + \dfrac{(\lambda^* + 2\mu^*)}{v_j^2}}{\rho_f - \left(m + i\dfrac{\eta_b}{\omega\chi}\right)\alpha^*} \qquad j=1,2 \qquad \text{.....(3.45)}$$

$$\alpha_0 = -\frac{\rho_f}{m + i\dfrac{\eta_b}{\omega\chi}} \qquad \text{.....(3.46)}$$

The potentials ϕ_{11}, ϕ_{12} and $\vec{\psi}_1$ satisfy the wave equations

$$\left(\nabla^2 + \frac{\omega^2}{v_j^2}\right)\phi_{ij} = 0 \qquad j=1,2 \qquad \text{.....(3.47)}$$

$$\left(\nabla^2 + \frac{\omega^2}{v_3^2}\right)\vec{\psi}_1 = 0 \qquad \text{.....(3.48)}$$

Equations (3.47 and 3.48) imply that in an unbounded viscoelastic porous solid saturated by a viscous fluid, there will be two dilatational waves and a shear wave. The two dilatational waves involve coupled motion in the fluid and solid. The wave corresponding to ϕ_{11} is the dilatational wave of the first kind, also called fast P wave. The wave corresponding to ϕ_{12} is dilatational wave of the second kind, also called slow P wave. The shear wave involves the coupling of the rotation of the solid and the liquid.

The velocities in equations (3.47 and 3.48) can be expressed as

$$v_j^2 = \frac{\lambda^* + 2\mu^*}{\rho_j^*} \qquad j=1,2 \qquad \text{.....(3.49)}$$

$$v_3^2 = \frac{\mu^*}{\rho_3^*} \qquad \text{.....(3.50)}$$

In what follows, $v_1 = \alpha_2^f$, $v_2 = \alpha_2^s$, $v_3 = \beta_2$. The notations α_2^f, α_2^s and β_2 are complex and frequency dependent velocities of fast P-wave, slow P-wave and S-wave, respectively, in the viscoelastic medium and have been used in the subsequent paragraphs.

The frequency dependent equivalent mass densities ρ_1^*, ρ_2^* and ρ_3^* are given by

$$\rho_1^* = \frac{B - \sqrt{(B^2 - 4AC)}}{2M^*} \qquad \text{.....(3.51)}$$

$$\rho_1^* = \frac{B + \sqrt{(B^2 - 4AC)}}{2M^*} \qquad \text{.....(3.52)}$$

$$\rho_3^* = \frac{C}{\left(m + i\frac{\eta_b}{\omega\chi}\right)} \qquad \text{.....(5.53)}$$

where

$$A = (\lambda^* + 2\mu^*)M^* \qquad \text{.....(3.54)}$$

$$B = \rho_b M^* + \left(m + i\frac{\eta_b}{\omega\chi}\right)H^* - 2\rho_f \alpha^* M^* \qquad \text{.....(3.55)}$$

$$C = \rho_b\left(m + i\frac{\eta_b}{\omega\chi}\right) - \rho_f^2 \qquad \text{.....(3.56)}$$

$$\lambda^* = K^* - \frac{2}{3}\mu^* \qquad \text{.....(3.57)}$$

$$H^* = \lambda^* + 2\mu^* + \alpha^{*2} M^* \qquad \text{.....(3.58)}$$

The displacements $\vec{u}$ and $\vec{w}$ can now be written as

$$\vec{u} = \nabla\phi_{11} + \nabla\phi_{12} + \nabla\times\vec{\psi}_1 \qquad \text{.....(3.59)}$$

$$\vec{w} = \mu_1\nabla\phi_{11} + \mu_2\nabla\phi_{12} + \alpha_0\nabla\times\vec{\psi}_1 \qquad \text{.....(3.60)}$$

Now consider the case of two half spaces in welded contact at $z = 0$. The material occupying the region $z < 0$, designated here as medium 1, is elastic, homogenous, isotropic. The other half space is a porous viscoelastic medium. Plane P-waves, traveling in the first half space are incident on the interface at an angle i_1. The displacements and stresses in the elastic half space are given by equations (A-6, A-7, A-8 & A-9).

In the viscoelastic half space, designated here as medium 2, the displacements and stresses are given as

$$u_x^2 = P_2^{df}(\alpha_2^f p)\exp\{i\omega(px+\xi_2^f z - t)\} + P_2^{ds}(\alpha_2^s p)\exp\{i\omega(px+\xi_2^s z - t)\} - S_2^d(\beta_2\eta_2)\exp\{i\omega(px+\eta_2 z - t)\} \quad \text{.....(3.61)}$$

$$u_z^2 = P_2^{df}(\alpha_2^f\xi_2^f)\exp\{i\omega(px+\xi_2^f z - t)\} + P_2^{ds}(\alpha_2^s\xi_2^s)\exp\{i\omega(px+\xi_2^s z - t)\} - S_2^d(\beta_2 p)\exp\{i\omega(px+\eta_2 z - t)\} \quad \text{.....(3.62)}$$

$$w_x = \mu_1 P_2^{df}(\alpha_2^f p)\exp\{i\omega(px+\xi_2^f z - t) + \mu_2 P_2^{ds}(\alpha_2^s p)\exp\{i\omega(px+\xi_2^s z - t) - \alpha_0 S_2^d(\beta_2\eta_2)\exp\{i\omega(px+\eta_2 z - t)\} \quad \text{.....(3.63)}$$

$$w_z = \mu_1 P_2^{df}(\alpha_2^f\xi_2^f)\exp\{i\omega(px+\xi_2^f z - t) + \mu_2 P_2^{ds}(\alpha_2^s\xi_2^s)\exp\{i\omega(px+\xi_2^s z - t) - \alpha_0 S_2^d(\beta_2 p)\exp\{i\omega(px+\eta_2 z - t)\} \quad \text{.....(3.64)}$$

$$\begin{aligned}\tau_{zx}^2 &= \rho_2\beta_2^2\left(\frac{\partial u_x}{\partial z}+\frac{\partial u_z}{\partial x}\right)\\ &= (i\omega)[P_2^{df}(2\rho_2\beta_2^2)p(\alpha_2^f\xi_2^f)\exp\{i\omega(px+\xi_2^f z - t)\}\\ &\quad - P_2^{ds}(2\rho_2\beta_2^2)p(\alpha_2^s\xi_2^s)\exp\{i\omega(px+\xi_2^s z - t)\}\\ &\quad + S_2^d(\rho_2\beta_2)(1-2\beta_2^2 p^2)\exp\{i\omega(px+\eta_2 z - t)\}\end{aligned} \quad \text{.....(3.65)}$$

$$\begin{aligned}\tau_{zz}^2 &= H^*\frac{\partial u_z}{\partial z} + (\lambda^* + \alpha_k^{*2}M^*)\frac{\partial u_x}{\partial x} + \alpha_k^* M^*\left(\frac{\partial w_x}{\partial x}+\frac{\partial w_z}{\partial z}\right)\\ &= (i\omega)H^*[P_2^{df}(\alpha_2^f\xi_2^{f^2})\exp\{i\omega(px+\xi_2^f z - t)\} + P_2^{ds}(\alpha_2^s\xi_2^{s^2})\exp\{i\omega(px+\xi_2^s z - t)\}\\ &\quad - S_2^d(\beta_2 p\eta_2)\exp\{i\omega(px+\eta_2 z - t)\}] + (i\omega)(\lambda^* + \alpha_k^{*2}M^*)[P_2^{df}(\alpha_2^f p^2)\exp\{i\omega(px+\xi_2^f z - t)\}\\ &\quad + P_2^{ds}(\alpha_2^s p^2)\exp\{i\omega(px+\xi_2^s z - t)\} + S_2^d(\beta_2\eta_2 p)\exp\{i\omega(px+\eta_2 z - t)\}] + (i\omega)\alpha_k^* M^*\\ &\quad [\mu_1 P_2^{df}(\alpha_2^f p^2)\exp\{i\omega(px+\xi_2^f z - t)\} + \mu_2 P_2^{df}(\alpha_2^f p^2)\exp\{i\omega(px+\xi_2^f z - t)\}\\ &\quad \alpha_0 S_2^d(\beta_2 p\eta_2)\exp\{i\omega(px+\eta_2 z - t)\} + \mu_1 P_2^{df}(\alpha_2^f\xi_2^{f^2})\exp\{i\omega(px+\xi_2^f z - t)\}\\ &\quad + \mu_2 P_2^{df}(\alpha_2^f\xi_2^{s^2})\exp\{i\omega(px+\xi_2^f z - t)\} - \alpha_0 S_2^d(\beta_2 p\eta_2)\exp\{i\omega(px+\eta_2 z - t)\}]\end{aligned} \quad \text{.....(3.66)}$$

where

u^2_x, u^2_z: components of particle displacement vector in the second medium

w^2_x, w^2_z: components of fluid displacement vector in the second medium

τ^2_{zx}, τ^2_{zz} : stress components

α^f_2 : complex and frequency dependent wave velocity of fast P-wave,

α^s_2 : complex and frequency dependent wave velocity of slow P-wave

β_2 : complex and frequency dependent wave velocity of S-wave

ρ_2 : matrix density

ρ_f : fluid density

φ : porosity

ρ_2 : bulk density

P^{df}_2: displacement amplitude of down- going fast P-wave

P^{uf}_2: displacement amplitude of up -going fast P-wave

P^{ds}_2: displacement amplitude of down -going slow P-wave

P^{us}_2: displacement amplitude of up- going slow P-wave

S^d_2: displacement amplitude of down -going S-wave

S^u_2: displacement amplitude of up -going S-wave

i^f_2 : angle made by fast P-ray with normal

i^s_2 : angle made by slow P-ray with normal

j_2 : angle made by S-ray with normal

p : ray parameter $\left(= \frac{\sin i^f_2}{\alpha^f_2} = \frac{\sin i^s_2}{\alpha^s_2} = \frac{\sin j_2}{\beta_2} \right)$

$$\sin i^f_2 = \alpha^f_2 p$$

$$\cos i^f_2 = \sqrt{(1 - \alpha^{f^2}_2 p^2)}$$

$$\sin i^s_2 = \alpha^s_2 p$$

$$\cos i^s_2 = \sqrt{(1 - \alpha^{s^2}_2 p^2)}$$

$$\sin j_2 = \beta_2 p$$

$$\cos j_2 = \sqrt{(1-\beta_2^2 p^2)}$$

$$\xi_2^f = \frac{\cos i_2^f}{\alpha_2^f} = \sqrt{\frac{1}{\alpha_2^{f^2}} - p^2}$$

$$\xi_2^s = \frac{\cos i_2^s}{\alpha_2^s} = \sqrt{\frac{1}{\alpha_2^{s^2}} - p^2}$$

$$\eta_2 = \frac{\cos j_2}{\beta_2} = \sqrt{\frac{1}{\beta_2^2} - p^2}$$

The boundary conditions at the interface ($z = 0$) between the two half spaces are:

$$1)\ u_x^1 = u_x^2 \qquad \text{.....(3.67)}$$

$$2)\ u_z^1 = u_z^2 \qquad \text{.....(3.68)}$$

$$3)\ \tau_{zx}^1 = \tau_{zx}^2 \qquad \text{.....(3.69)}$$

$$4)\ \tau_{zz}^1 = \tau_{zz}^2 \qquad \text{.....(3.70)}$$

$$5)\ 0 = \frac{\partial}{\partial t}(u_z^2 - w_z) \qquad \text{.....(3.71)}$$

The last boundary condition arises due to vanishing of fluid pressure at the boundary and can be written as $-i\omega(u^2_z - w_z) = 0$ or $0 = u^2_z - w_z$

Application of boundary conditions leads to following equations:

$$P_1^d(\alpha_1 p) + P_1^u(\alpha_1 p) + S_1^u(\beta_1\eta_1) = P_2^{df}(\alpha_2^f p) + P_2^{ds}(\alpha_2^s p) + S_2^d(\beta_2\eta_2) \qquad \text{.....(3.72)}$$

$$P_1^d(\alpha_1\xi_1) - P_1^u(\alpha_1\xi_1) + S_1^u(\beta_1 p) = P_2^{df}(\alpha_2^f\xi_2^{f^2}) + P_2^{ds}(\alpha_2^s\xi_2^{s^2}) - S_2^d(\beta_2 p) \qquad \text{.....(3.73)}$$

$$P_1^d(2\rho_1\beta_1^2)p\alpha_1\xi_1 - P_1^u(2\rho_1\beta_1^2)p\alpha_1\xi_1 - (\rho_1\beta_1)(1-2\beta_1^2p^2)S_1^u$$
$$= P_2^{df}(2\rho_2\beta_2^2)p(\alpha_2^f\xi_2^{f^2}) - P_2^{ds}(2\rho_2\beta_2^2)p(\alpha_2^s\xi_2^{s^2}) + S_2^d(\rho_2\beta_2)(1-2\beta_2^2p^2)$$

.....(3.74)

$$P_1^d(\rho_1\alpha_1)(1-2\beta_1^2p^2)+P_1^u(\rho_1\alpha_1)(1-2\beta_1^2p^2)-(2\rho_1\beta_1^2)p\beta_1\eta_1S_1^u$$

$$=P_2^{df}\left\{H^*\alpha_2^f\xi_2^{f^2}+(\lambda^*+\alpha_k^{*2}M^*)(\alpha_2^fp^2)+\alpha_k^*M^*\mu_1\frac{1}{\alpha_2^f}\right\}$$

$$+P_2^{ds}\left\{H^*\alpha_2^s\xi_2^{s^2}+(\lambda^*+\alpha_k^{*2}M^*)(\alpha_2^sp^2)+\alpha_k^*M^*\mu_1\frac{1}{\alpha_2^s}\right\} \qquad \text{.....(3.75)}$$

$$+S_2^d\left\{-H^*p\beta_2\eta_2+(\lambda^*+\alpha_k^{*2}M^*)p\beta_2\eta_2\right\}$$

$$0=P_2^{df}(1-\mu_1)(\alpha_2^f\xi_2^{f^2})+P_2^{ds}(1-\mu_2)(\alpha_2^s\xi_2^{s^2})-S_2^d(\beta_2p)(1-\alpha_0) \qquad \text{.....(3.76)}$$

These equations can be put in the following form

$$M\begin{bmatrix}P_1^u\\S_1^u\\P_2^{df}\\P_2^{ds}\\S_2^d\end{bmatrix}=N\begin{bmatrix}P_1^d\\0\\0\\0\\0\end{bmatrix} \qquad \text{.....(3.77)}$$

M is a 5x5 matrix and is given on the next page

$$M=\begin{pmatrix}-\alpha_1p & -(1-\beta_1^2p^2)^{1/2} & \alpha_2^fp & \alpha_2^sp & (1-\beta_2^2p^2)^{1/2}\\ (1-\alpha_1^2p)^{1/2} & -\beta_1p & (1-\alpha_2^{f^2}p^2)^{1/2} & (1-\alpha_2^{s^2}p^2)^{1/2} & -\beta_2p\\ 2\rho_1\beta_1^2p(1-\alpha_1^2p)^{1/2} & \rho_1\beta_1(1-2\beta_1^2p^2) & 2(\rho_2\beta_2^2)p(1-\alpha_2^{f^2}p^2)^{1/2} & 2(\rho_2\beta_2^2)p(1-\alpha_2^{f^2}p^2)^{1/2} & (\rho_2\beta_2)(1-2\beta_2^2p^2)\\ -(\rho_1\alpha_1)(1-2\beta_1^2p^2) & 2\rho_1\beta_1^2p(1-\beta_1^2p^2)^{1/2} & D1 & D2 & -D3\\ 0 & 0 & (1-\mu_1)(1-\alpha_2^{f^2}p^2)^{1/2} & (1-\mu_2)(1-\alpha_2^{s^2}p^2)^{1/2} & -(1-\alpha_0)\beta_2p\end{pmatrix}$$

.....(3.78)

The elements of the column vector N are

$$N=\begin{pmatrix}\alpha_1p & (1-\beta_1^2p^2)^{1/2} & -\alpha_2^fp & -\alpha_2^sp & -(1-\beta_2^2p^2)^{1/2}\\ (1-\alpha_1^2p)^{1/2} & -\beta_1p & (1-\alpha_2^{f^2}p^2)^{1/2} & (1-\alpha_2^{s^2}p^2)^{1/2} & -\beta_2p\\ 2\rho_1\beta_1^2p(1-\alpha_1^2p)^{1/2} & \rho_1\beta_1(1-2\beta_1^2p^2) & 2(\rho_2\beta_2^2)p(1-\alpha_2^{f^2}p^2)^{1/2} & 2(\rho_2\beta_2^2)p(1-\alpha_2^{f^2}p^2)^{1/2} & (\rho_2\beta_2)(1-2\beta_2^2p^2)\\ (\rho_1\alpha_1)(1-2\beta_1^2p^2) & -2\rho_1\beta_1^2p(1-\beta_1^2p^2)^{1/2} & -D1 & -D2 & D3\\ 0 & 0 & (1-\mu_1)(1-\alpha_2^{f^2}p^2)^{1/2} & (1-\mu_2)(1-\alpha_2^{s^2}p^2)^{1/2} & -(1-\alpha_0)\beta_2p\end{pmatrix}$$

.....(3.79)

In case of P-wave incident from above (Figure 3.4(a)) the first column of N will be operative. The above form of N takes into the account the fact that waves may be incident

at the boundary from above as well as from below as shown in Figure 3.4. The matrix equation 3.77 in the expanded form now reads as follows:

$$\mathbf{M}\begin{bmatrix} \backslash P/P & \backslash S/P & P_f/\!/P & P_s/P & S/\!/P \\ \backslash P/S & \backslash S/S & P_f/S & P_s/S & S/S \\ \backslash P P_f & \backslash S P_f & P_f P_f & P_s P_f & S P_f \\ \backslash P P_s & \backslash S P_s & P_f P_s & P_s P_s & S P_s \\ \backslash P S & \backslash S S & P_f S & P_s S & S S \end{bmatrix} = \mathbf{N}$$

.....(3.80)

The symbol '\' denotes an downgoing wave, and '/' denotes an upgoing wave. The reflection and transmission coefficients are obtained through the following relation

$$\begin{bmatrix} \backslash P/P & \backslash S/P & P_f/\!/P & P_s/P & S/\!/P \\ \backslash P/S & \backslash S/S & P_f/S & P_s/S & S/S \\ \backslash P P_f & \backslash S P_f & P_f P_f & P_s P_f & S P_f \\ \backslash P P_s & \backslash S P_s & P_f P_s & P_s P_s & S P_s \\ \backslash P S & \backslash S S & P_f S & P_s S & S S \end{bmatrix} = \mathbf{M^{-1}N}$$

.....(3.81)

The case of a fast P-wave traveling through a viscoelastic upper half space, characterized by velocities α_2^f , α_2^s and β_2 and incident at the interface separating it from the elastic half space, characterized by velocities α_3 and β_3, below can be treated similarly. The 5x5 matrix M in this case is given on the next page

$$M = \begin{pmatrix} -\alpha_2^f p & -\alpha_2^s p & -(1-\beta_2^2 p^2)^{1/2} & \alpha_3 p & (1-\beta_3^2 p^2)^{1/2} \\ (1-\alpha_2^{f'} p^2)^{1/2} & (1-\alpha_2^{s'} p^2)^{1/2} & -\beta_2 p & (1-\alpha_3^2 p)^{1/2} & -\beta_3 p \\ 2(\rho_2\beta_2^2)p(1-\alpha_2^{f'} p^2)^{1/2} & 2(\rho_2\beta_2^2)p(1-\alpha_2^{f'} p^2)^{1/2} & (\rho_2\beta_2)(1-2\beta_2^2 p^2) & 2\rho_3\beta_3^2 p(1-\alpha_3^2 p)^{1/2} & \rho_3\beta_3(1-2\beta_3^2 p^2) \\ -D1 & -D2 & D3 & (\alpha_3\rho_3)(1-2\beta_3^2 p^2) & -(2\beta_3^2\rho_3)p(1-\beta_3^2 p^2)^{1/2} \\ (1-\mu_1)(1-\alpha_2^{f'} p^2)^{1/2} & (1-\mu_2)(1-\alpha_2^{s'} p^2)^{1/2} & -(1-\alpha_0)\beta_2 p & 0 & 0 \end{pmatrix}$$

.....(3.82)

The elements of the column vector N are

$$N = \begin{pmatrix} \alpha_2^f p & \alpha_2^s p & (1-\beta_2^2 p^2)^{1/2} & -\alpha_3 p & -(1-\beta_3^2 p^2)^{1/2} \\ (1-\alpha_2^{f'} p^2)^{1/2} & (1-\alpha_2^{s'} p^2)^{1/2} & -\beta_2 p & (1-\alpha_3^2 p)^{1/2} & -\beta_3 p \\ 2(\rho_2 c_s^2)p(1-\alpha_2^{f'} p^2)^{1/2} & 2(\rho_2 c_s^2)p(1-\alpha_2^{f'} p^2)^{1/2} & (\rho_2\beta_2)(1-2\beta_2^2 p^2) & 2\rho_3\beta_3^2 p(1-\alpha_3^2 p)^{1/2} & \rho_3\beta_3(1-2\beta_3^2 p^2) \\ D1 & D2 & -D3 & -(\alpha_3\rho_3)(1-2\beta_3^2 p^2) & (2\beta_3^2\rho_3)p(1-\beta_3^2 p^2)^{1/2} \\ (1-\mu_1)(1-\alpha_2^{f'} p^2)^{1/2} & (1-\mu_2)(1-\alpha_2^{s'} p^2)^{1/2} & -(1-\alpha_0)\beta_2 p & 0 & 0 \end{pmatrix}$$

.....(3.83)

In equations 3.78, 3.79, 3.82 and 3.83

$$D1 = H^* \frac{(1-\alpha_2^{f'} p^2)}{\alpha_2^f} + (\lambda^* + \alpha^{*2} M^*)\alpha_2^f p^2 + \alpha^* M^* \mu_1 \frac{1}{\alpha_2^f}$$

$$D2 = H^* \frac{(1-\alpha_2^{s'} p^2)}{\alpha_2^s} + (\lambda^* + \alpha^{*2} M^*)\alpha_2^s p^2 + \alpha^* M^* \mu_2 \frac{1}{\alpha_2^s}$$

$$D3 = H^*(1-\beta_2^2 p^2)^{1/2} p - (\lambda^* + \alpha^* M^*)(1-\beta_2^2 p^2)^{1/2} p$$

and the relation for getting reflection-transmission coefficients is

$$\begin{bmatrix} P_f P_f & P_s P_f & SP_f & PP_f & SP_f \\ P_f P_s & P_s P_s & SP_s & PP_s & SP_s \\ P_f S & P_s S & SS & PS & S\,S \\ P_f P & P_s P & SP & P\;P & S\,P \\ P_f S & P_s S & SS & P\;S & S\,S \end{bmatrix} = \mathbf{M^{-1}N}$$

.....(3.84)

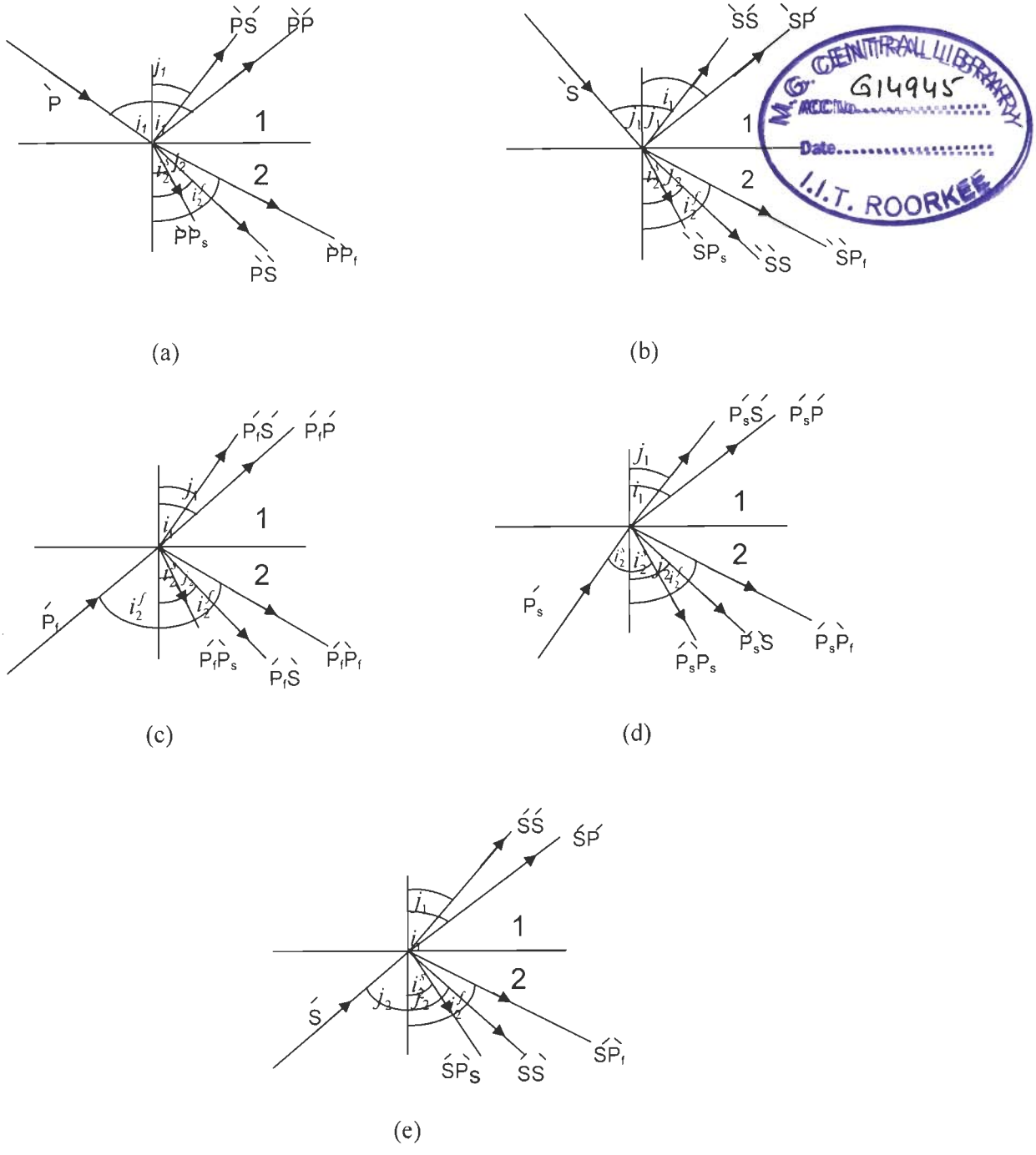

Figure 3.4: ***Notation for 25 possible reflection and transmission coefficients arriving from waves at the welded interface between an elastic (medium 1) and porous viscoelastic medium (medium 2).***

3.5 SYNTHETIC SEISMOGRAMS

Consider a stack of n elastic, homogeneous and isotropic layers overlying a half space with prescribed values of density (ρ) and P- and S-wave velocities (α and β), as shown in Figure 3.5. Plane P- waves propagate through the stack of layers. The reflected P-wave paths from the (n-1) th and nth interfaces are shown in Figure 3.6. The z-component of reflected P-wave displacement at the surface of the layered half space can be written as follows:

$$u_z(x,0,\omega) = -2\alpha_1\zeta_1(1-2\beta_1^2 p^2)\times\frac{PRODUCT\times \overset{\backslash}{P}\overset{/}{P}}{(1-2\beta_1^2 p^2)^2+4\beta_1^4 p^2\zeta_1\eta_1} \qquad \text{.....(3.85)}$$

where

PRODUCT = *Product of downgoing and upgoing transmission coefficients of P-waves at n-1 interfaces*

The above expression is a slightly modified version of the relation given by Aki and Richards (2002). The effect of the free surface has been included in the above expression and has the following form: $-2\alpha_1\zeta_1(1-2\beta_1^2 p^2)/((1-2\beta_1^2 p^2)^2+4\beta_1^4 p^2\zeta_1\eta_1)$. The effect of the free surface represents the modification of amplitude of upcoming P-waves by the downgoing reflected P-wave and S-waves at z = 0. In the present case n=1 for the first interface and n=2 for the second interface.

The expression 3.85 yields the spectrum of vertical component of reflected P-wave spikes that includes the effect of viscoelasticity and solid-fluid interaction of second layer of the model assumed in the present study. The reflected P-waves come from top and bottom surfaces of the viscoelastic layer. This attenuated spectrum is multiplied with the spectrum of the source wavelet and Fourier inverted to yield the reflected wavelet at a given offset. The synthetic seismograms are obtained by plotting the wavelets at the appropriate travel times.

In order to use the expressions of reflection and transmission coefficients derived on the basis of theory of propagation of plane waves, it is assumed that the region occupying the region $z<0$ is occupied by air to enable P-waves to propagate. The plane waves are generated by a remote source incident on at $z=0$ at such an angle so that these emerge into the region $z>0$ making an angle i_o with the normal appropriate for the reflected ray to emerge at a prescribed offset at the surface z = 0 (Figure 3.7). The point at which the waves enter the layered half space at $z = 0$ is taken as the source point and the distance at which reflected wave emerges at $z = 0$ is measured from this source point and called offset.

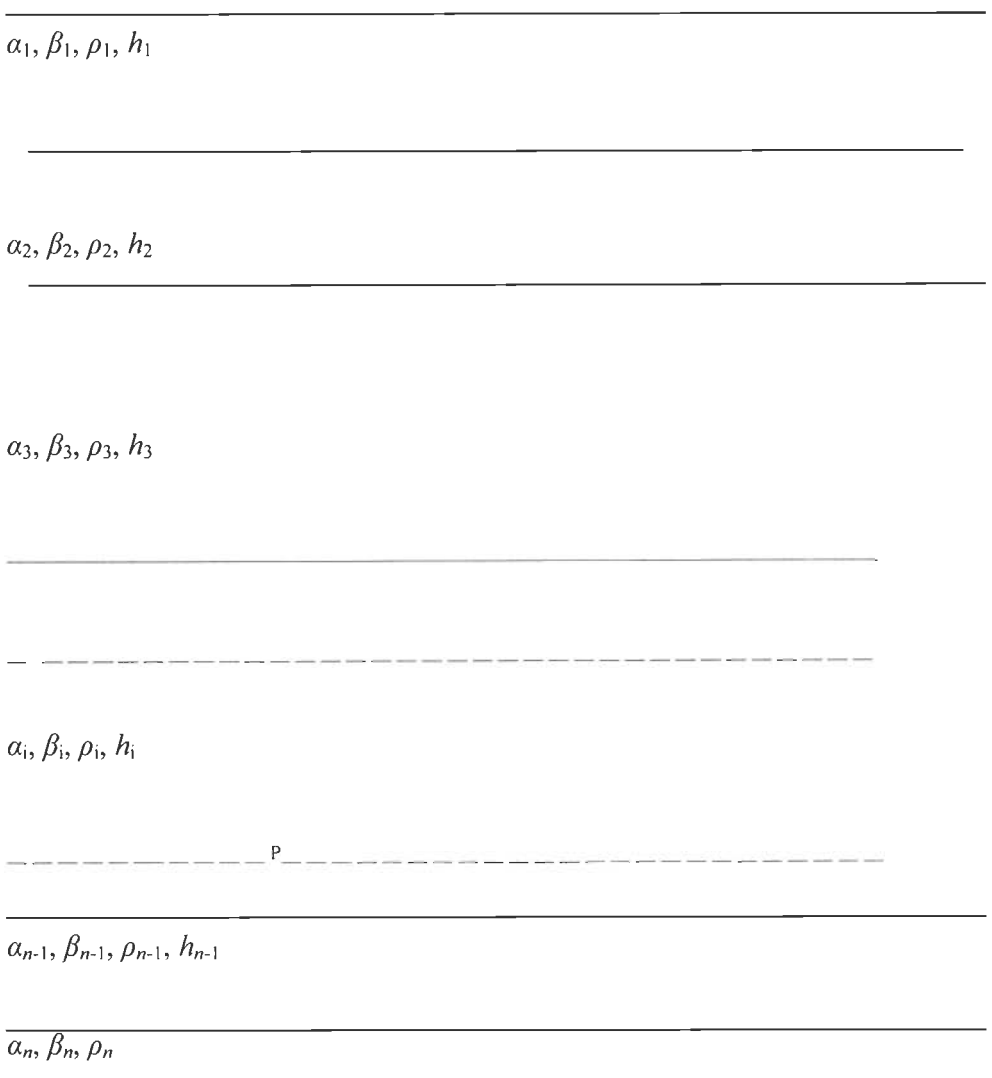

Figure 3.5: ***Layered half space with densities (ρ_i i =1,2,…,n), velocities (α_i, β_i, i =1,2,..,n) and thicknesses (h_i , I = 1, 2, n-1).***

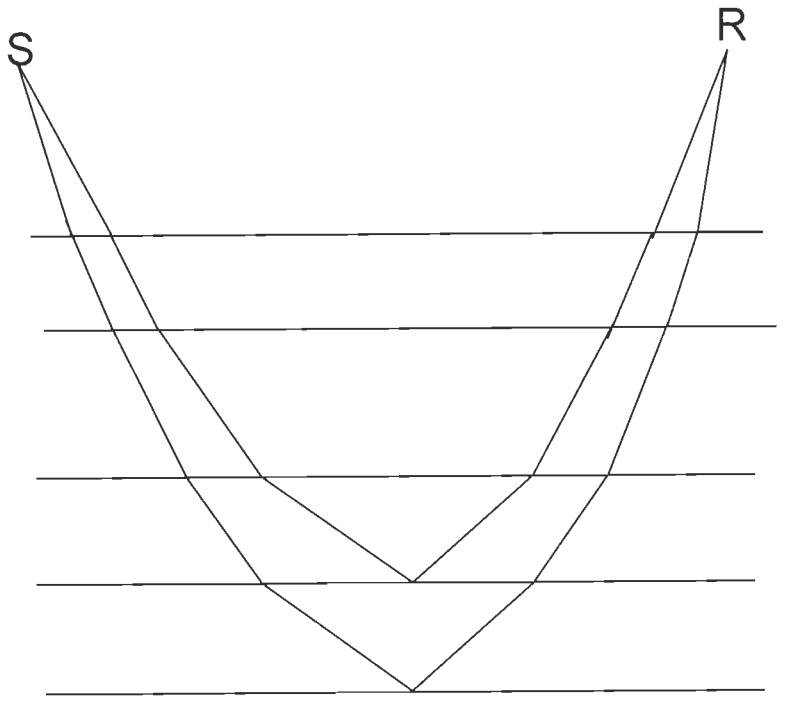

Figure 3.6: ***The reflected P-wave paths from the (n-1) th and nth interfaces.***

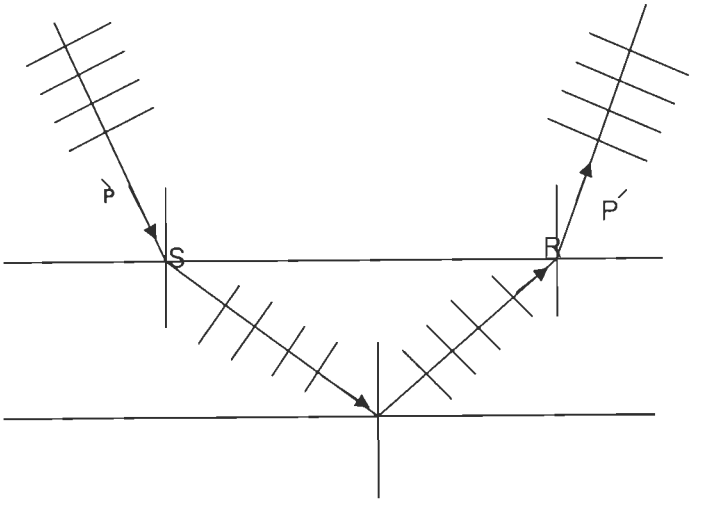

Figure 3.7: ***Plane waves from the remote source are incident at S, the source point. The wave propagating in the earth model are plane waves.***

3.6 AVO INVERSION

Amplitude – versus - offset (AVO) inversion has been applied to detect gas sands and to determine physical parameters of the media across the reflecting boundary. For this purpose, linearized versions of Zoepprtiz equations are used. The data to which such

inversion is applied is recorded in seismic data acquisition where seismic waves propagate in a real earth. In the present work, the propagation of waves in a porous viscoelastic medium has been considered. The synthetic seismograms have been generated at the surface of a three layered earth model of which the second layer is porous and viscoelastic. The AVO inversion of the synthetic seismic data will reveal the effect that porosity, fluid content and viscoelasticity have on the AVO attributes.

The Aki – Richards approximation of the Zoeppritz equations for P to P reflection coefficient, R_{pp}, is given below (Aki and Richards, 2002):

$$R_{pp} = \frac{1}{2}(1-4\beta^2 p^2)\frac{\Delta\rho}{\rho} + \frac{1}{2\cos^2 i}\frac{\Delta\alpha}{\alpha} - 4\beta^2 p^2 \frac{\Delta\beta}{\beta} \qquad \text{.....(3.86)}$$

where α, β and ρ are the mean P-wave velocity, mean S-wave velocity and mean density on two sides of the reflector and $\Delta\alpha$ $(=\alpha_2-\alpha_1)$, $\Delta\beta$ $(=\beta_2-\beta_1)$ and $\Delta\rho$ $(=\rho_2-\rho_1)$ are the respective contrasts. The above equation holds when the ratios $\Delta\alpha/\alpha$, $\Delta\beta/\beta$ and $\Delta\rho/\rho$ are much less than unity.

For the purposes of inversion, α can be estimated using $T^2 - X^2$ method of velocity estimation. The S-wave velocity is obtained by multiplying α with 0.6. The estimate of ρ is obtained by using Gardner's relation:

$$\rho = 0.31(\alpha^{0.25}) \qquad \text{.....(3.87)}$$

The reflection coefficients, R_{pp}, are obtained from the amplitudes of seismic reflections. The offsets are converted into angle of incidence, i. The equation 3.86 is now inverted to get the values of ratios $\Delta\alpha/\alpha$, $\Delta\beta/\beta$ and $\Delta\rho/\rho$. The AVO attributes, A and B, are now obtained from the following relations:

$$A = \frac{1}{2}\left(\frac{\Delta\alpha}{\alpha} + \frac{\Delta\rho}{\rho}\right) \qquad \text{.....(3.88)}$$

$$B = \frac{1}{2}\frac{\Delta\alpha}{\alpha} - 2\left(\frac{\beta}{\alpha}\right)^2\left(\frac{\Delta\rho}{\rho} + 2\frac{\Delta\beta}{\beta}\right) \qquad \text{.....(3.89)}$$

CHAPTER – 4

COMPUTATIONAL PROCEDURE

4.1 INTRODUCTION

In this chapter the methodology of computation of synthetic seismograms at the surface of a three layered earth model have been presented. At first, the selection of the model parameters has been dealt with and is followed by essential aspects of computational methodology.

4.2 MODEL

In this study, the model of earth consists of two layers overlying a half space. In the following, the half space has been termed the third layer. The materials comprising the layers are assumed to be homogeneous and isotropic. The first and the third layer are assumed to be elastic. The second layer has been assumed to be viscoelastic and porous and saturated with more than one viscous fluid, i.e., gas and water or oil and water or only water.

Plane P-waves, generated by a remote source, pass into the earth model at a point designated as source point. For this purpose, the space above the model, occupying the region $z<0$, is assumed to be filled with air so that P-waves can propagate through it. The source wavelet is assumed to be a Ricker wavelet of 50 Hz. frequency. Synthetic seismograms have been generated at 20 offsets simulating an AVO situation. For porous second layer the above exercise is repeated for different values of porosities and water saturations. The ray path in the above model has been shown in Figure 4.1.

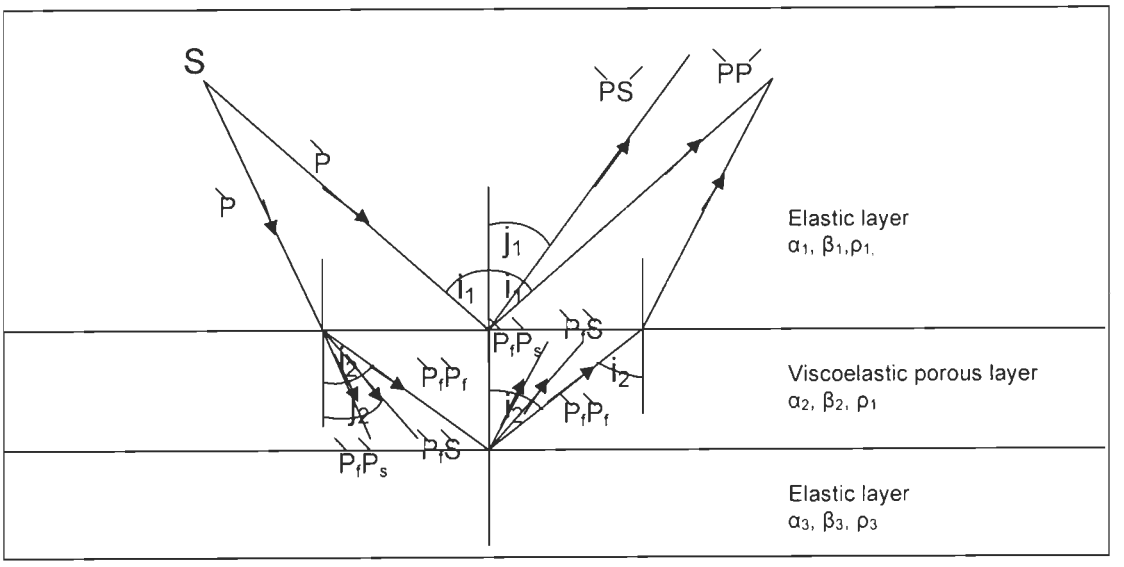

Figure 4.1: ***Raypaths in the three layered earth model considered for the present computation.***

The viscous fluids which are considered as the pore fluid in this study are oil, gas and water. The hydrocarbon, oil or gas, fills part of the pore space along with water. Following cases have been considered:

(a) Oil with 25%, 50 % and 75 % water saturation and 20% porosity.

(b) Gas with 25%, 50 % and 75 % water saturation and 20% porosity.

(c) 100% water saturation and 20% porosity.

(d) Oil with 50 % water saturation and 10%, 20% and 30% porosity.

(e) Gas with 50 % water saturation and 10%, 20% and 30% porosity .

4.3 CHOICE OF MODEL PARAMETERS

The physical properties of the three layers in the model have been selected so as to resemble a sandstone reservoir enclosed by impervious strata above and below.

It has been assumed that the sandstone reservoir lies at a depth of 2500 m from the surface and its thickness is 100 m. The density and seismic wave velocities for the upper

and lower layers are taken corresponding to the rock types usually present above and below the reservoir.

For the second layer that is taken to represent the reservoir, the appropriate parameters have been taken from the table of values given in Gregory, (1977) Table (4.5). This table contains data for P-wave velocity, S-wave velocity, depth of the reservoir, porosity of the rock and the type of the fluid present in a sandstone reservoir. This data pertains to the Gulf coast region.

The value for seismic wave velocities given in this table incorporates the effect of porosity of the reservoir rock. Consequently, this velocity is lower than velocity in the mineral particles constituting the solid framework, also called matrix velocity. The same is true in case of density of the rock. To estimate the matrix velocity and matrix density from the available data, following procedure has been adopted: The sandstone layer at a depth of 2500 m is selected and the P and S wave velocities, density and porosity are picked up from the table. It has been assumed that the velocity and density values pertain to the reservoir having 100% water saturation. The water filling the pores has been assumed to be brine having a salt content of 20% NaCl. Its density, ρ_w, is obtained from McQuillin et al. (1986).

From the S-wave velocity of the saturated rock, μ_{sat} i.e. the shear modulus of the saturated rock, can be estimated by the following way

$$\mu_{sat} = \rho_b * \beta_{sat}^2 \qquad \text{.....(4.1)}$$

and

$$\mu_{dry} = \mu_{sat} \qquad \text{.....(4.2)}$$

where μ_{dry} is shear modulus of dry rock, β_{sat} is the S-wave velocity of saturated rock, ρ_b is the bulk density of the rock. From μ_{dry}, the shear modulus of the solid matrix (μ_m) can be calculated by (Nolen-Hoeksema, 2000)

$$\mu_m = \frac{\mu_{dry}}{\left(1 - \frac{\varphi}{\varphi_c}\right)} \qquad \text{.....(4.3)}$$

where φ is the porosity of the rock and φ_c is the critical porosity (taken as 40% in this study) of the rock.

The density of the solid rock (ρ_s) has been calculated by

$$\rho_s = \frac{\rho_b - \varphi\rho_f}{1 - \varphi} \qquad \text{.....(4.4)}$$

where ρ_f is the density of the fluid. S-wave velocity of the matrix is obtained from

$$\beta_{solid} = \sqrt{\frac{\mu_m}{\rho_s}} \qquad \text{.....(4.5)}$$

where β_{solid} is the S-wave velocity of the solid rock. P-wave velocity for the solid rock has been estimated by

$$\frac{\beta}{\alpha} \cong 0.6 \qquad \text{.....(4.6)}$$

where α is the P-wave velocity and β is the S-wave velocity.

4.4 PHYSICAL PROPERTIES OF PORE FLUIDS

The physical properties i.e. density, the seismic wave velocities and viscosity of the pore fluids (oil, gas and water) are also important parameters in seismic wave propagation in porous media.

4.4.1 *Density of Pore Fluids*

The density of gas depends on its composition. The composition of gas present in the pores has been obtained from Sheriff (2002) and given in Table 4.1. Density values have been obtained from Levorsen (1967). The density of the gas comes out to be 0.983 kg/m^3.

Table 4.1: ***Volume Fractions and Densities of Constituents of Natural Gas***

Constituent gas	Methane	Ethane	Propane	Isobutane	Butane	Pentane
Fraction by volume	0.80	0.07	0.06	0.015	0.025	0.03
Density (kg/m^3)	0.715	1.339	1.963	2.588	2.588	3.213

The water present in the reservoir rocks being highly saline, its density has been obtained from Mcquillin et al. (1986) for a salinity of 20% NaCl. It is given in Table 4.2.

Oils of different API gravity values have been considered (10^0 to 60^0). The density and viscosity is different for different API gravity values. Density of oil for particular API oil can be calculated from

$$API = \frac{141.5}{\rho_f} - 131.5 \qquad \text{.....(4.7)}$$

and is given in Table 4.3. Here ρ_f is the density of oil.

4.4.2 *Viscosity of Pore Fluids*

Viscosity of fluid varies with temperature. To get the appropriate value of viscosity at the depth of the reservoir (2500 m) the temperature gradient of the Gulf Coast region, as shown in Figure 4.2 has been considered. From Figure 4.2 temperature has been found to be about 220^0 F at the depth of 2500 m.

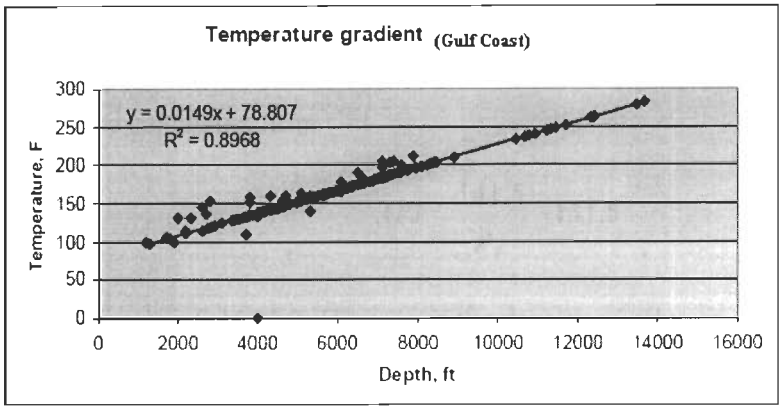

Figure 4.2: ***The temperature gradient of Gulf coast region. (Source: Internet, PPT presentation by Holtz, M.H., NúñezLópez, V., Breton, K.L.).***

The value of viscosity of gas, oil and water at 220^0 F have been obtained from Stine (2004) and are given in Table 4.2 and Table 4.3.

4.4.3 *P-wave Velocity in Pore Fluids*

Velocity of P-waves in gas is taken from Sheriff (2002) and is given in Table 4.2. The bulk modulii, K, of oil and brine are obtained from Mcquillin et al. (1986) and velocity, V, calculated using the following relation:

$$V = \sqrt{\frac{K}{\rho_f}} \qquad \text{.....(4.8)}$$

where ρ_f is the density of the fluid. The velocity in oil for different densities have been obtained and an average has been used in computations.

Table 4.2: ***Properties of Brine and Gas***

Fluid	Density (kg/m^3)	P-wave velocity (m/sec)	Viscosity (at 220^0F) (Poise)
Gas	0.983	440	0.000095
Brine	1140	1613	0.003

Table 4.3: ***Properties of Oil***

API Gravity	10	20	30	40	50	60
Density ($kg/m^{3)}$	1000	933	904	876	849	825
Viscosity (at 220°F, in Poise)	2.0	0.08	0.03	0.01	0.009	0.007
P-wave velocity	1394 m/s					

4.4.4 *Relaxation Times*

The viscoelastic behavior of the solid constituents of the second layer has been modeled as a Standard Linear Solid with a single relaxation mechanism. To compute frequency dependent values of wave velocities and quality factors (Q_p and Q_s), a knowledge of

relaxation times τ_σ and τ_ε is required. These have been obtained from Carcione (1988) and given in Table 4.4.

Table 4.4: ***Relaxation Times of Seismic Waves***

	Relaxation Times	
	(P-wave)	(S-wave)
τ_σ	0.0311465	0.0304655
τ_ε	0.0325305	0.0332577

The physical properties of solid constituents of the three layers and those of pore fluids in the second layer, as described above, are assumed to represents the closest real value that may be encountered in a real earth. The model parameters for solid constituent of the three layers are given Table 4.5, which have been used in the present study.

Table 4.5: ***Model Parameters for Solid Constituents***

Layer No:	P-wave velocity (m/sec)	S-wave velocity (m/sec)	Density (kg/m^3)	Thickness (m)
1.	2957	1258	2236	2500
2.	5411*	3246*	2593*	100
3.	3048	1297	2340	-

* Matrix velocity and density

Matrix velocity and density in the second layer have been computed from real data using assuming a porosity of 20%.

4.4.5 *Permeability*

The permeability of the second layer is needed for use in relation (Eq. 3.45 and 3.46). It is taken as equal to average value of a sandstone and is 10^{-12} m^2.

4.5 SOURCE WAVELET

The source wavelet used in this present study is a Ricker wavelet of 50 Hz frequency. It has been computed from the following relation given by the Sheriff (2002):

$$f(t) = (1 - 2\pi^2 f_M{}^2 t^2) e^{-\pi^2 f_M{}^2 t^2} \qquad \text{.....(4.9)}$$

where f_M is the frequency of the source wavelet. This is shown in Figure 4.3 along with its spectrum. The source wavelet has been sampled at 0.001 s and its duration is 0.2 s. For computing its Fourier transform, its duration has been increased through zero-padding. The total duration of the expanded source wavelet is 8.192 s, giving a frequency interval of nearly 0.122 Hz. This has been done to obtain a smooth spectrum. The Nyquist frequency of the sampled source wavelet is 500 Hz. The spectrum of the source wavelet has negligible amplitude beyond 150 Hz.

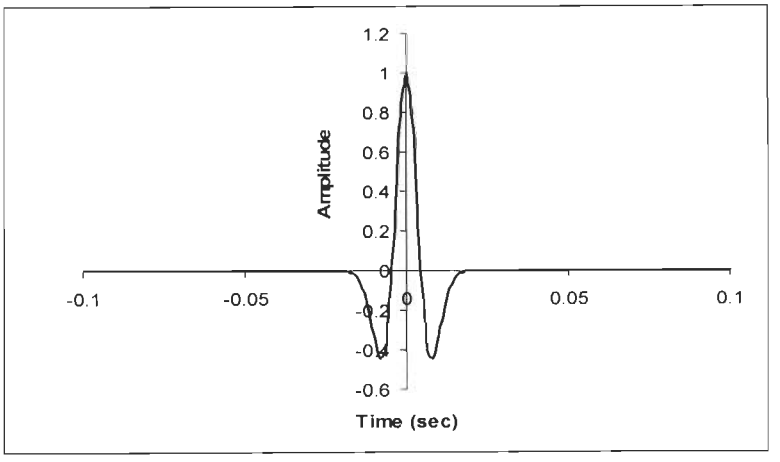

(a)

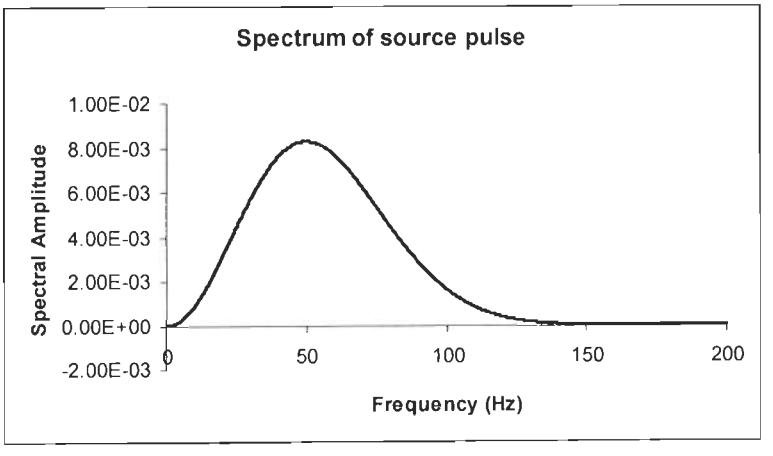

(b)

Figure 4.3: ***(a) Source wavelet used for the present computation; (b) Spectrum of the source wavelet.***

4.6 SYNTHETIC SEISMOGRAMS GENERATION

Synthetic seismograms have been generated using relation (Eq. 3.85), at 20 offsets with 100m being the offset interval. This has been carried out in following steps.

(a) First, the angle at which the P-waves start from the source point (the take-off angle) is computed for a given offset, using ray tracing. The velocities of these waves are complex and frequency dependent and are computed using relations (Eq. 3.12). When the P-wave velocity in the second layer is complex and frequency dependent, the real value of the velocity at 50 Hz has been used so that all the angles that the seismic rays make with the normal to the interface are real. For the two interfaces, two take-off angles are thus computed for all the 20 offsets.

(b) The two-way travel times for reflections from each interface are computed for all the 20 offsets. As before, the real value of the velocity at 50 Hz has been used for the second layer when the P-wave velocity in the second layer is complex and frequency dependent. This ensures that the angles that the seismic rays make with the normal are real.

(c) The effect that the presence of free surface has on the amplitudes of seismic reflections has also been computed.

(d) The velocities in the porous medium are computed using relations (Eq. 3.49 and 3.50). Since the pores are filled with one or two viscous fluids, two types of P-waves exist: fast and slow along with an S-wave. All the velocities are complex and frequency dependent. Consequently, the reflection and transmission coefficients are also complex. These are evaluated using relations (Eq. 3.81 and 3.84). First, the frequency dependent values of the amplitude of reflected spike from each interface is computed and multiplied with the Fourier spectrum of the source wavelet. The frequency dependent velocities, reflection and transmission coefficients and amplitudes of seismic reflection spikes are computed for all the frequencies that are present in the spectrum of source wavelet. The resulting spectrum of the reflected seismic wavelet is inverse Fourier transformed to get the wavelet in the

time domain. These wavelets are plotted at the correct two way geometrical travel time to give the synthetic seismogram.

Since the velocities in the second layer are complex and frequency dependent, ray parameter, p, is also complex and frequency dependent. For every frequency, a separate angle of refraction has been computed in this layer. Thus, there will be 4096 ray paths for waves traveling in this layer, as shown schematically in Figure 4.5. For every ray path the distance traveled in this layer and the resulting attenuation of the wave has been computed. For each ray, the reflection coefficients at the two interfaces have also been separately computed. This has been repeated for all the 20 offsets.

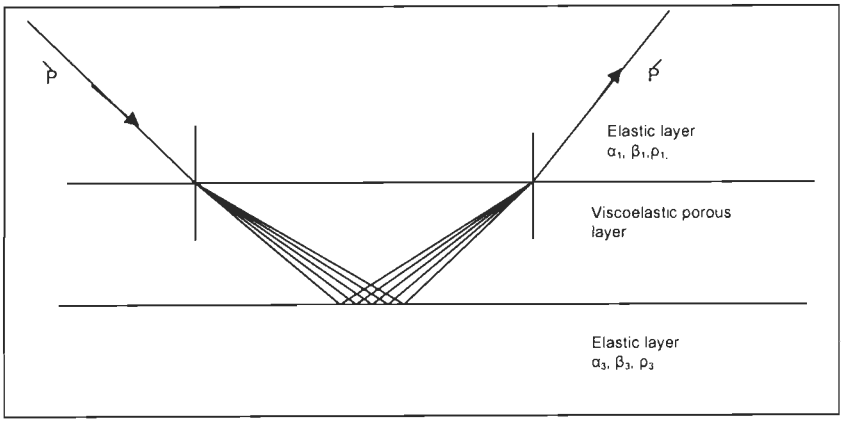

Figure 4.4: Ray paths in the viscoelastic second layer.

4.7 FLOW CHART OF COMPUTATIONAL PROCESS

A flow chart showing the sequence of steps in numerical computation has been given below:

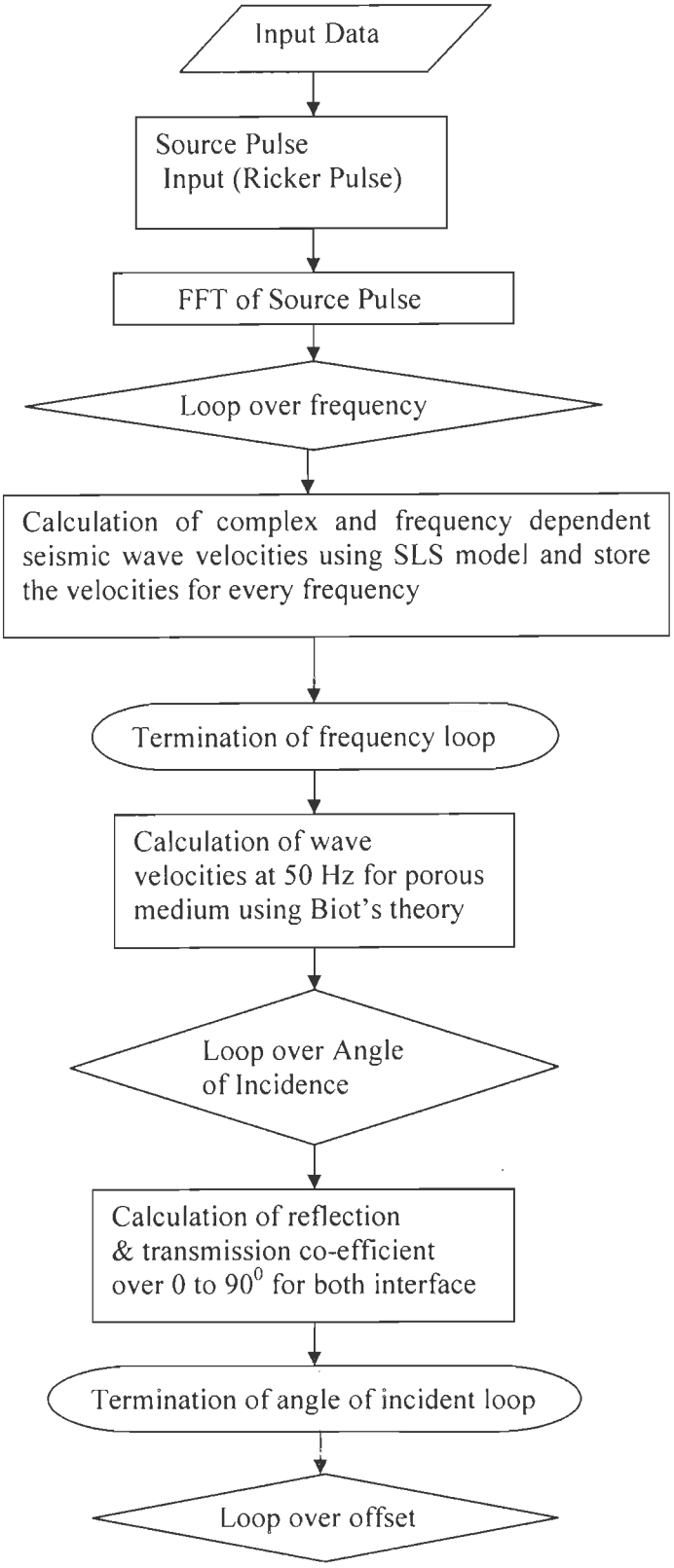

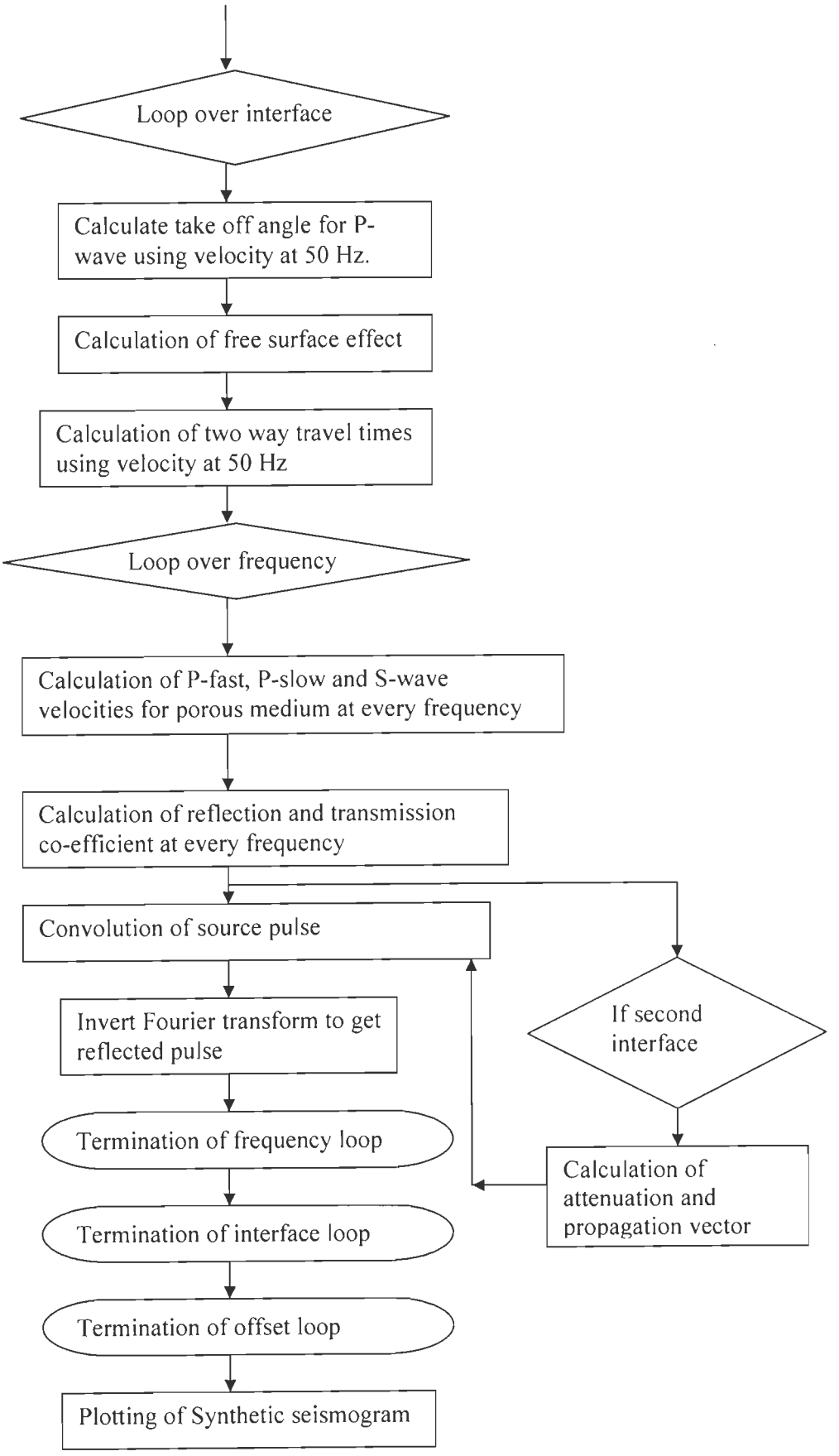
Loop over interface
Calculate take off angle for P-wave using velocity at 50 Hz.
Calculation of free surface effect
Calculation of two way travel times using velocity at 50 Hz
Loop over frequency
Calculation of P-fast, P-slow and S-wave velocities for porous medium at every frequency
Calculation of reflection and transmission co-efficient at every frequency
Convolution of source pulse
Invert Fourier transform to get reflected pulse
Termination of frequency loop
Termination of interface loop
Termination of offset loop
Plotting of Synthetic seismogram
If second interface
Calculation of attenuation and propagation vector

CHAPTER – 5

RESULTS AND DISCUSSIONS

5.1 INTRODUCTION

The main objective of the present work is to investigate the effect that viscoelasticity and solid - fluids interaction have on the shape of the reflected seismic wavelets. For this purpose, firstly, synthetic seismograms have been generated at 20 offsets varying from 100 to 2000 m, on the surface of a three-layered earth model. The first and third layers of the model are assumed to be elastic and the second layer is porous and viscoelastic. For purposes of comparison, computations have also been carried out when the second layer is elastic and non-porous, viscoelastic and non-porous and elastic and porous wherein P-wave velocity has been estimated using time average relationship. These seismograms simulate a CMP gather prior to AVO analysis. The source wavelet is assumed to be a Ricker wavelet having a frequency of 50 Hz. Secondly, normally incident synthetic seismograms have been generated when the second layer has thicknesses of 100 m. Finally, normally incident synthetic seismograms have been generated for a wedge shaped second layer.

Following notations have been used for identifying the different curves in figures:

(a) "EL" when the second layer is elastic and non-porous;

(b) "VNP" when the second layer is viscoelastic and non-porous;

(c) "TAR" when the second layer is elastic and porous and the seismic wave velocities in the porous medium have been estimated using Time Average Relationship, e.g., Willies equation (Willie, 1956) , and

(d) "VP" when the second layer is viscoelastic and porous and the seismic wave velocities in the porous medium have been estimated using Biot's theory.

The presentation and interpretation of results has been arranged in four parts. In Part I, the second layer is viscoelastic but non-porous. In Part II, the second layer is

viscoelastic and porous. In Part III, a comparative study has been made of the results obtained in the present study with those obtained when the velocity in the second layer are estimated using time average relationship. In Part IV, quantification of the results has been presented.

5.2 PART I: SECOND LAYER IS VISCOELASTIC AND NON-POROUS

With the objective of quantifying the effect of viscoelasticity alone on the shape of the reflected wavelets, the second layer is assumed to be viscoelastic and non-porous. In this case, the seismic waves will be attenuated while propagating through the viscoelastic layer. The Standard Linear Solid model has been adopted to represent the linear viscoelastic behavior of the second layer, leading to the complex and frequency dependent nature of elastic moduli (Eq. 3.9) and hence of seismic wave velocities. The shape of the computed seismic wavelets have been compared to that obtained when the second layer is elastic.

5.2.1 Wave Velocities

As mentioned above, the seismic wave velocities are complex and frequency dependent when the solid matrix is viscoelastic. Figure 5.1(a) and (b) depict the frequency dependence of P and S wave velocities respectively, in a viscoelastic layer. Both the curves show similar trend. The maximum changes in the velocities take place between 1 to 50 Hz and the velocities attain their maximum values near 100 Hz. The total variation is 2.19% for P-waves and 4.47% for S-waves. It is a characteristic of the SLS model that at high frequencies the velocities approach the values for elastic solids asymptotically.

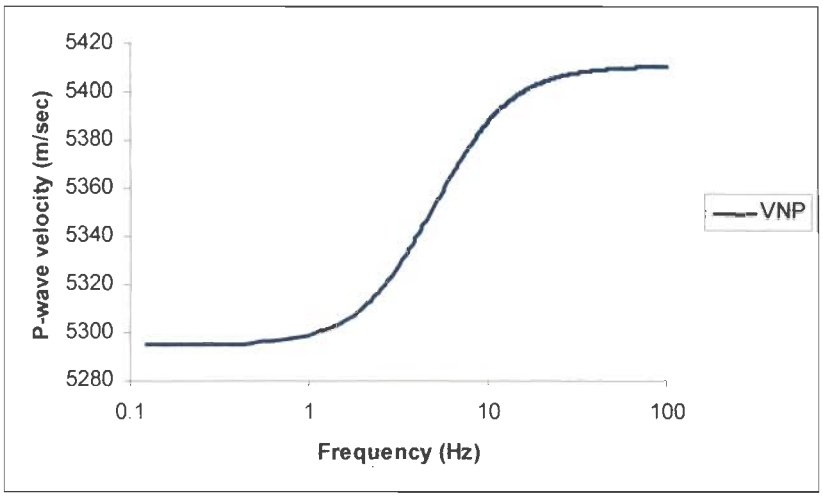

(a)

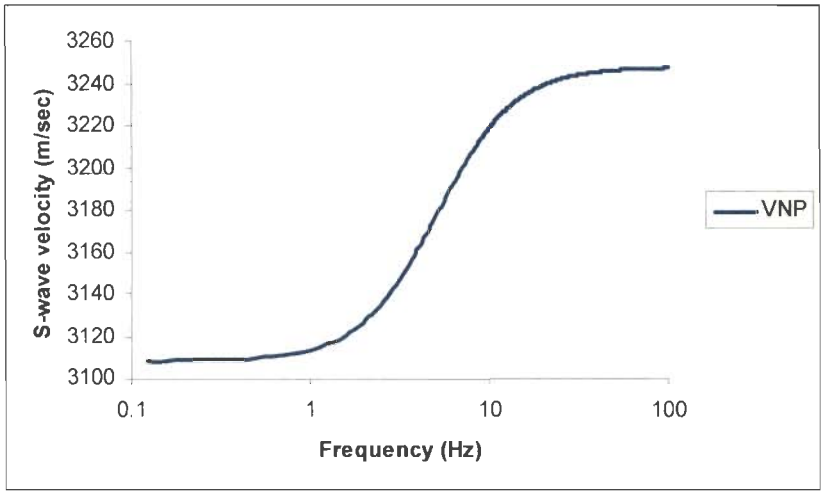

(b)

Figure 5.1: ***Variation of (a) P-wave velocity and (b) S-wave velocity with frequency for the viscoelastic layer modeled as a standard linear solid. The frequency range, 1-100 Hz, is commonly accepted in seismic prospecting.***

5.2.2 Quality Factors and Attenuation Coefficient

Figure 5.2 (a) and (b) show the frequency dependence of quality factors (Q_p and Q_s) and attenuation coefficient respectively in a viscoelastic medium. For a single mechanism SLS model, used here for representing the viscoelastic solid, Q is frequency dependent. Both Q_p and Q_s attain a minimum between 1 to 10 Hz., with Q_p remaining greater than Q_s. In Figure 5.2 (b), the attenuation coefficient increases between 1 to 10Hz. The trend of the frequency dependence of attenuation coefficient is similar to that of seismic wave

velocities, with the difference that the former attains its highest value over a smaller frequency range.

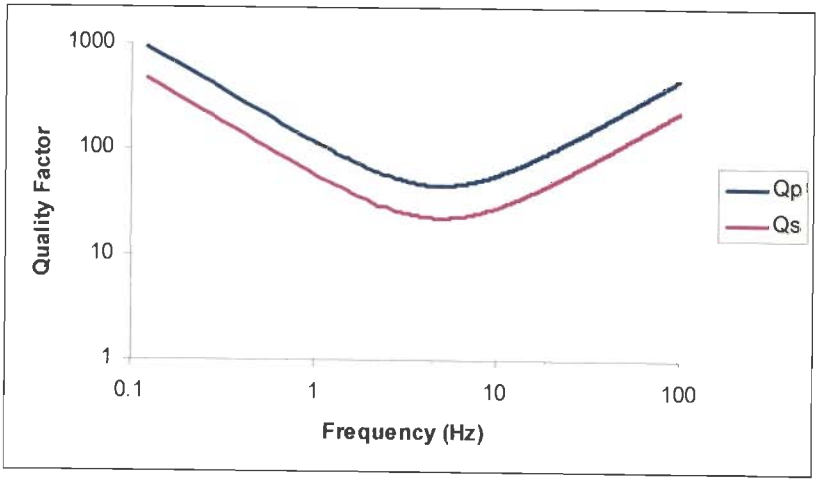

(a)

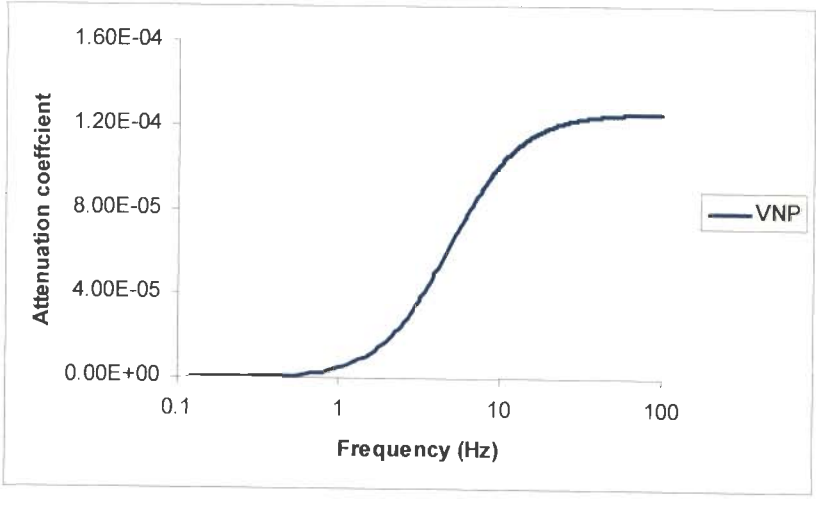

(b)

Figure 5.2: ***Variation of (a) quality factor and (b) attenuation coefficient with frequency for the viscoelastic layer modeled as a single mechanism standard linear solid.***

5.2.3 Reflection Coefficients

A consequence of complex and frequency dependent nature of seismic wave velocities is that reflection and transmission coefficients at the boundaries of the viscoelastic layer also show similar behavior. Figure 5.3 (a) and (b) show the variation of real part of the P-wave reflection coefficients (Rpp) with offset for first and second interfaces, respectively. The reflection coefficients displayed are at a frequencies of 1 and 50 Hz. The reflection

coefficients for the viscoelastic case at a 50 Hz. frequency do not differ significantly from those when the second layer is itself elastic. This is because the P- and S-wave velocities at 50 Hz (5409.82 m/s and 3246.32 m/s respectively) are very nearly equal to those of elastic layer (5411 m/s and 3247.76 m/s respectively). At the lowest velocities values at low frequencies (such as 1 Hz.) (5294.71 m/s and 3108.52 m/s respectively), the reflection coefficients are about 2.9% of their values at 50 Hz. However the complex and frequency dependent nature of the reflection coefficients leads to dispersion in the shape of reflected wavelets. The same is true for transmission coefficients also.

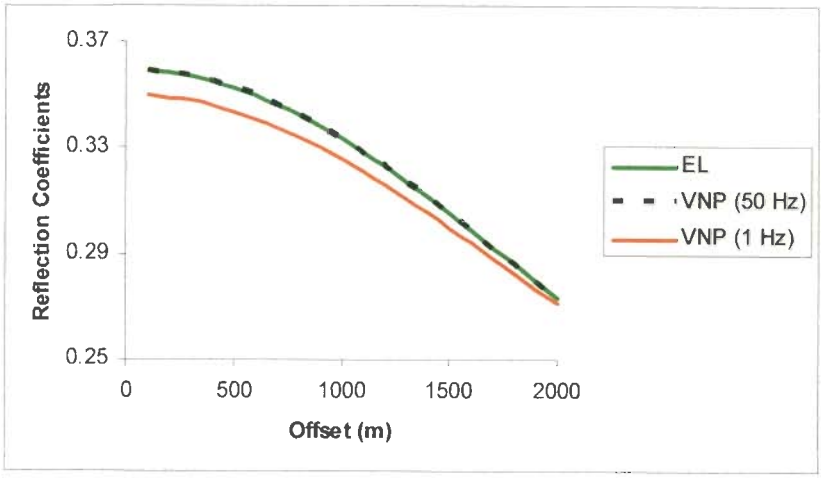

(a)

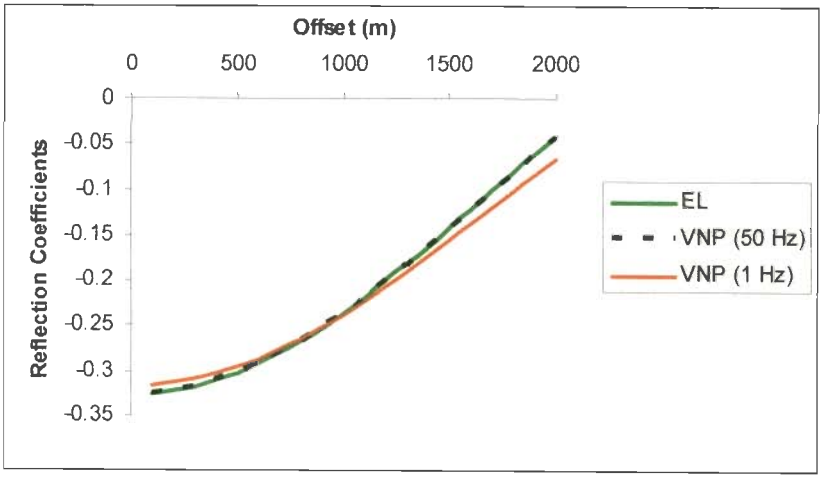

(b)

Figure 5.3: ***Variation of reflection co-efficients with incident angle of reflected P-waves from the (a) first interface and (b) second interface. Only the real parts of the reflection coefficient at a frequency of 1 Hz. and 50 Hz. have been plotted. For comparison, the reflection coefficients when the second layer is elastic have also been plotted.***

5.2.4 Synthetic Seismograms

Figure 5.4 shows the synthetic seismograms when second layer is viscoelastic and non-porous. It is observed very clearly that the amplitude of the reflected wavelet is getting more and more attenuated with increasing offset.

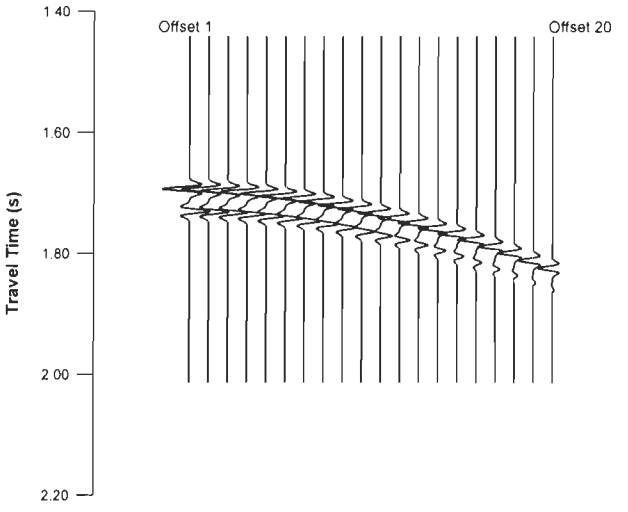

Figure 5.4: ***Synthetic seismograms at the surface of three-layer model simulating an AVO situation from the both interfaces. There are 20 traces at offsets varying from 100 m to 2000 m.***

5.2.5 Seismic Wavelets

Figures 5.5 (a) and (b) show a comparative study of the reflected wavelet when the second layer is viscoelastic and when it is elastic, at two offsets: 1500m and 2000m. The figures show the effect of viscoelasticity on the shapes of reflected wavelets. The reflected pulses at 1500m offset show amplitude loss of the order of 0.9 dB whereas at 2000 m, the amplitude loss is of the order of 1.38 dB. These losses refer to the amplitude of the central lobe. There is also a phase delay due to velocities being complex and frequency dependent. The amplitudes of the side lobes of the wavelets are slightly different (this difference is greater at 2000 m) and the widths of the wavelets are also different when compared with those for elastic case. Thus, the effect of viscoelasticity alone on the shape of reflected seismic wavelets is clearly demonstrated even in the narrow frequency range of 1 – 100 Hz.

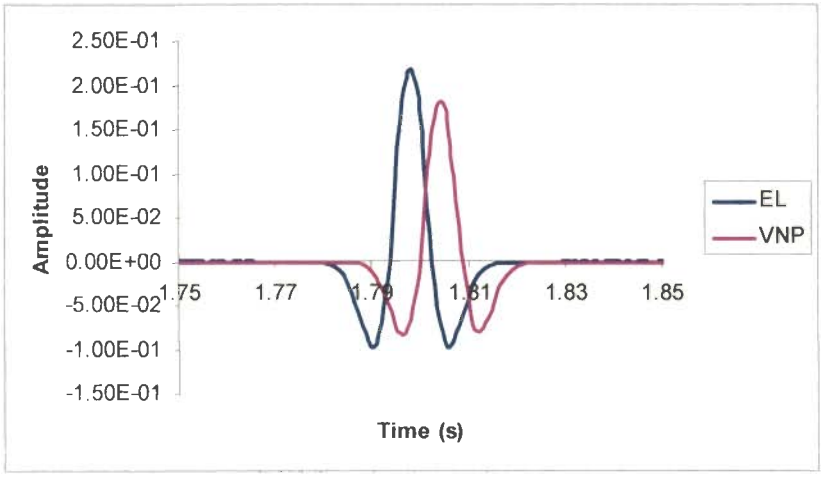

(a)

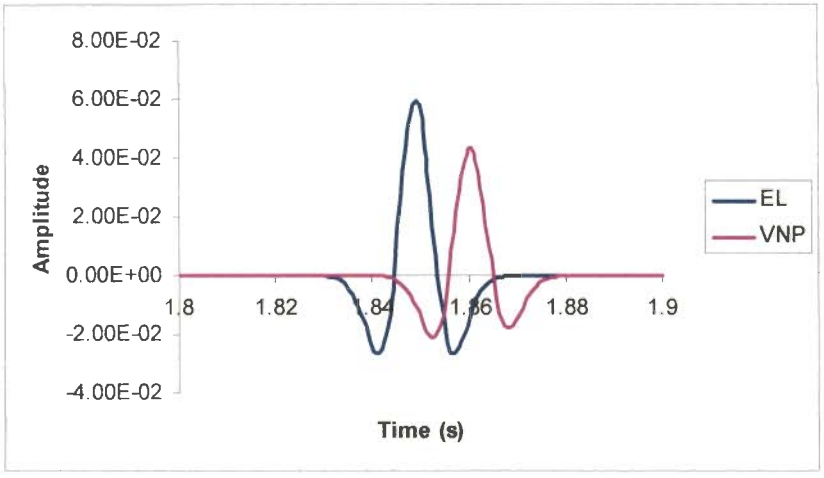

(b)

Figure 5.5: ***Comparison of seismic pulses at offset (a) 1500m and (b) 2000m from second interface, for viscoelastic and elastic cases, depicting significant changes in pulse shapes due to dispersion and attenuation.***

5.3 PART II: SECOND LAYER IS VISCOELASTIC AND POROUS

The second layer is now viscoelastic and porous containing oil or gas and water in different proportions. The porous layer is assumed to contain oil and water, gas and water or only water. The propagation of seismic waves in the porous layer is now affected by solid-fluid interaction. The presence of fluids in the pore spaces gives rise to two coupled longitudinal waves (the fast and slow P-waves) and a shear wave, in accordance with Biot's theory (Biot, 1956). The computations of the velocities of these waves have been

described in Chapter 3. In the following paragraphs the effects of the presence of different types and amount of fluids on the behavior of seismic wave velocities, quality factors, attenuation coefficients, reflection coefficients and shapes of reflected seismic wavelets have been presented and analyzed. In addition, AVO analysis is carried out on synthetic data to determine whether the AVO attributes (i.e., intercept A and slope B of the linear relation between reflection coefficient and $sin^2 i$ where i is angle of incidence) are significantly affected by the amount of gas or not.

In the following description, when the pore spaces contain gas and water or oil and water, the water saturation, when not stated, is assumed to be 50%, and, in the same way, porosity, when not stated, is assumed to be 20%. When only water is present, the saturation, of course, is 100%. P-wave, without any prefix, means fast P-waves.

5.3.1 Frequency Dependence of Wave Velocities

5.3.1.1 *Variation with Porosity*

Figure 5.6 (a) and (b) show respectively the frequency dependence of P and S wave velocity in the viscoelastic layer. The trend of the curves for oil and water, gas and water and only water is similar to that shown in Figure 5.1 (a). Smallest P-wave velocity in the presence of gas and water is observed. However, S-wave velocity is largest in the presence of gas and water. This is because pore fluids influence both the bulk modulus and bulk density. The change in bulk modulus is more pronounced than bulk density resulting in greater decrease in P-wave velocity. On the other hand, shear modulus remains unchanged. The decrease in bulk density is greater in the presence of gas and water leads to greater S-wave velocity.

Frequency dependence of velocities of fast P-wave, slow P-wave and S-wave for a viscoelastic layer having different porosities are shown in (i) Figure 5.7 (a) to (c) when pores contain gas and water, (ii) Figure 5.8 (a) to (c) when pores contain oil and water and (iii) Figure 5.9 (a) to (c) when pores contain only water. The rate of change of P- and S-

wave velocities increases with increase of porosity with S-wave velocity changing at a faster rate than P-wave velocity.

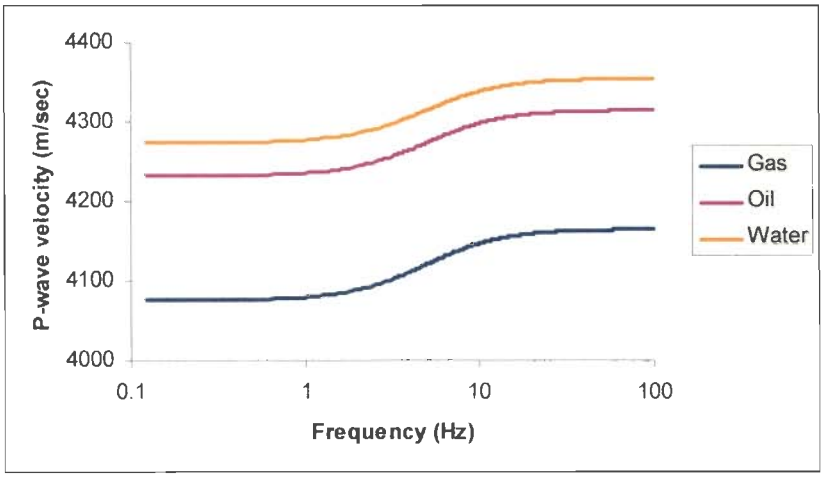

(a)

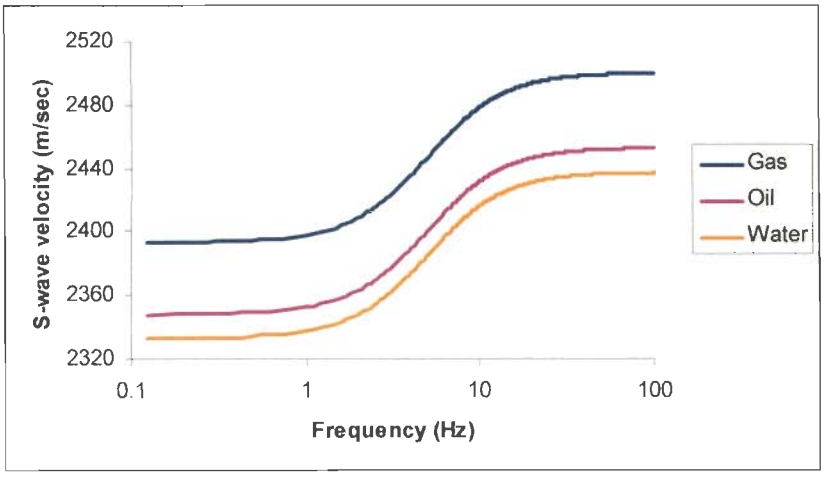

(b)

Figure 5.6 ***Variation of (a) Fast P-wave velocity and (b) S-wave velocity with frequency in porous viscoelastic layer for different fluids.***

For comparison purposes, the velocities at a frequency of 50 Hz and 50% water saturation are shown in Table 5.1.

Table 5.1 ***Seismic Wave Velocities at 50 Hz in the Porous Viscoelastic Layer***

Wave Type	Velocity in m/s when pores contain								
	Gas			Oil			Water		
Porosity	10%	20%	30%	10%	20%	30%	10%	20%	30%
Fast P-wave	4879.2	4163.9	3090.6	4928.3	4313.9	3474.7	4941.3	4353.8	3571.9
Slow P-wave	0.6209	0.4390	0.3585	22.66	15.79	12.42	37.59	26.08	20.43
S-wave	2927.9	2498.6	1854.5	2902.2	2451.5	1797.8	2893.6	2436.0	1779.6

5.3.1.2 *Variation with Water Saturation*

Frequency dependence of velocities of fast P-wave, slow P-wave and S-wave in a viscoelastic layer having different saturations are shown in (i) Figure 5.10 (a) to (c) when pores contain gas and water, and (ii) Figure 5.11 (a) to (c) when pores contain oil and water. The change of P- and S-wave velocities with increasing saturation is more pronounced when gas and water is present than when oil and water is present.

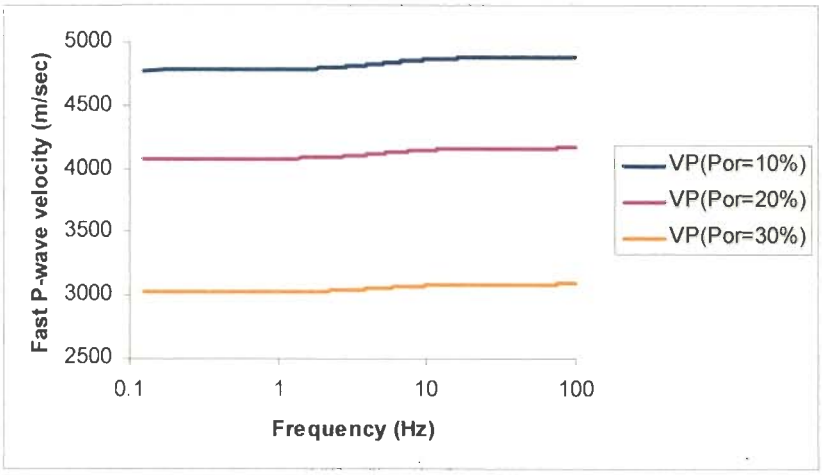

(a)

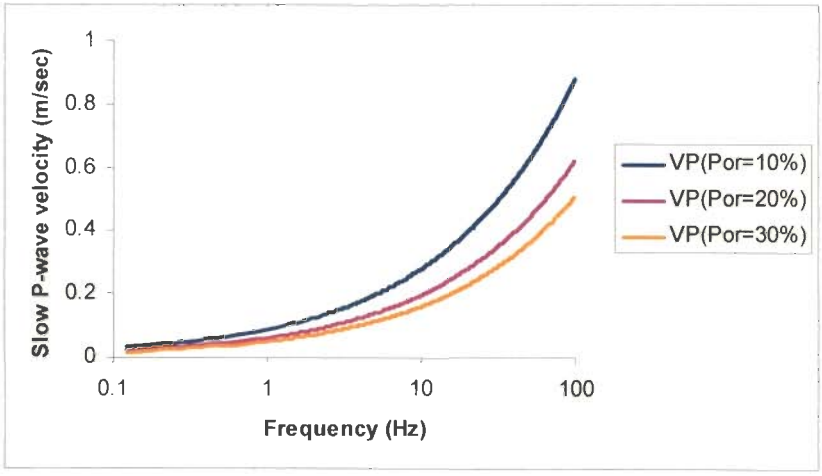

(b)

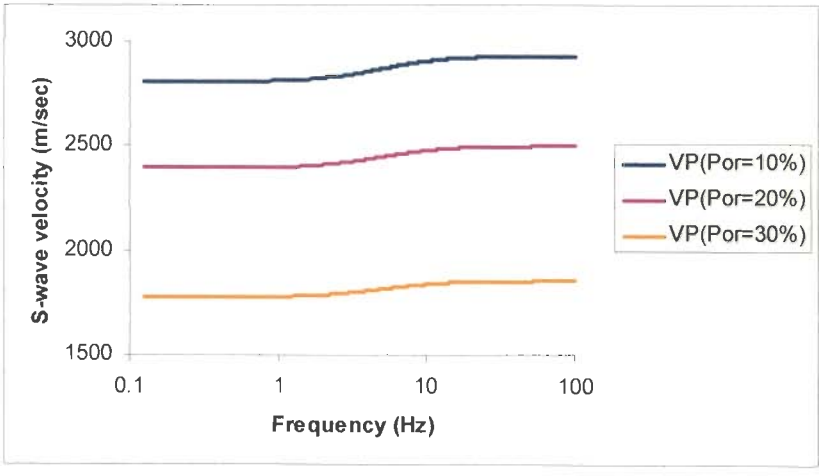

(c)

Figure 5.7: ***Variation of (a) Fast P-wave velocity (b) Slow P-wave velocity and (c) S-wave velocity with frequency in porous viscoelastic layer for different porosities. The pore fluid is gas and water.***

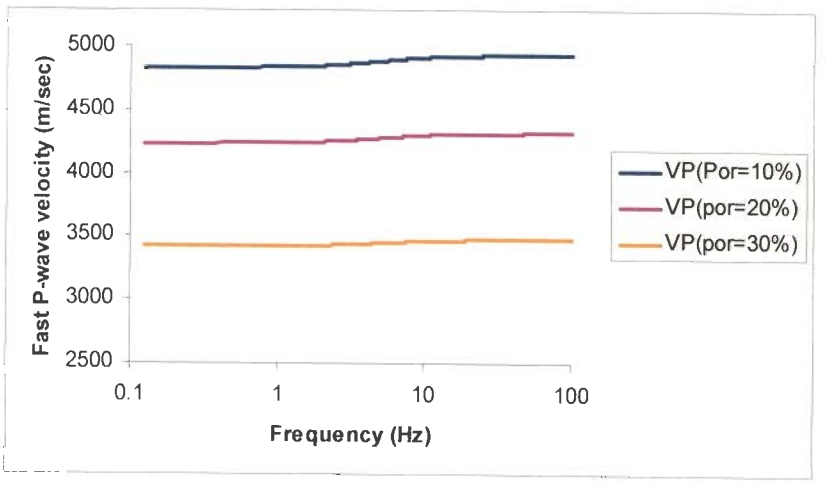

(a)

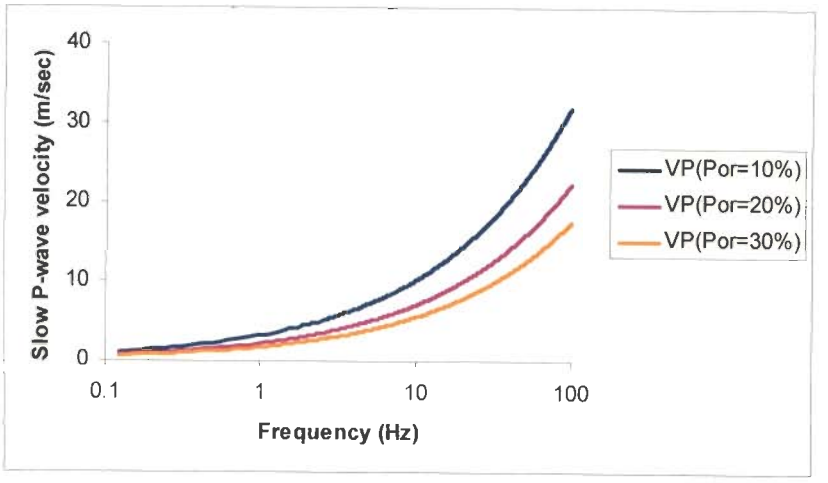

(b)

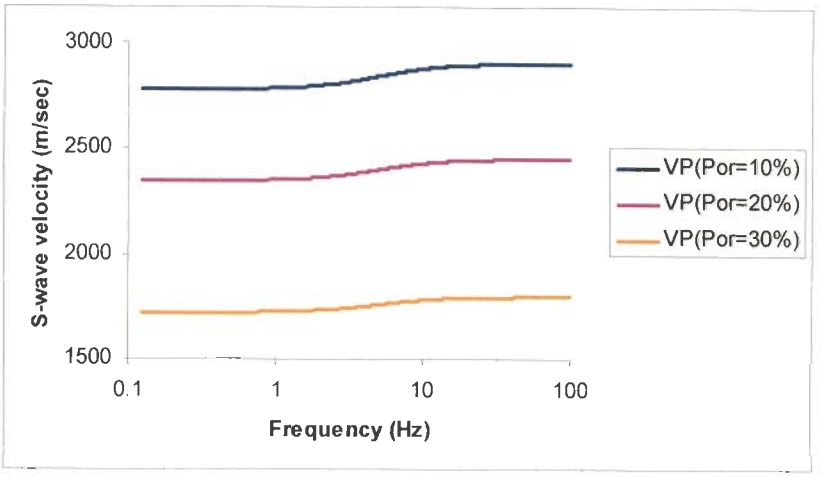

(c)

Figure 5.8: ***Variation of (a) Fast P-wave velocity (b) Slow P-wave velocity and (c) S-wave velocity with frequency in porous viscoelastic layer for different porosities. The pore fluid is oil and water.***

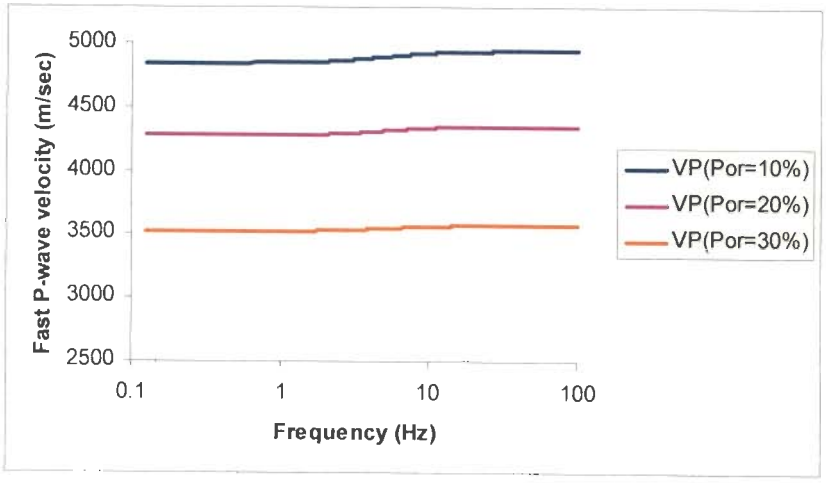

(a)

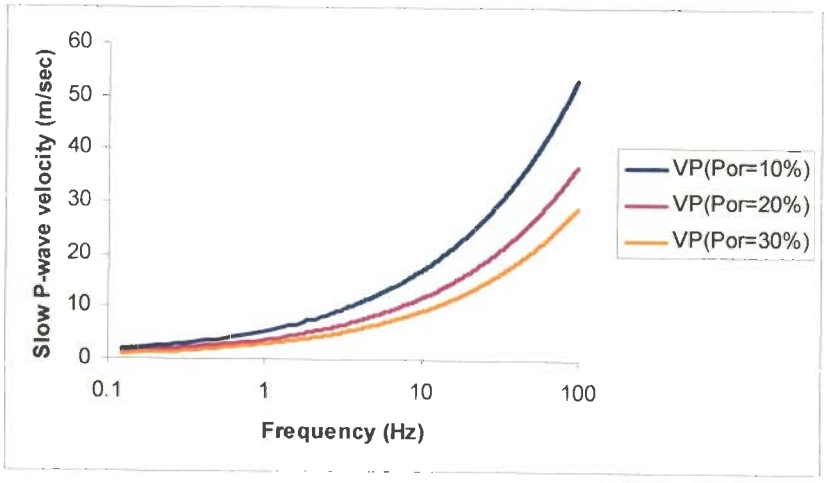

(b)

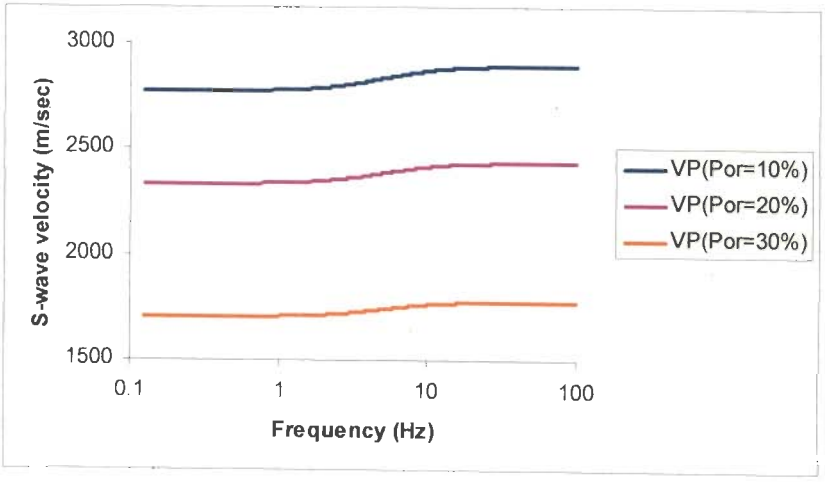

(c)

Figure 5.9: ***Variation of (a) Fast P-wave velocity (b) Slow P-wave velocity and (c) S-wave velocity with frequency in porous viscoelastic layer for different porosities. The pore fluid is water.***

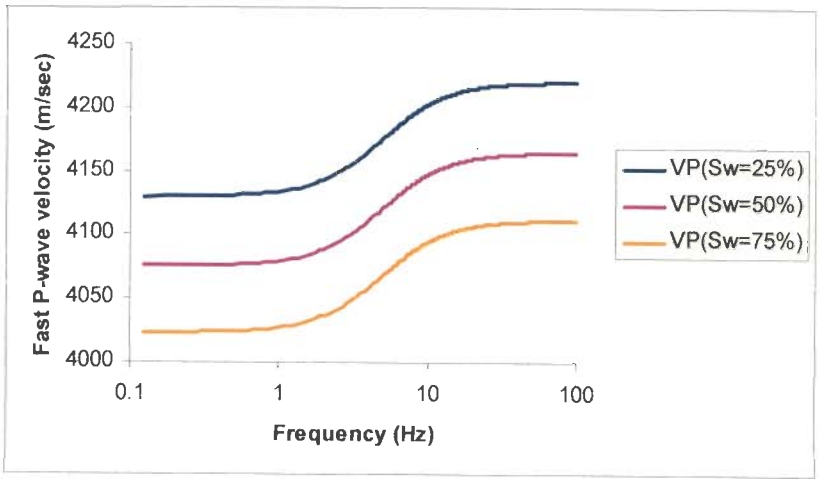

(a)

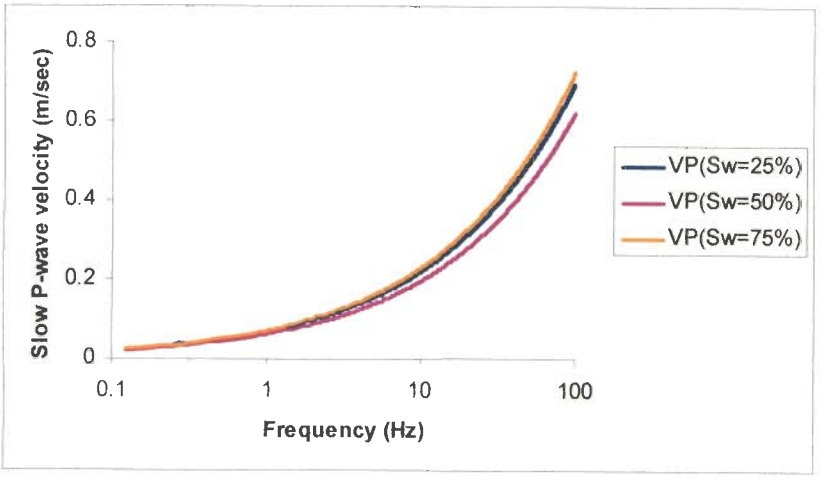

(b)

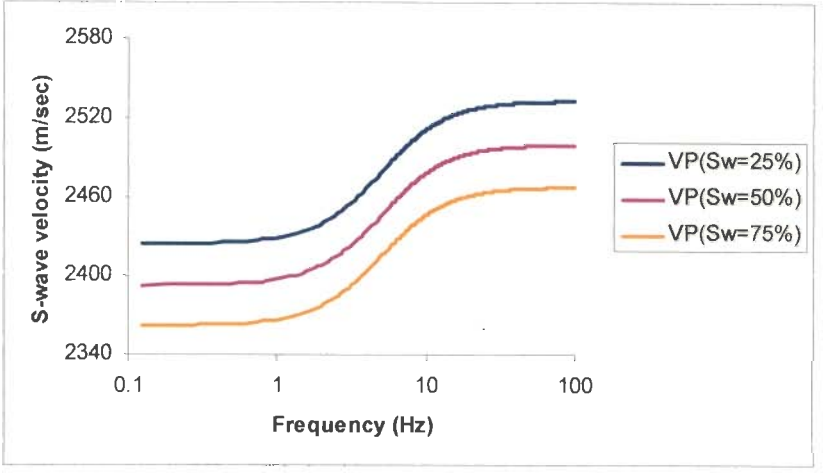

(c)

Figure 5.10: ***Variation of (a) Fast P-wave velocity (b) Slow P-wave velocity and (c) S-wave velocity with frequency in porous viscoelastic layer for different water saturations. The pore fluids gas and water.***

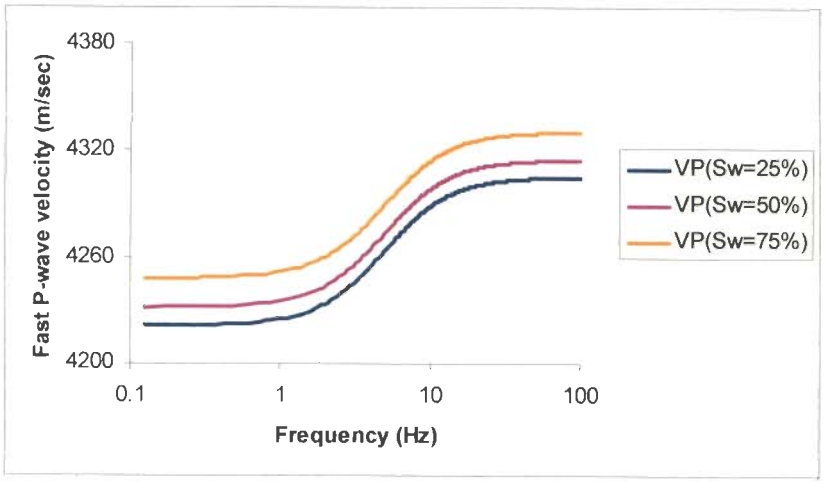

(a)

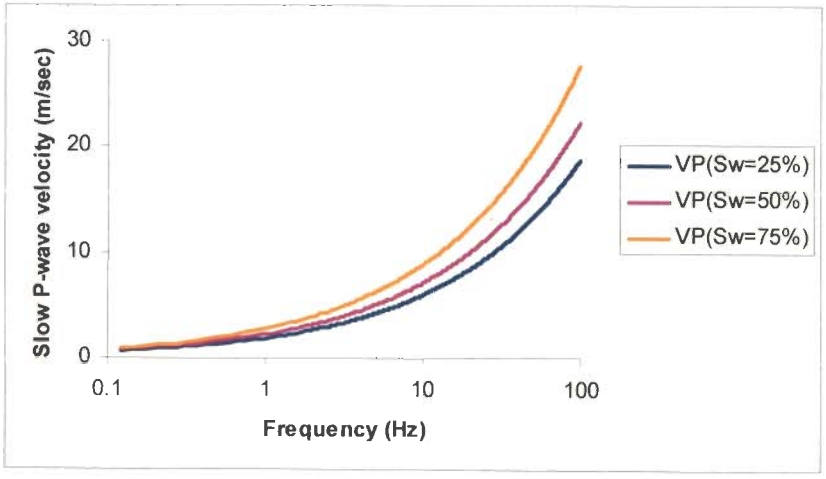

(b)

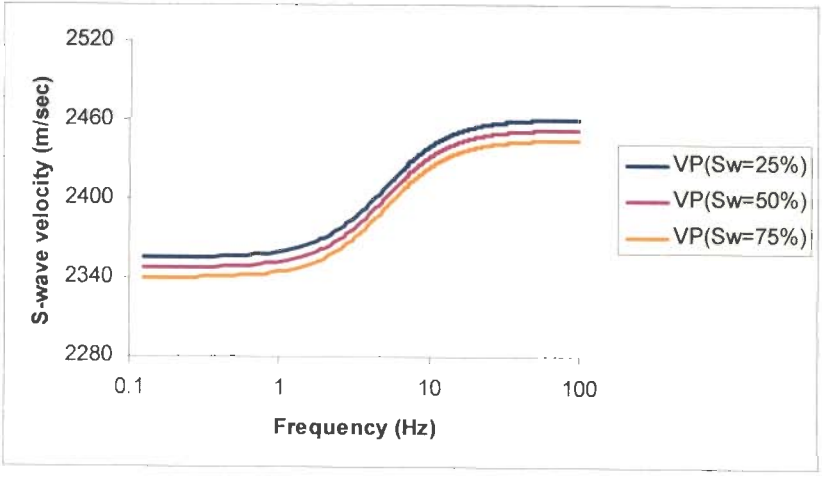

(c)

Figure 5.11: ***Variation of (a) Fast P-wave velocity (b) Slow P-wave velocity and (c) S-wave velocity with frequency in porous viscoelastic layer for different water saturations. The pore fluid is oil and water.***

5.3.2 Frequency Dependence of Quality factors

5.3.2.1 *Variation with Porosity*

Figure 5.12 shows the frequency dependence of quality factors of P-wave in the viscoelastic layer. The trend of the curves is similar to that shown in Figure 5.2 (a) and is the same irrespective of the type of fluid present in the pore spaces.

Frequency dependence of quality factors of P-waves in a viscoelastic layer having different porosities are shown in (i) Figure 5.13 when pores contain gas and water, (ii) Figure 5.14 when pores contain oil and water, and (iii) Figure 5.15 when pores contain only water. These curves are typical for a single mechanism relaxation model. All the curves for different fluids and porosities attain a minimum between 1 to 10 Hz. It is also observed that when gas and water is present in the pore spaces, Q_p does not vary with increase in porosity. There is some variation with porosity when oil and water or only water is present in the pore spaces, the increase being nearly 29.46 % and 37.8 % respectively when porosity changes from 10% to 30%.

The small variation in Q values with porosity (Figure 5.14 and 5.15) is due to the effect of viscosity of the pore fluid on the dynamic coefficients that affects real and imaginary parts of complex elastic modulus $M(\omega)$. More the porosity, larger the amount of fluid in the pore spaces and greater the influence of viscosity on the dynamic coefficients, complex wave velocities.

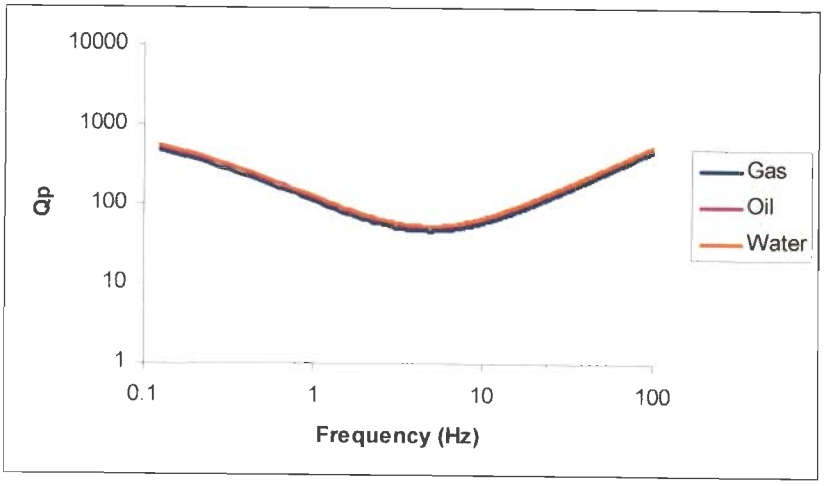

Figure 5.12: ***Variation of quality factor with frequency in viscoelastic porous layer for different fluids.***

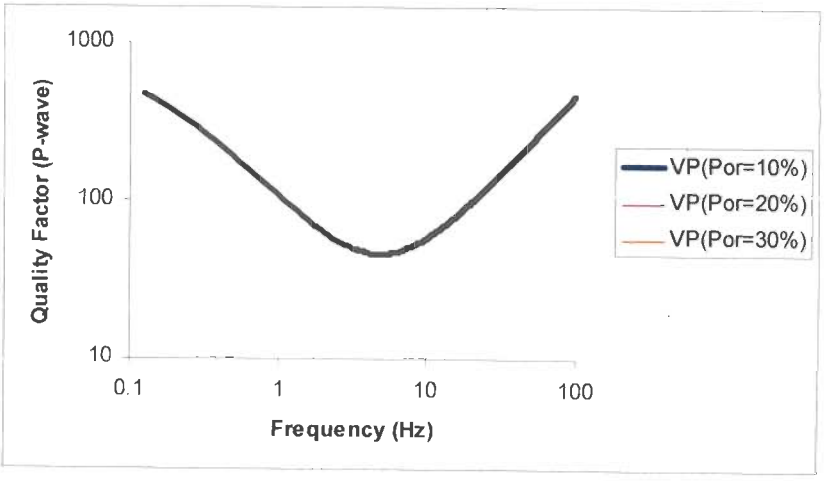

Figure 5.13: ***Variation of quality factor with frequency in viscoelastic porous layer for different porosities. The pore fluid is gas and water.***

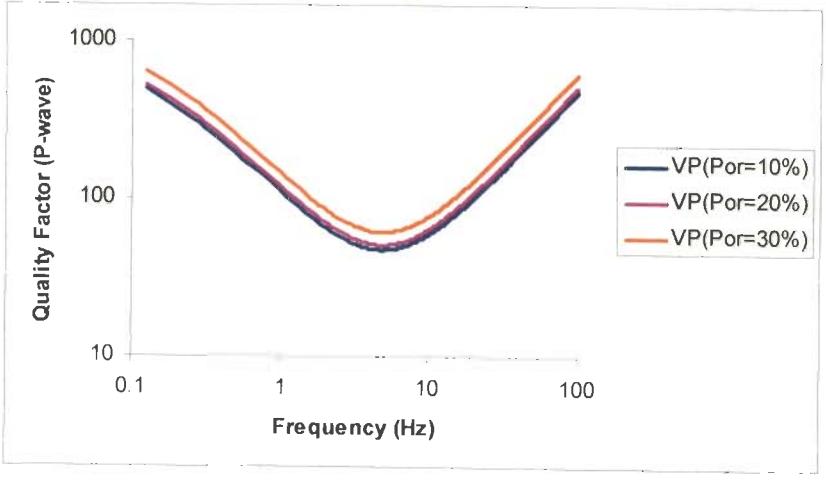

Figure 5.14: ***Variation of quality factor with frequency in viscoelastic porous layer for different porosities. The pore fluid is oil and water.***

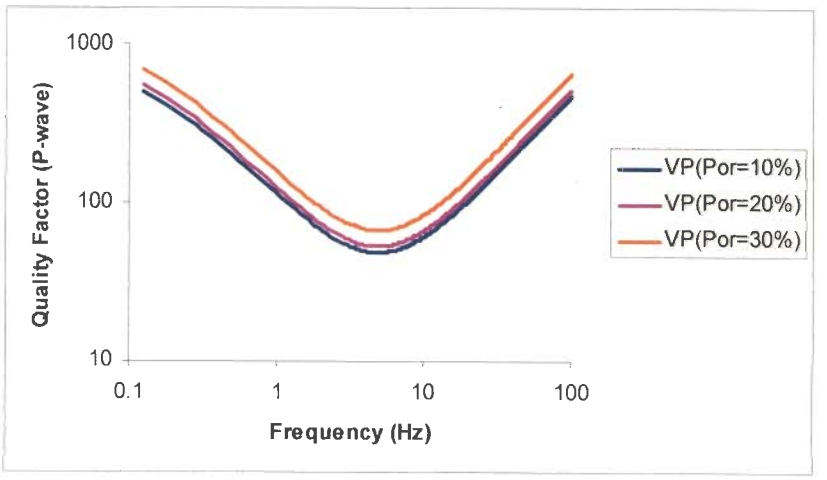

Figure 5.15: ***Variation of quality factor with frequency in viscoelastic porous layer for different porosities. The pore fluid is water.***

5.3.2.2 *Variation with Water Saturation*

Frequency dependence of quality factors of P-waves in a viscoelastic layer having different water saturations are shown in (i) Figure 5.16 when pores contain gas and water, and (ii) Figure 5.17 when pores contain oil and water. All the curves for different fluids and saturations show similar trend attaining a minimum between 1 to 10 Hz. It is also observed that there is no significant effect of increasing water saturation on quality factors. Thus, the amount of different fluids in a viscoelastic layer with a given porosity does not seem have to have any significant effect on the quality factors.

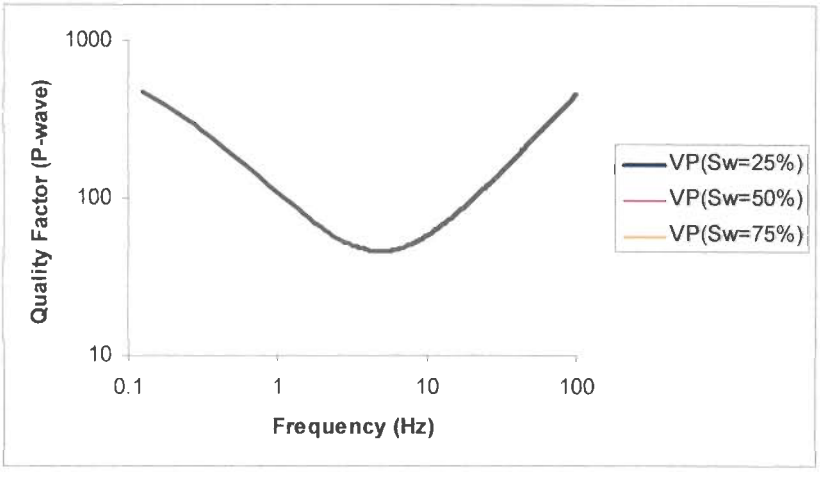

Figure 5.16: ***Variation of quality factor with frequency in viscoelastic porous layer for different water saturations. The pore fluid is gas and water.***

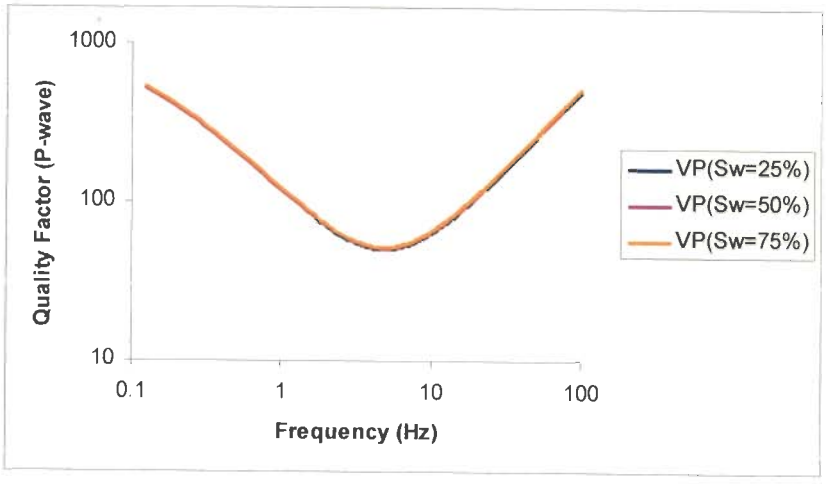

Figure 5.17: ***Variation of quality factor with frequency in viscoelastic porous layer for different water saturations. The pore fluid is oil and water.***

5.3.3 Frequency Dependence of Attenuation Coefficient

5.3.3.1 *Variation with Porosity*

Figure 5.18 shows the frequency dependence of attenuation coefficient of P-wave in the viscoelastic layer. The trend of the curves is similar to that shown in Figure 5.2 (b) and is the same irrespective of the type of fluid present in the pore spaces. The attenuation coefficient increases with increasing frequency but the trend becomes steeper when gas and water is present, signifying higher increase with frequency than when oil and water or only water are present. The attenuation coefficient in the presence of gas and water in the pores is significantly higher in the frequency range of interest. The curves for oil and water and only water are nearly coincident over most of the frequency range.

Frequency dependence of attenuation coefficient of P-waves in a viscoelastic layer having different porosities are shown in (i) Figure 5.19 when pores contain gas and water, (ii) Figure 5.20 when pores contain oil and water, and (iii) Figure 5.21 when pores contain only water.

These curves are typical for a single mechanism relaxation model. The overall trend of the variation of attenuation coefficient with frequency is almost same for different fluids and different porosity values. These curves bring out the effect of porosity and fluid

content on the attenuation coefficient. The attenuation is significantly greater at high frequencies when the viscoelastic layer is porous and fluid saturated. It is observed that the attenuation coefficient in the presence of gas and water is more sensitive to change of porosity than when oil and water or only water is present in the pores. This means that if gas and water will present in the pore space the seismic wavelets will be more attenuated. Water shows the least effect of porosity on the attenuation coefficient. The effect is noticeable only at higher frequencies. The higher attenuation coefficients in the presence of gas and water are due to the greater reduction of P-wave velocity than when oil and water or only water is present. Since velocity enters into the definition of attenuation coefficients (Eq. 3.2), these are bound to be higher than when velocity is small.

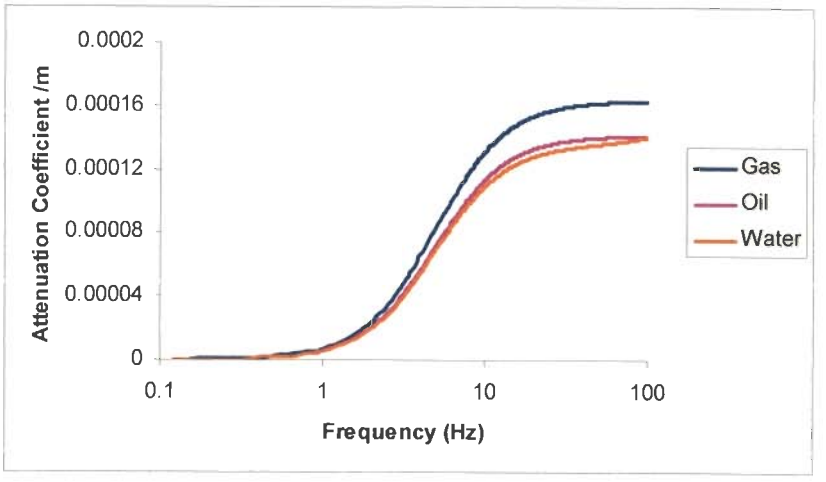

Figure 5.18: ***Variation of attenuation coefficient of fast P-waves with frequency in viscoelastic porous layer for different fluids.***

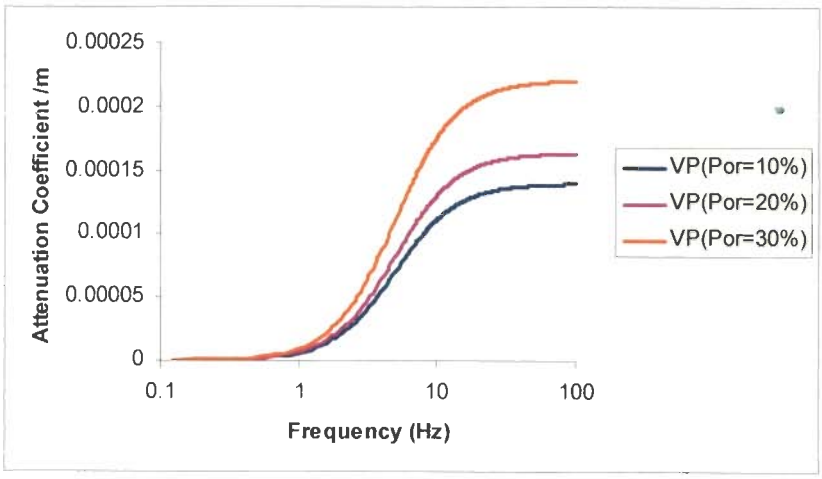

Figure 5.19: ***Variation of attenuation coefficient of fast P-waves with frequency in viscoelastic porous layer for different porosities. The pore fluids is gas and water.***

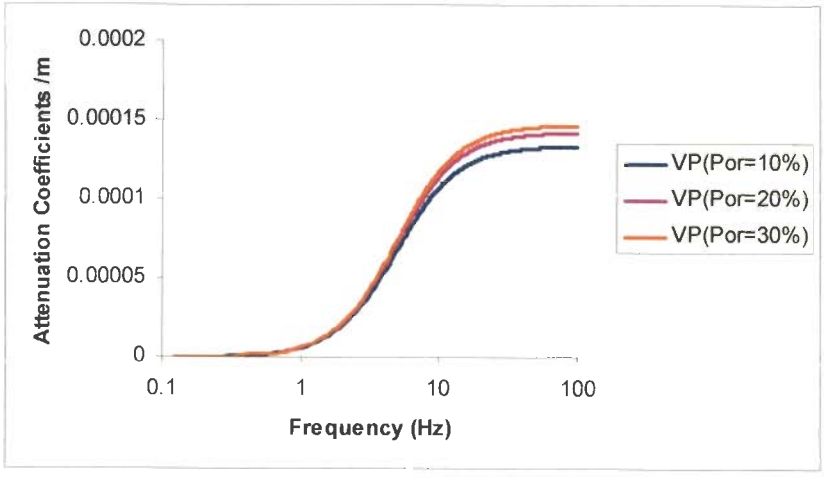

Figure 5.20: ***Variation of attenuation coefficient of fast P-waves with frequency in viscoelastic porous layer for different porosities. The pore fluid is oil and water.***

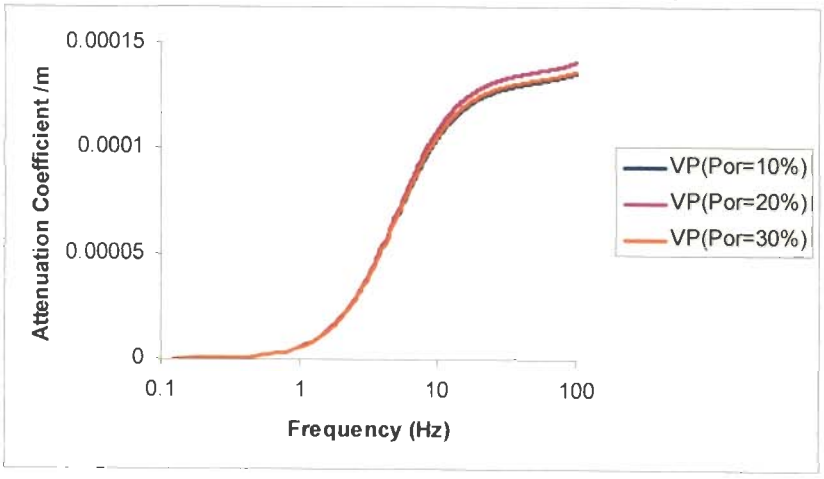

Figure 5.21: ***Variation of attenuation coefficient of fast P-waves with frequency in viscoelastic porous layer for different porosities. The pore fluid is water.***

5.3.3.2 *Variation with Water Saturation*

Frequency dependence of attenuation coefficient of P-waves in a viscoelastic layer having different saturations are shown in (i) Figure 5.22 when pores contain gas and water and (ii) Figure 5.23 when pores contain oil and water. All the curves for different fluids and saturations show a trend similar to that of previous section. It is observed that there is no significant effect of increasing water saturation on attenuation coefficients. Thus, the attenuation coefficients are not sensitive to change in the amount of fluid present in the pore space at constant porosity.

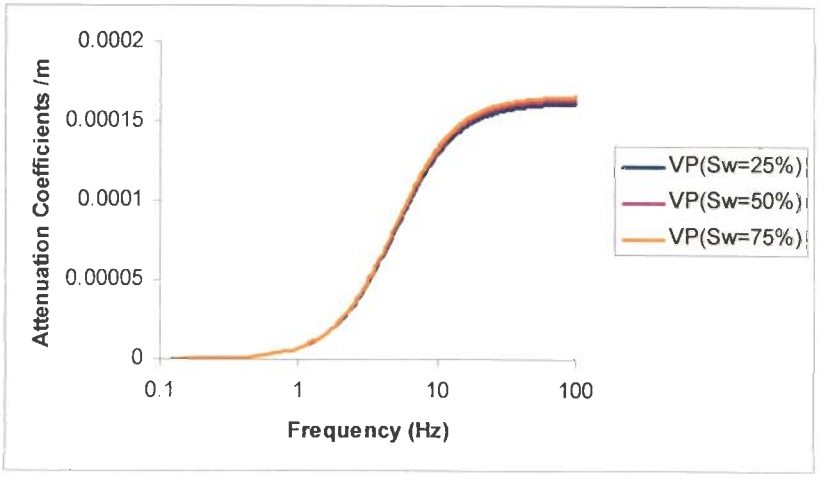

Figure 5.22: ***Variation of attenuation coefficient with frequency in viscoelastic porous layer for different water saturations. The pore fluid is gas and water.***

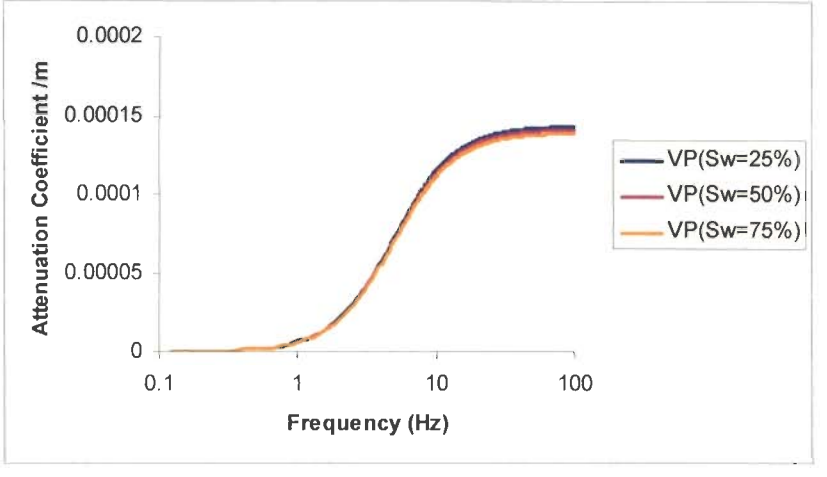

Figure 5.23: ***Variation of attenuation coefficient with frequency in viscoelastic porous layer for different water saturations. The pore fluid is oil and water.***

5.3.4 Variation of Wave Velocities with Porosity and Water Saturation

5.3.4.1 *Variation with Porosity*

Figure 5.24 (a) and (b) show respectively the porosity dependence of P- and S-wave velocity in the viscoelastic layer containing either gas and water, oil and water or only water in pore spaces. The dependence of P-wave velocity – porosity variation on the type of pore fluids is significant for porosities exceeding 10%, with lowest velocities in the presence of gas and water. The S-wave velocity – porosity variation does not show much significant dependence on type of pore fluids. Whatever little dependence is seen in Figure 5.24(b) is the result of the influence of porosity and pore fluids on bulk density.

Variation of P-wave and S-wave velocities with porosity for different water saturations are shown in (i) Figure 5.25(a) and (b) when pore fluid is gas and wate and (ii) Figure 5.26(a) and (b) when pore fluid is oil and water. The trend of velocity – porosity variation is the same irrespective of the type of fluid present. These variations are sensitive to increasing water saturation when gas and water is present in the pores.

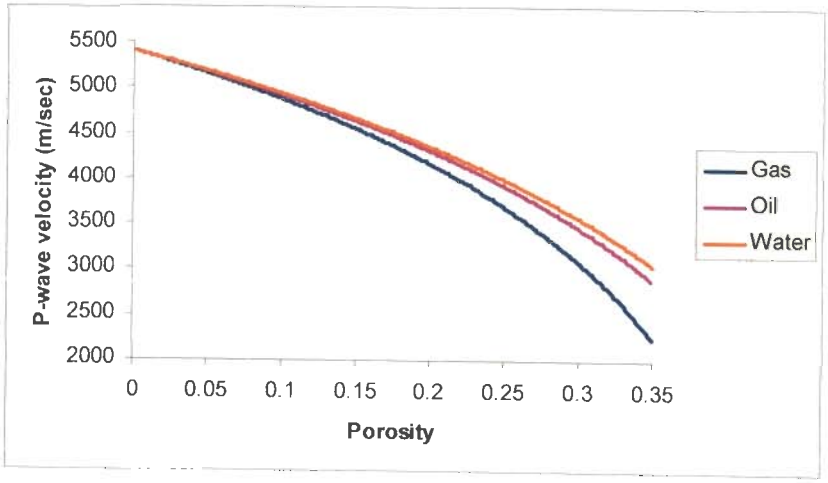

(a)

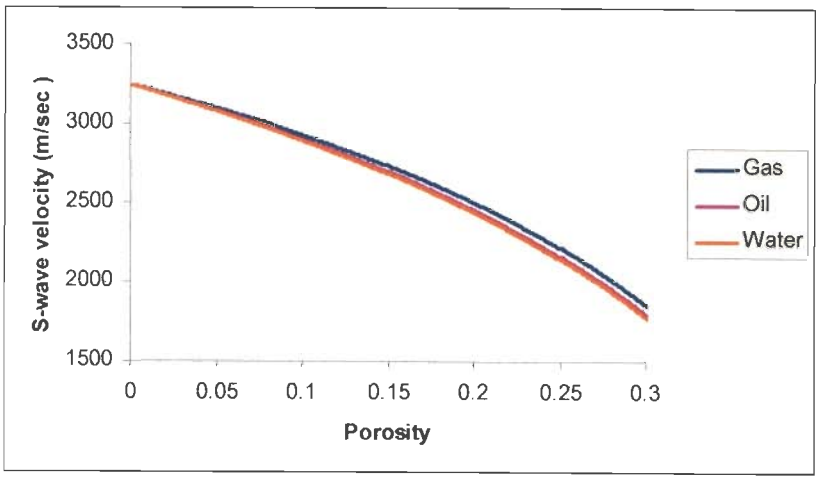

(b)

Figure 5.24: ***Variation of (a) P-wave velocity, and (b) S-wave velocity, with porosity in the porous viscoelastic layer for different fluids.***

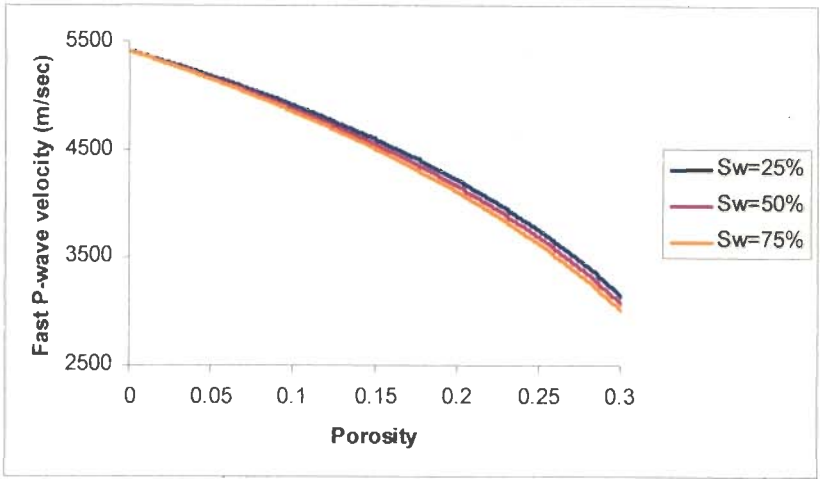

(a)

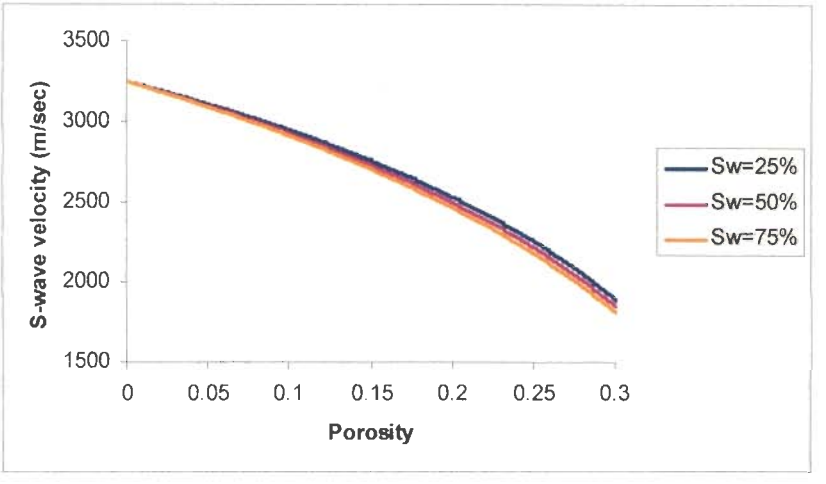

(b)

Figure 5.25: ***Variation of (a) P-wave velocity (b) S-wave velocity with porosity for different saturations in porous viscoelastic layer. The pore fluid is gas and water.***

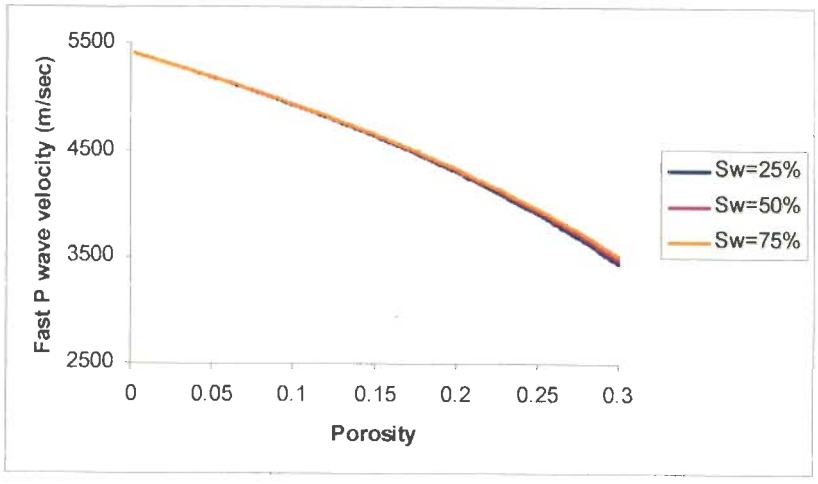

(a)

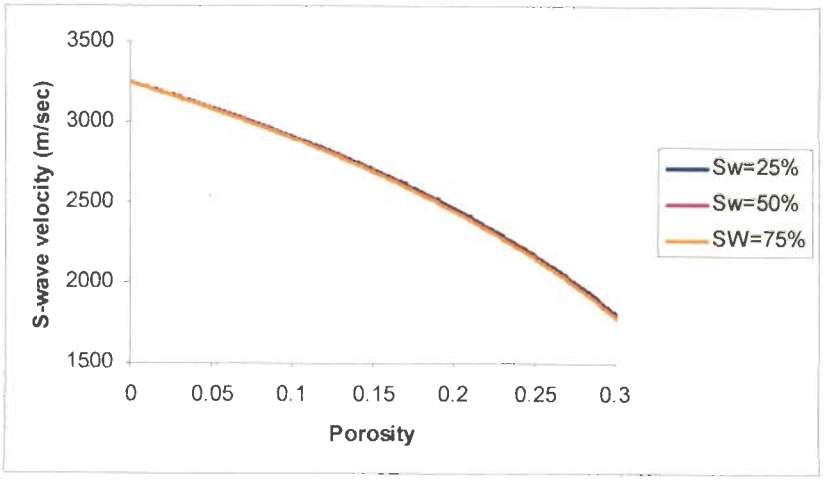

(b)

Figure 5.26: ***Variation of (a) P-wave velocity (b) S-wave velocity with porosity for different saturations in porous viscoelastic layer. The pore fluid is oil and water.***

5.2.4.2 *Variation with Water Saturation*

Variations of P-wave and S-wave velocities with water saturation in a porous viscoelastic layer are shown in (i) Figure 5.27 (a) and (b) when pores contain gas and water and (ii) Figure 5.28 (a) and (b) when pores contain oil and water. The velocities decrease slightly with increasing water saturation (i.e., decreasing gas saturation). The rate of decrease is greater when porosity is 30%. The increase of bulk density with water saturation leads to this decrease of velocities. The velocities do not vary much with water saturation when oil

and water is present in the pores. The P-wave velocity increases slightly with water saturation when the porosity is 30%.

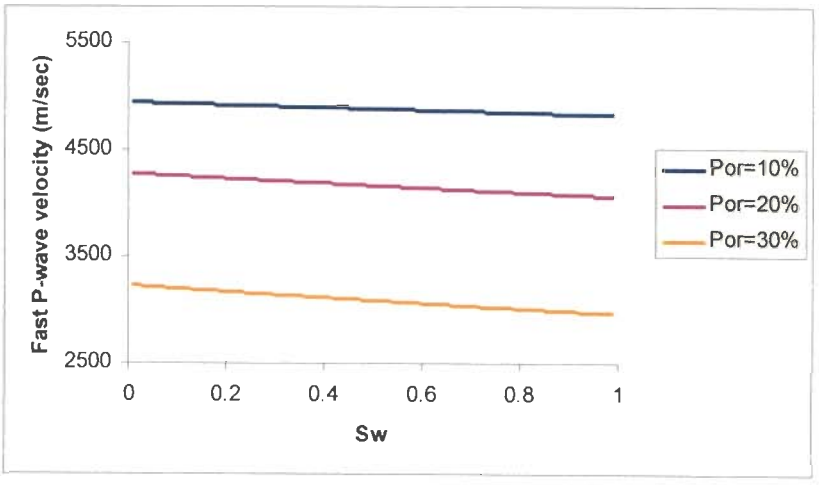

(a)

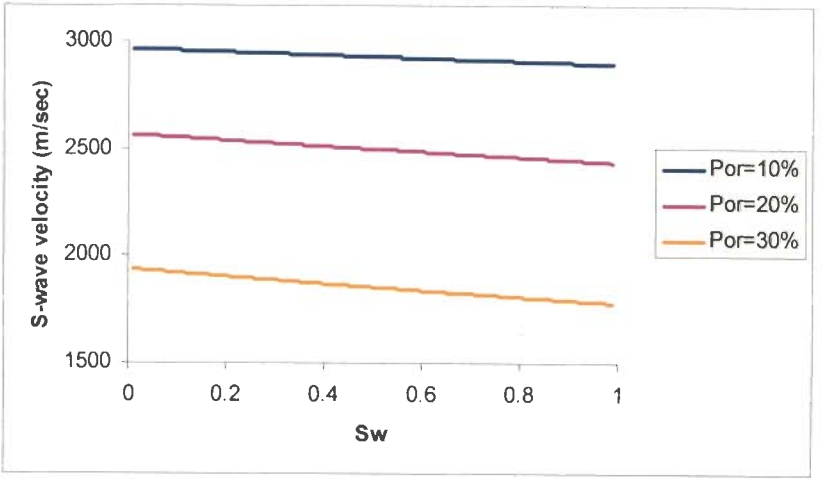

(b)

Figure 5.27: ***Variation of (a) fast P-wave velocity (b) S-wave velocity with saturation for different porosities in porous viscoelastic layer. The pore fluid is gas and water.***

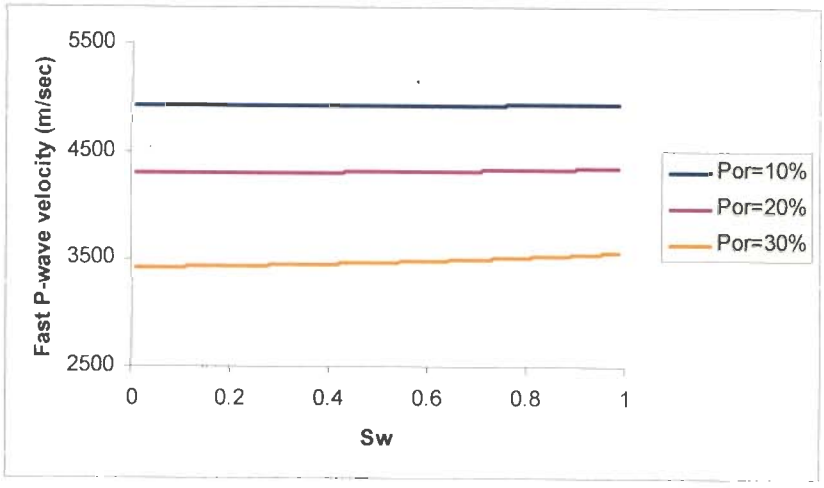

(a)

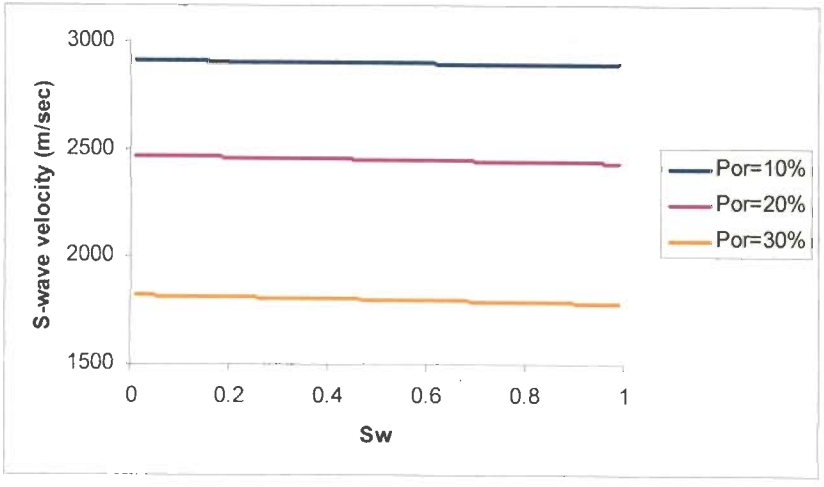

(b)

Figure 5.28: ***Variation of (a) P-wave velocity (b) S-wave velocity with saturation for different porosities in porous viscoelastic layer. The pore fluid is oil and water.***

5.3.5 Reflection Coefficients

Following figures show the variation of reflection coefficients with angle of incidence for both interfaces calculated using equations 3.81 and 3.84. The curves depict the real part of reflection coefficients and pertain to a frequency of 50 Hz. Figure 5.29 (a) shows the reflection coefficient curves when P-waves are incident from above at the first interface and the pores contain gas and water or oil and water or only water.

Figure 5.29(b) show these curves when P-waves are incident from above at the second interface. The reflection coefficients, in the presence of gas and water, are lowest at

all angles of incidence, except for a small region near critical angle at the first interface. This reflection coefficient at the second interface is largest (and positive) in case of gas and water over a broad region, from nearly 30° to 70°. This feature is due to greater reduction in P-wave velocities in the presence of gas and water. This character of the angle dependent variation is dependent on porosity. At a higher porosity, there will be still greater reduction in P-wave velocity and the reflection coefficients at the second interface will become negative for all angles, the general trend remaining the same.

Figure 5.30 shows the reflection coefficients at the first interface for different porosities plotted for angles of incidence smaller than 30°, typical for AVO analysis. Pores contain gas and water. Increasing porosity decreases the seismic wave velocities, and the impedance contrast, positive at lower porosities, becomes negative at higher porosities and the character of the curve changes. It is noticeable that the curves for 25% and 30% porosity resemble those for class II type gas sand and those for porosity exceeding 30% porosity resemble the typical response for class III type gas sand.

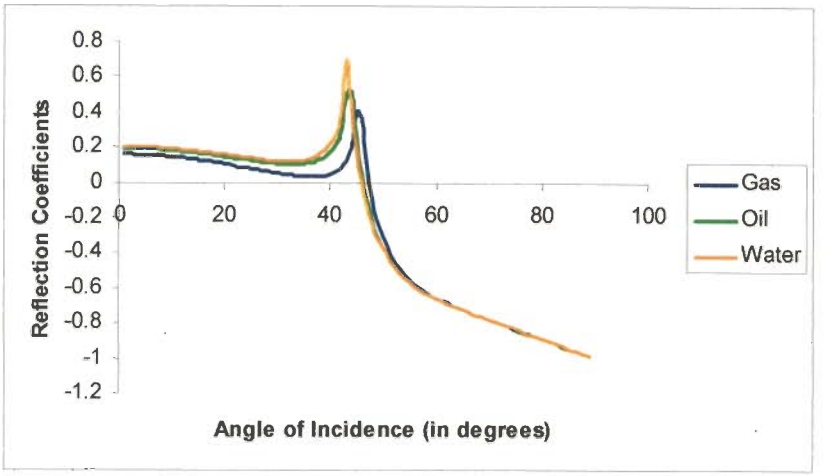

(a)

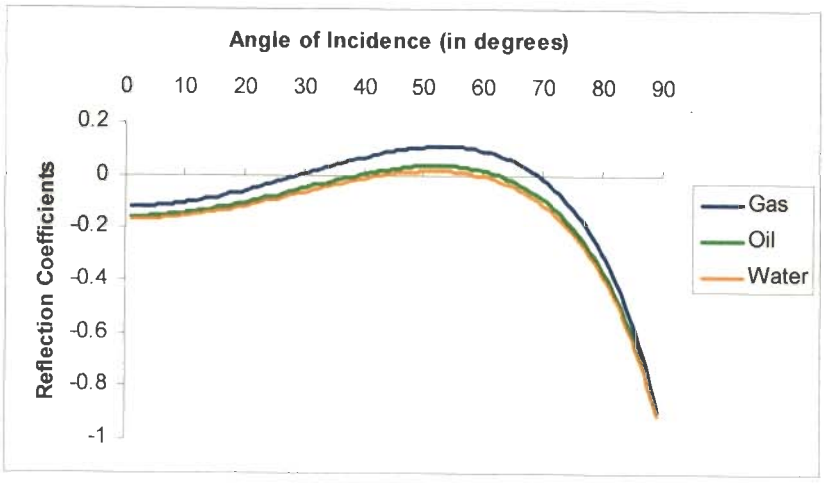

(b)

Figure 5.29: ***Comparison of the variation of reflection coefficients with incident angle of reflected P-waves at the (a) first interface and (b) second interface for different fluids. Only the real part of the reflection coefficients at a frequency of 50 Hz have been plotted.***

The variation of reflection coefficients with angle of incidence, shown in Figure 5.30 is based on computations based on the model given in Table 4.5. In this model the elastic layer overlying the viscoelastic porous layer is assumed to be a soft, having V_p/V_s ratio of 2.38 which leads to a large contrast in the Poisson's ratio between the first layer and the second layer at higher porosity (>30%) values in the presence of gas and water in the pore spaces. However, if the overlying layer is hard, having V_p/V_s of the order of 1.6, the variation of the reflection coefficients with the angle of incidence at different porosities will be different. One such model is given in Table 5.2 where first layer has V_p/V_s value of the order of 1.66. In this case, the variation of reflection coefficient at a porosity of 35% resembles the response of class IV type gas sand (Roden, 2005), as shown in Figure 5.31, which is similar to Figure 5.30. It is observed that at higher porosity, in contrast to Figure 5.31, the reflection coefficients decrease with the angle of incidence which is characteristic of class IV type gas sand.

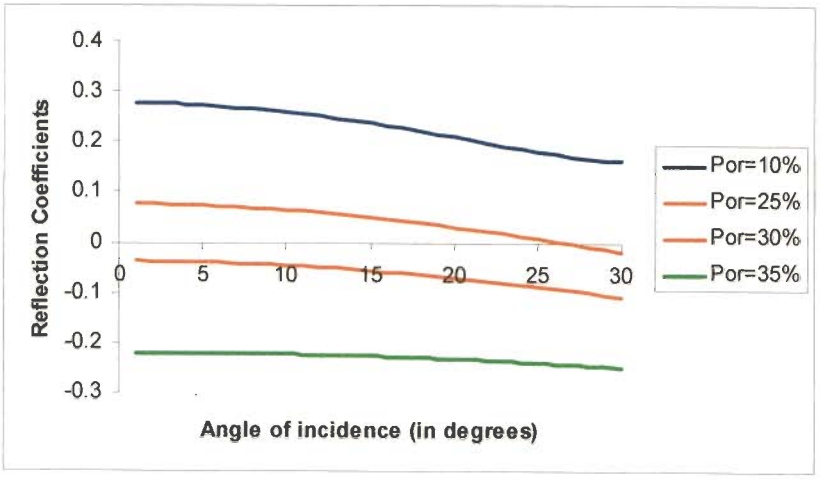

Figure 5.30: ***Variation of P-wave reflection co-efficients with incident angle at the first interface for different porosities. Pore fluid is gas and water.***

Table 5.2: ***Model Parameters for Solid Constituents***

Layer No:	P-wave velocity (m/sec)	S-wave velocity (m/sec)	Density (kg/m^3)	Thickness (m)
1.	2957	1774	2330	2500
2.	5411*	3246*	2593*	100
3.	3048	1829	2340	-

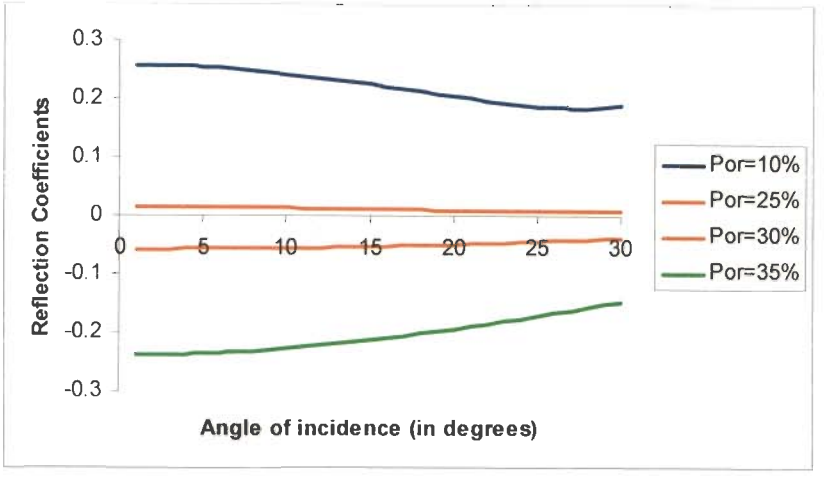

Figure 5.31: ***Variation of P-wave reflection co-efficients with incident angle at the first interface for different porosities. Pore fluid is gas and water.***

5.3.6 Synthetic Seismograms

Figure 5.32 shows the synthetic seismograms, computed at 20 offsets, varying from 100 m to 2000 m. simulating a CMP gather. The second layer is porous and viscoelastic. The

attenuation suffered by the seismic wavelet depends on the length of the path of seismic waves in the dissipative layer. This path in the second layer is longer for far offsets. The broadening of the wavelets with increasing offset can be easily noticed in Figure 5.33, which shows all the 20 wavelets reflected from the second interface plotted on the same time axis.

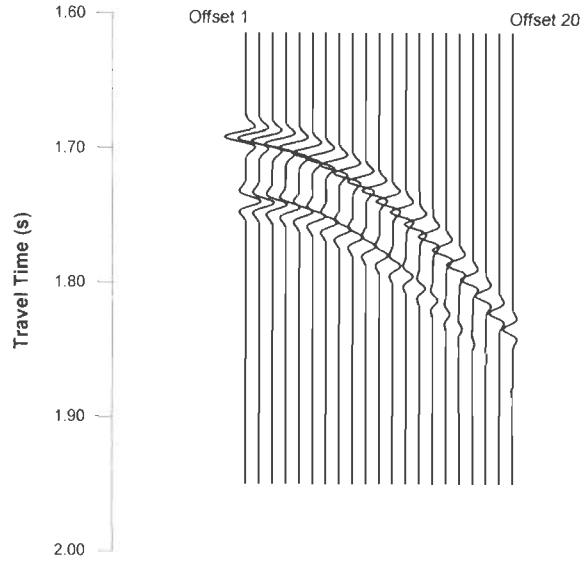

Figure 5.32: ***Synthetic seismograms for 20 offset simulating an AVO situation when second layer is viscoelastic and porous. The pore fluid is gas and water.***

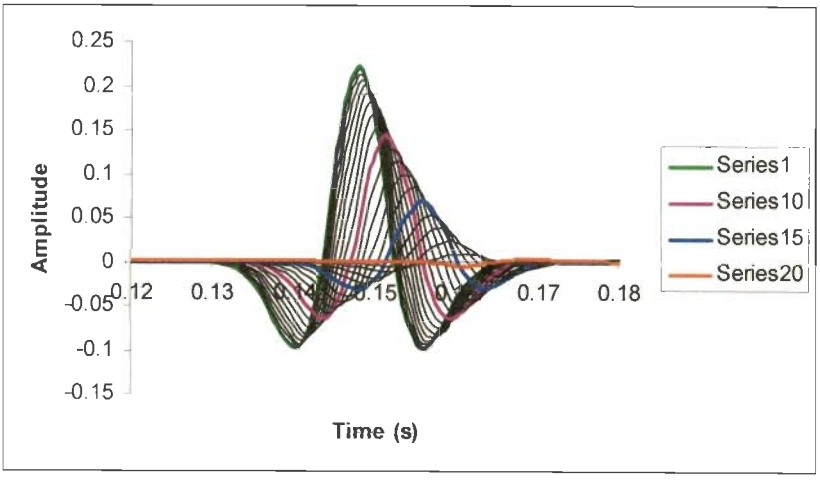

Figure 5.33: ***The wavelets reflected from second interface plotted on the same time axis, showing the attenuation and broadening of wavelets with offset. The pore fluid is gas and water.***

5.3.7 Amplitudes of Seismic Wavelets

Variation of the peak amplitude of seismic wavelets with offset, reflected from the second interface, show the influence of the interstitial fluids on the amplitudes.

Figure 5.34 depicts the variation of peak amplitude with offset for different fluids. The amplitudes are highest in the presence of gas and water. These curves indicate the influence of pore fluids on the peak amplitudes of seismic wavelets is quite distinct and significant. The observed differences are due to the fluid-dependent reduction in seismic wave velocities that affect reflection coefficients.

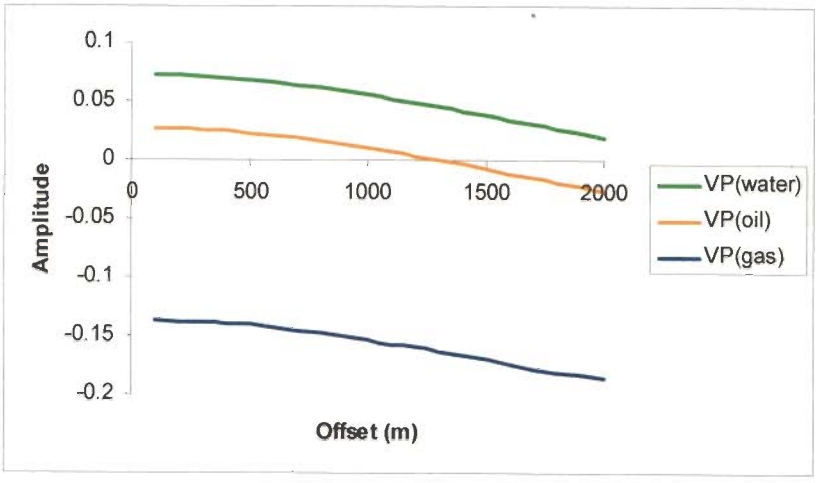

Figure 5.34: ***Comparison of the variation of peak amplitude of the wavelets with offset for different fluids. The porosity is 30%.***

Figure 5.35 (a) and Figure 5.36 (a) show the variation of the peak amplitude at different offsets for different water saturations for gas (and water) and oil (and water) respectively. It is observed that amplitudes increase with increasing water saturation. This effect is more pronounced in the presence of gas and water. This effect will be more pronounced at higher porosity. Lowering of P-wave velocity with increasing oil and gas saturation that leads smaller impedance contrast is the cause of this effect. Figure 5.35 (b), Figure 5.36 (b) and Figure 5.37 show the variation of the peak amplitude of the wavelets with offset for gas (and water), oil (and water) and only water respectively for different porosity values. It is observed that the amplitude – offset curves are quite distinct for

different porosities. The differences in amplitudes at different porosities are observed to be greater at near offsets. The smaller difference at far offsets is due to greater attenuation in the viscoelastic layer. These curves display the influence that porosity and pore fluids have on amplitudes of seismic wavelets.

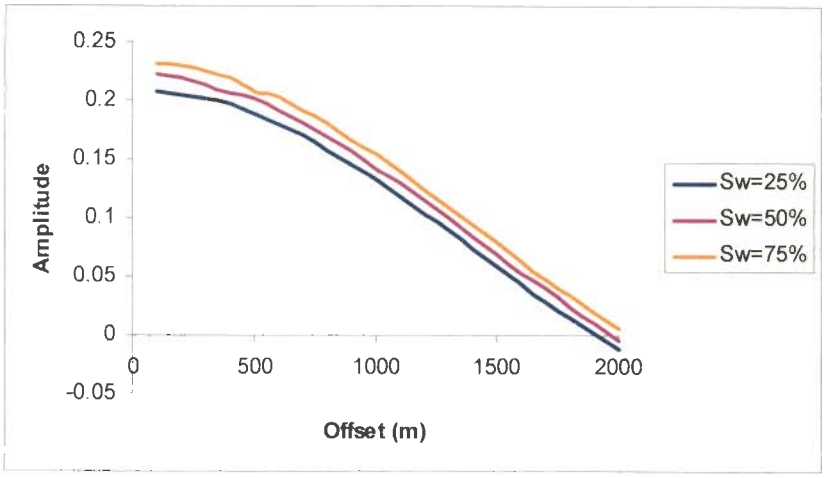

(a)

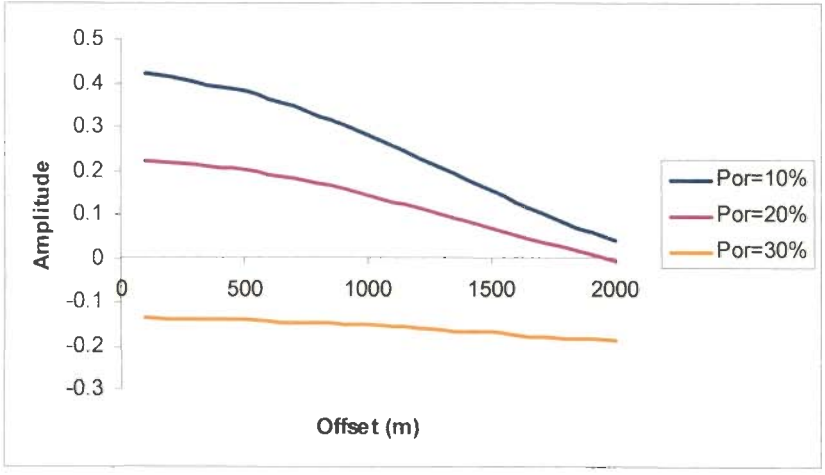

(b)

Figure 5.35: ***Variation of peak amplitude of the reflected wavelets with offset when pore fluid present in the reservoir is gas and water; (a) for different saturations (b) for different porosities.***

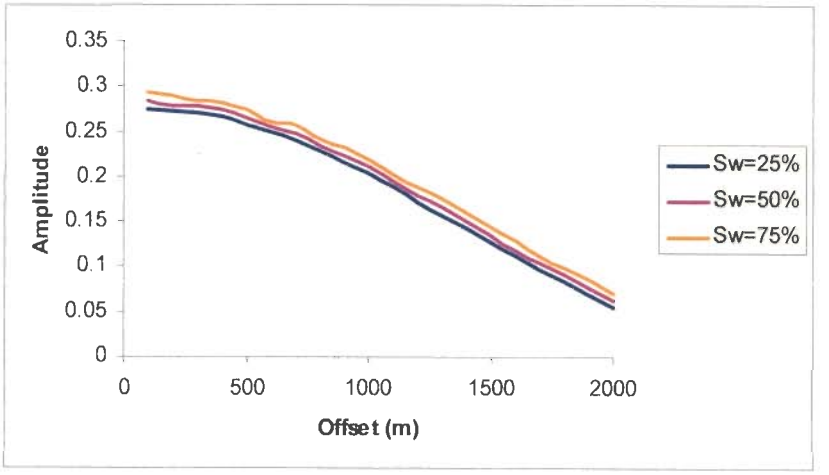

(a)

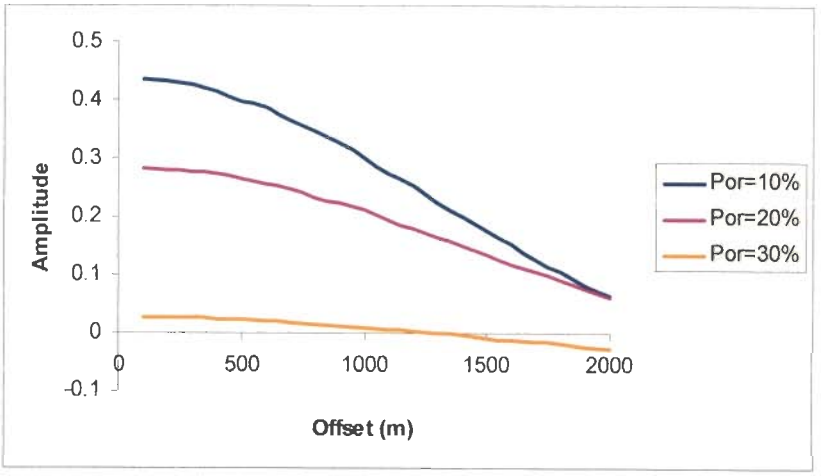

(b)

Figure 5.36: ***Variation of peak amplitude of the reflected wavelets with offset when pore fluid is oil and water; (a) for different saturations (b) for different porosities.***

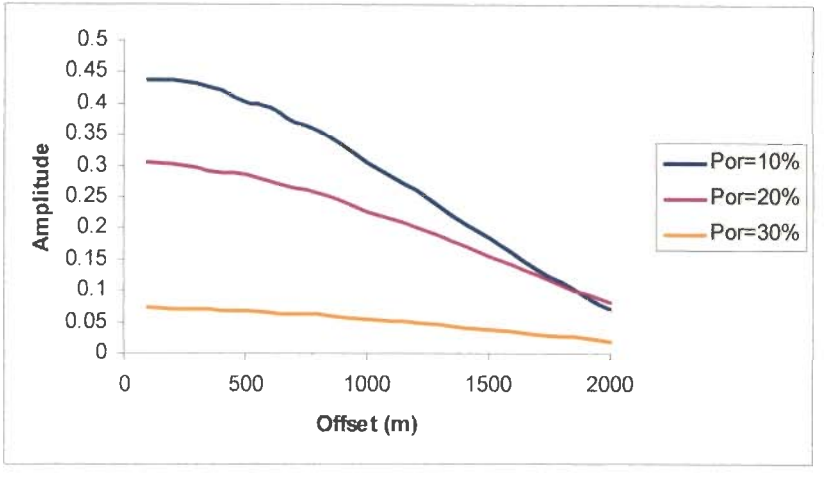

Figure 5.37: ***Variation of peak amplitude of the reflected wavelet with offset for different porosities when reservoir is 100% saturated with water.***

In order to bring out more clearly the effect of porosity and pore fluids on seismic wavelets, the NMO (normal move out) corrected synthetic seismograms have been shown in Figure 5.38 for 20% and 30% porosity values in the presence of gas and water. Similar NMO corrected synthetic seismograms have been shown in Figure 5.39 based on the model parameters given in Table 5.2. In this case, the first layer resembles a hard rock. It is observed that amplitudes of seismic wavelets reflected from first interface, at 20% porosity decrease with offsets for both models. However, for 30% porosity, the amplitudes of seismic wavelets increase with offset when the overlying medium is soft but decrease when the overlying medium is hard.

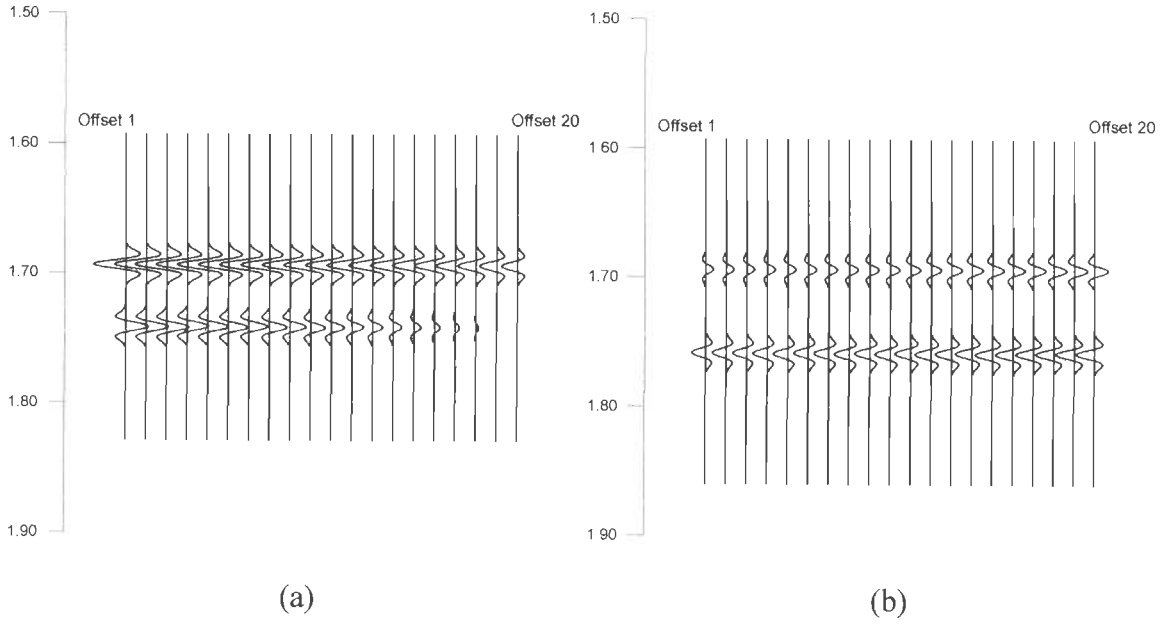

Figure 5.38: ***NMO corrected synthetic seismograms showing variation of amplitude of the reflected wavelets with offset when porosity is (a) 20% and (b) 30%. The pore fluid is gas and water.***

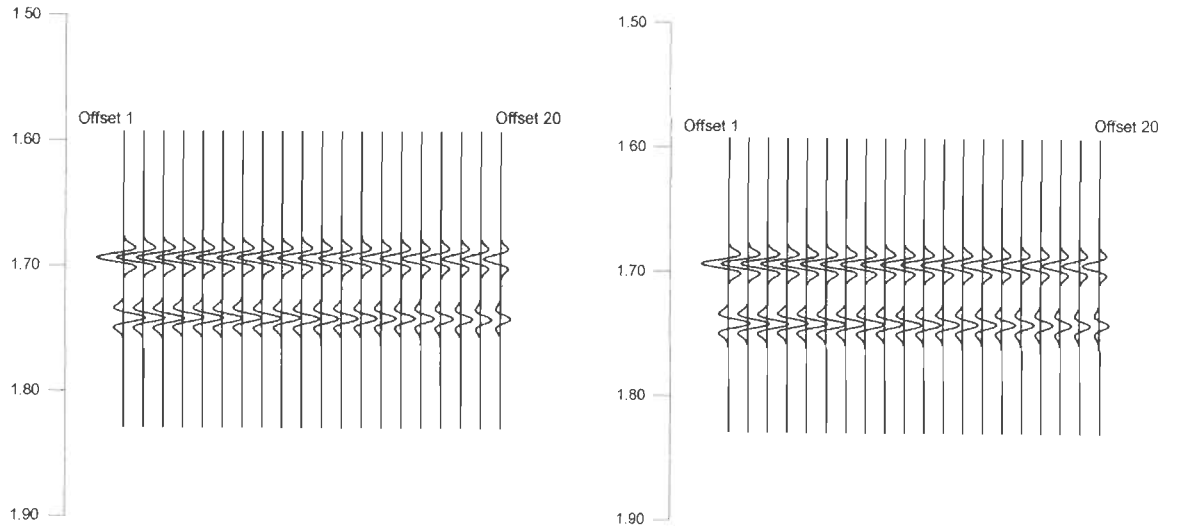

(a) (b)

Figure 5.39: ***NMO corrected synthetic seismograms, based on model parameters given in Table 5.2, showing variation of amplitude of the reflected wavelets with offset when porosity is (a) 20% and (b) 30%. The pore fluid is gas and water.***

Similar NMO corrected synthetic seismograms have been shown in Figure 5.40 when pores contain oil and water and in Figure 5.41 when pores contain only water.

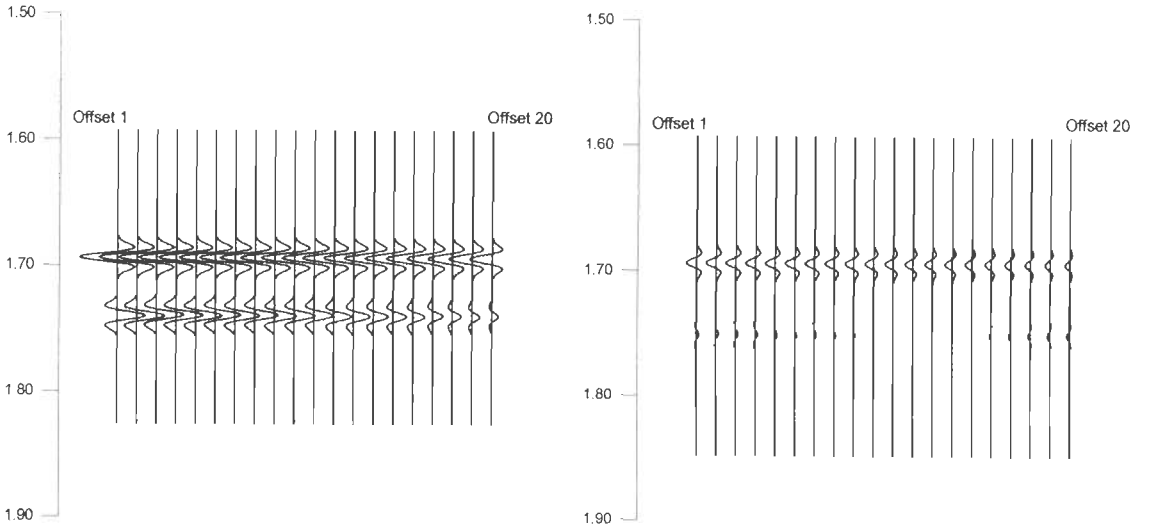

(a) (b)

Figure 5.40: ***NMO corrected synthetic seismograms showing variation of amplitude of the reflected wavelets with offset when porosity is (a) 20% and (b) 30%. The pore fluid is oil and water.***

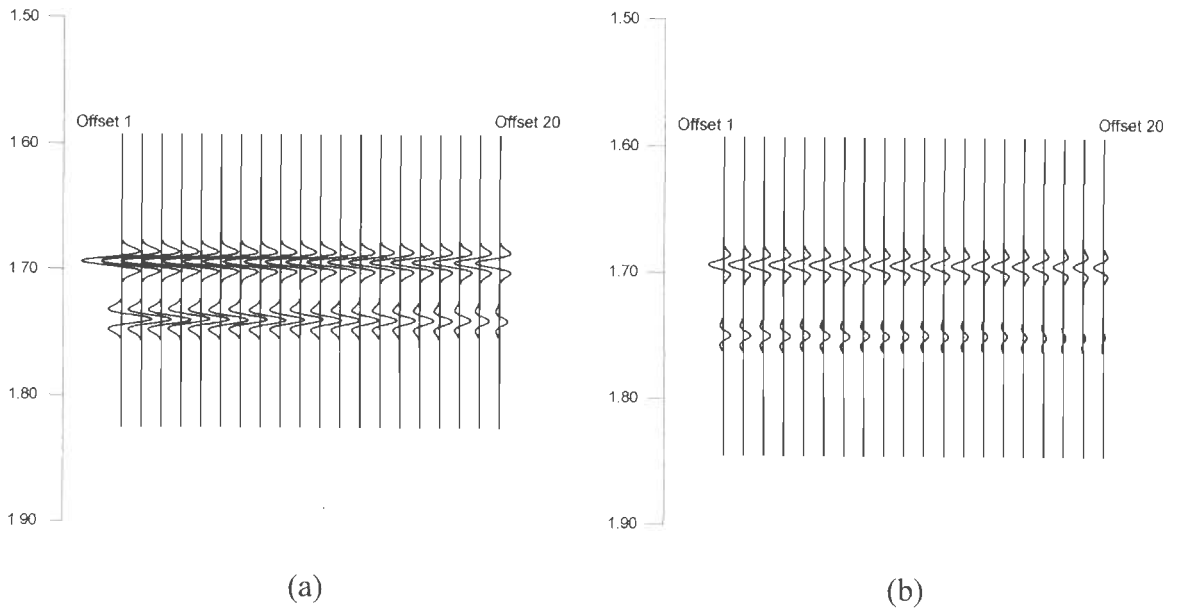

Figure 5.41: ***NMO corrected synthetic seismograms showing variation of amplitude of the reflected wavelets with offset when porosity is (a) 20% and (b) 30%. The pore fluid is water.***

It is observed that, the amplitudes of the wavelets from first interface decrease with offset irrespective of porosity in the presence of oil and water. The wavelets from second interface also decrease in amplitude with offset at 20% porosity. However wavelets from the second interface first decrease in amplitude at near offsets, undergo change of polarity and then increase in amplitude at far offsets. When only water is present in the pores, the amplitudes of wavelets at both interfaces always decrease with offset irrespective of porosity. The broadening of wavelets is observed with increase in offset in all cases due to progressive loss of high frequency components. This change in amplitudes at different offsets are mainly governed by impedance contrasts and hence reflection coefficients (described below) which depend on model parameters.

Figure 5.42 and Figure 5.43 show the variation of reflection coefficients with offset at first and second interface respectively at 30% porosity for different fluids. It is observed that for gas and water, the reflection coefficients increase with offset at both the interfaces. When oil and water is present in the pores, reflection coefficients at first interface decrease with offset. However, at second interface, the reflection coefficients first decreases with

the offset, change sign and then increase with offset (Figure 5.43). The reflection coefficients decrease with increasing offset at both interfaces when only water is present in the pore spaces.

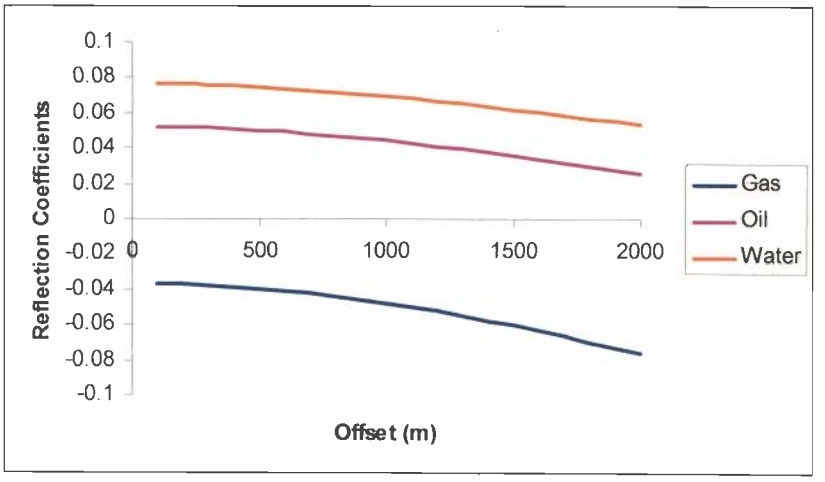

Figure 5.42: ***Comparison of the variation of reflection coefficients with offset at the first interface in the porous viscoelastic layer with 30% porosity for different fluids.***

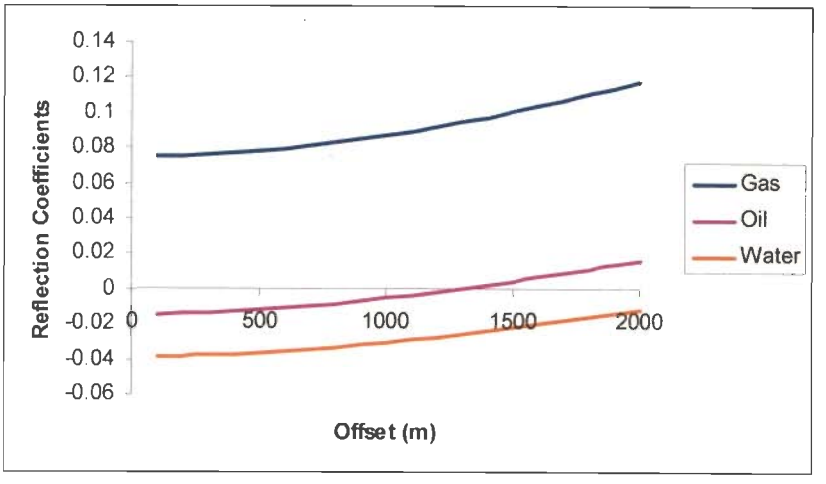

Figure 5.43: ***Comparison of the variation of reflection coefficients with offset at the second interface in the porous viscoelastic layer with 30% porosity for different fluids.***

5.3.8 Shapes of Seismic Wavelets

The shape of the reflected wavelets depends on the varying porosity and the saturation and also on the type of fluid present in the reservoir rock.

5.3.8.1 *Variation with Porosity*

Figure 5.44, shows the wavelets for different porosities in the presence of gas and water at an offset of 100m. There is a change of polarity of the wavelet at 30% porosity. The decrease of amplitude with porosity is the combined effect of reflection coefficient and attenuation. The change in shape of the pulses is not evident due to very small path length in the viscoelastic layer. Figure 5.45 shows the wavelets when oil and water is present, and Figure 5.46, when only water is present. In both these cases, there is no change of polarity even at high porosity.

5.3.8.2 *Variation with Water Saturation*

From Figure 5.47 and 5.48 that show seismic wavelets for different water saturations at 100 m offset, it can be observed that the shapes show small variation with water saturation in the presence of gas and water, but no significant variation when oil and water is present. Overall, it can be stated that water saturation does not have any pronounced effect on the shape of seismic wavelets.

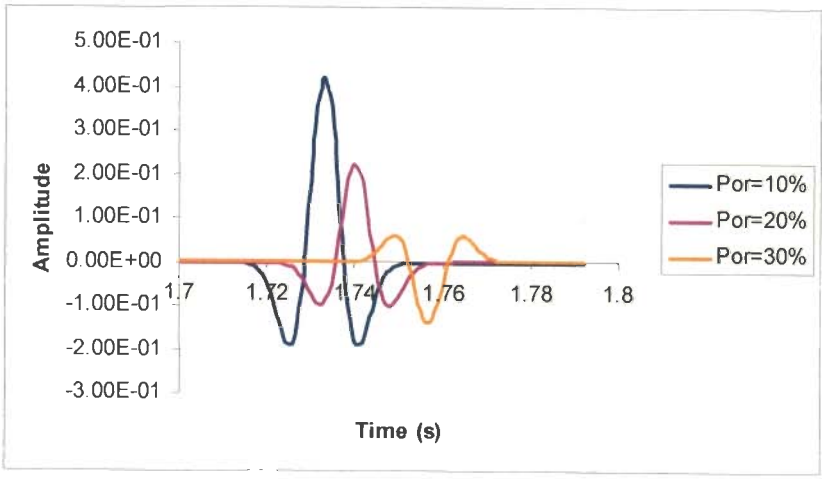

Figure 5.44: ***Comparison of seismic wavelets from second interface at 100m offset for different porosities. The pore fluid is gas and water.***

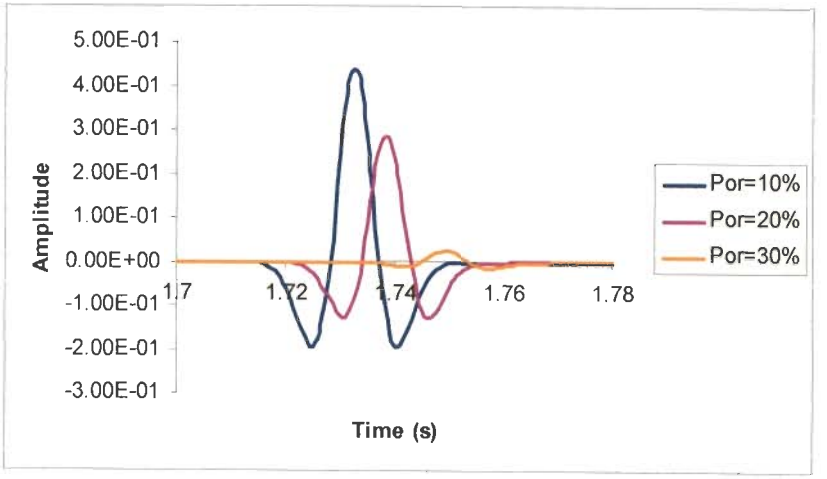

Figure 5.45: ***Comparison of seismic wavelets from second interface at 100m offset for different porosities. The pore fluid is oil and water.***

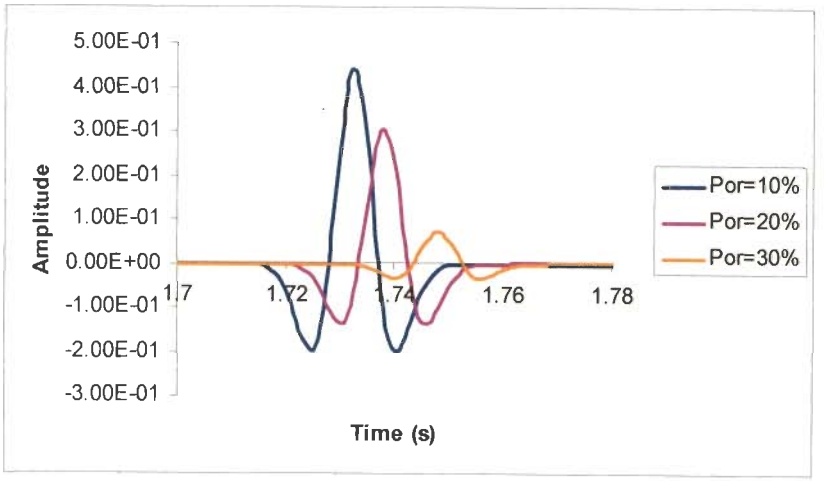

Figure 5.46: ***Comparison of seismic wavelets from second interface at 100m offset for different porosities. The pore fluid is water.***

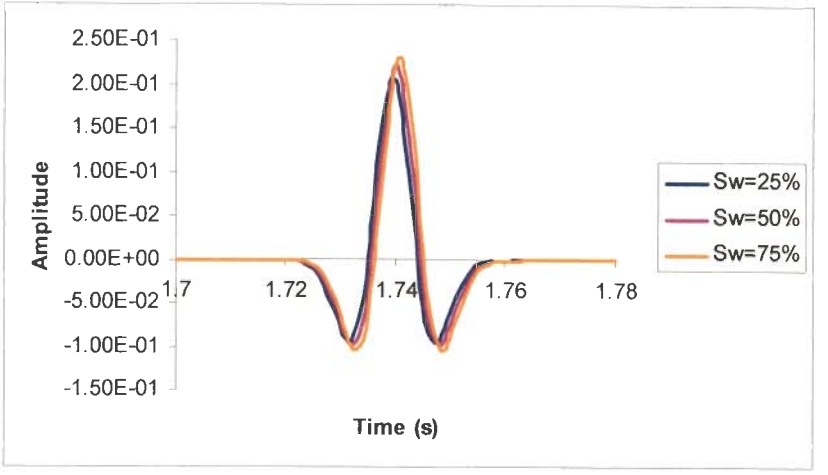

Figure 5.47: ***Comparison of seismic wavelets from second interface at 100m offset for different water saturations. The pore fluid is gas and water.***

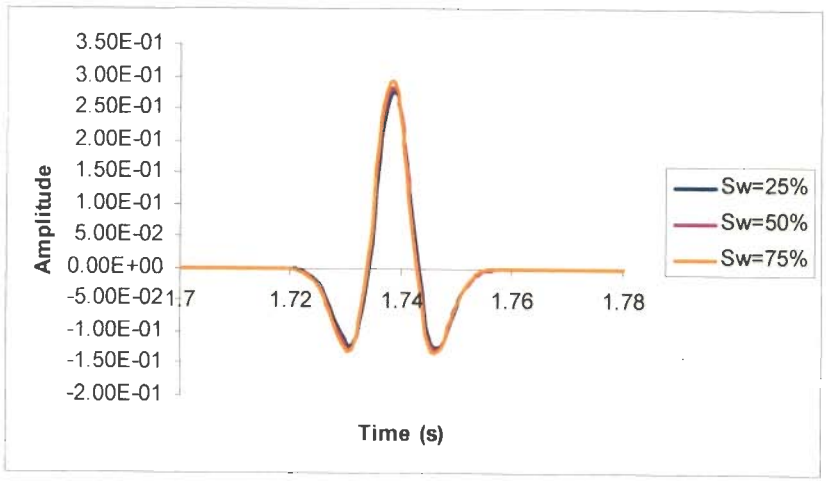

Figure 5.48: ***Comparison of seismic wavelets from second interface at 100m offset for different water saturations. The pore fluid is oil and water.***

5.3.8.3 *Variation with Different API Gravity Oil*

Figure 5.49 shows the seismic wavelets at 2000 m offset for oils having different API gravity. The details of viscosity and density values assumed to define different API gravity oils have been given in the Chapter 4 (Table 4.3). Overall, the pulses show less amplitude for lighter oils. However, the sensitivity of shape of the wavelets to different API gravity oils is not very pronounced. The asymmetric shape of the seismic wavelet in the presence of oil in the pore spaces is easily recognized.

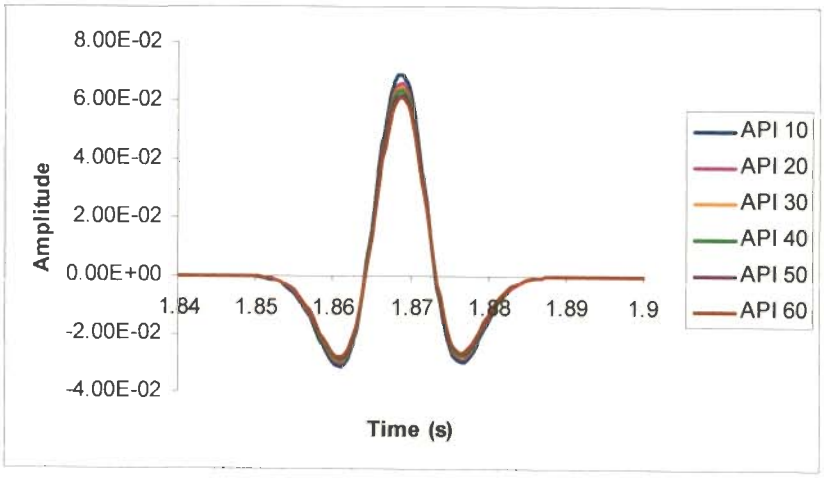

Figure 5.49: ***Comparison of seismic wavelets from second interface at 2000 m offset for oils of different API gravity.***

5.3.8.4 *Variation with Offsets*

The change in the shape of the wavelets with offset due to the effect of viscoelasticity along with the solid – fluid interaction have been shown in the following figures. Figure 5.50, Figure 5.51 and Figure 5.52 show seismic wavelets, reflected from the second interface, at 100 m, 1500 m and 2000 m offset respectively when porosity is 20%, and water saturation is 50 % in the presence of oil (and water) or gas (and water) or only water in the porous viscoelastic layer. From these figures, it is seen that wavelets in the case of gas (and water) is present, wavelets have significantly smaller amplitude at all offsets. At 2000 m, there is a change of polarity too. The fluid dependent change of shape and delay induced due to frequency dependent nature of wave velocities is also evident with increase of offset.

Figure 5.53 and Figure 5.54 compare the shape of reflected wavelets from second interface for different fluids at 1500m and 2000m offsets respectively when the porosity of the second layer is 30% and water saturation is 50%. The amplitudes of wavelets are highest when gas (and water) is present. The changes in the shape are marked by unequal amplitudes of side lobes of the wavelets. The changes in shape of the pulses for different fluids and the delays with increasing offsets are also seen. These figures depict the combined effect of reflection coefficients at the second interface, attenuation, and complex and frequency dependent nature of the seismic wave velocities on the shapes of seismic wavelets. Thus, it can be stated that the change shapes of seismic wavelets with offset are distinct for a given fluid type. These variations can be used to identify the type of fluids in the porous viscoelastic layer.

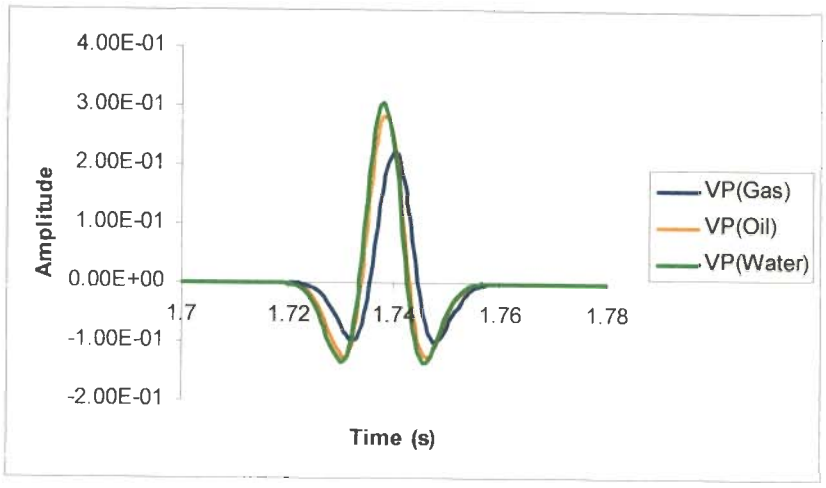

Figure 5.50: ***Comparison of seismic wavelets from second interface at 100m offset for different fluids***

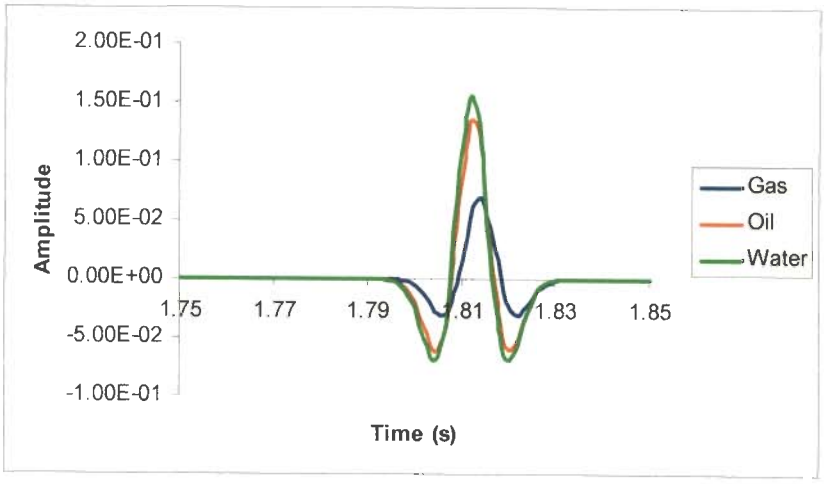

Figure 5.51: ***Comparison of seismic wavelets from second interface at 1500m offset for different fluids.***

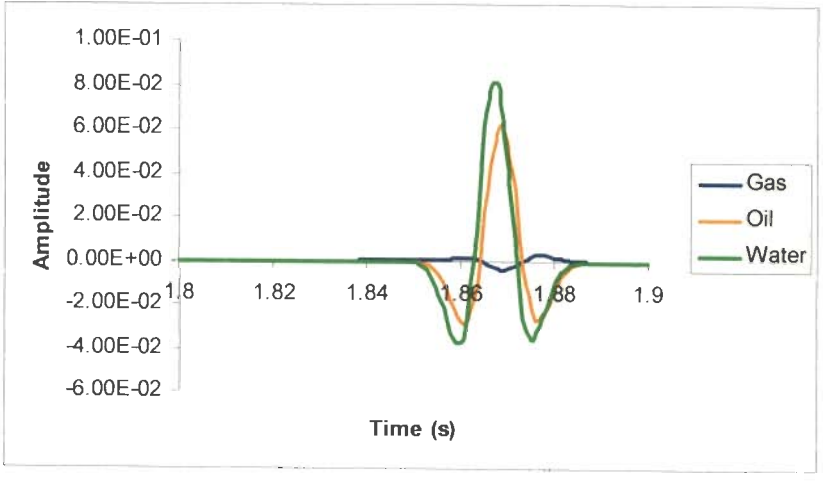

Figure 5.52: ***Comparison of seismic wavelets from second interface at 2000m offset for different fluids.***

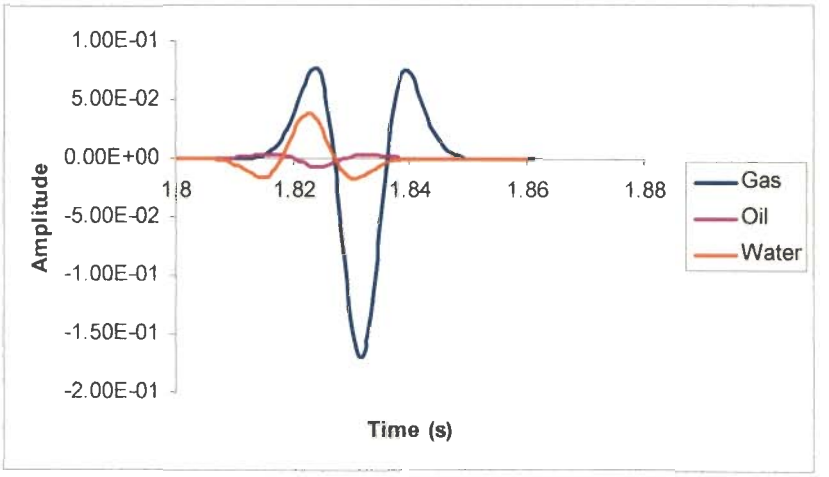

Figure 5.53: ***Comparison of seismic wavelets from second interface at 1500m offset for different fluids when porosity is 30%.***

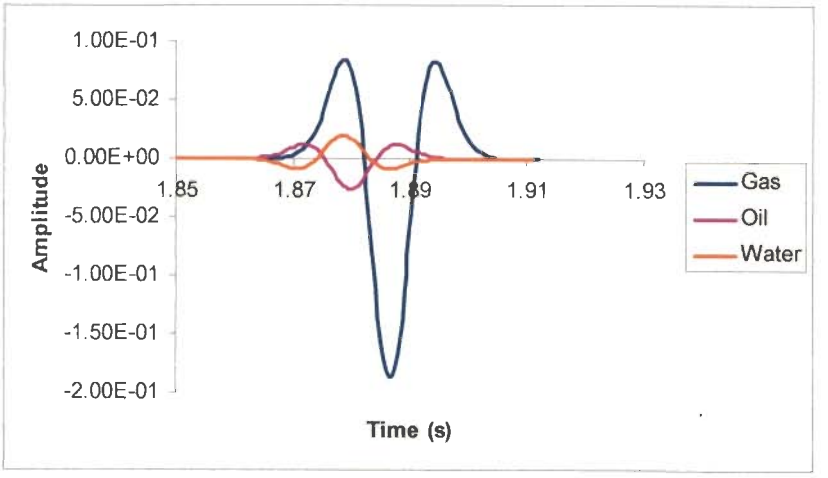

Figure 5.54: ***Comparison of seismic wavelets from second interface at 2000m offset for different fluids when porosity is 30%.***

5.3.9 AVO Attributes

Values of AVO attributes A and B have been computed when gas is present in the pores and are shown in Table 5.3 and 5.4. These A and B values can be used to differentiate different types of gas sands. A and B values have been given in Table 5.3 for different porosities and in Table 5.4, for different water saturations. The errors have been calculated from deviations of computed from actual values. It can be seen that values of A and B are quite sensitive to changes in porosity and water saturations.

Table 5.3: ***A and B Values for Varied Porosities***

Porosity	Actual (A)	Inverted (A)	Actual (B)	Inverted (B)	Error in % (A)	Error in % (B)
10%	0.279	0.277	-0.702	-0.623	0.7	11.2
20%	0.159	0.159	-0.487	-0.553	0.23	11.9
30%	-0.0371	-0.0372	-0.321	-0.277	0.11	13.7

Table 5.4: ***A and B Values for Varied Water Saturations***

Sw	Actual (A)	Inverted (A)	Actual (B)	Inverted (B)	Error in % (A)	Error in % (B)
25%	0.152	0.153	-0.546	-0.488	0.48	10.7
50%	0.159	0.159	-0.487	-0.553	0.23	11.9
75%	0.165	0.165	-0.559	-0.487	0.009	12.9

5.4 PART III: COMPARISON WITH CONVENTIONAL APPROACH

In the present work, a three layered earth model has been considered where the second layer is considered to be viscoelastic and porous having viscous fluid in the pore spaces. The seismic wave velocities in the porous medium have been estimated using Biot's theory. However, conventionally, it is assumed that the solid medium of the earth behaves elastically and the seismic wave velocities are predicted by using the time average relationship (TAR), an empirical relation. In the following paragraphs, results of a comparative study have been presented wherein the results of the present work and those obtained using the conventional approach have been compared.

The attenuation of the seismic wavelets and its shape has been compared with the seismic wavelets obtained on assuming the second layer to be elastic and porous and the seismic wave velocities estimated using the time average relationship. This comparison has been carried out at selected offsets. This comparative study has been carried out when the reservoir contains gas and water, and oil and water when porosity is 30% and water saturation, 50%.

5.4.1 Variation of Seismic Wave Velocities with Porosity

The Figure 5.55 (a) and (b) compares the variation of the P- wave velocities with porosity obtained using Biot's theory (at 50 Hz frequency) with those obtained from conventional time average relationship, when the reservoir is saturated with gas and water or with oil and water respectively. These velocity – porosity curves show different trends. The velocities estimated using time average relationship show much greater change with porosity. The changes are greater when gas (and water) is present. Consequently, the impedance contrasts will be greater and reflection coefficients will be higher with conventional approach.

5.4.2 Reflection Coefficients

Figure 5.56 (a) and (b) compare the variation of reflection coefficients with offset for VP and TAR at the first and second interface respectively when reservoir is saturated with gas and water. Similarly, Figure 5.57 (a) and (b) compare the variation of reflection coefficients with offset at first and second interface, respectively, when oil and water is present in the pore spaces.

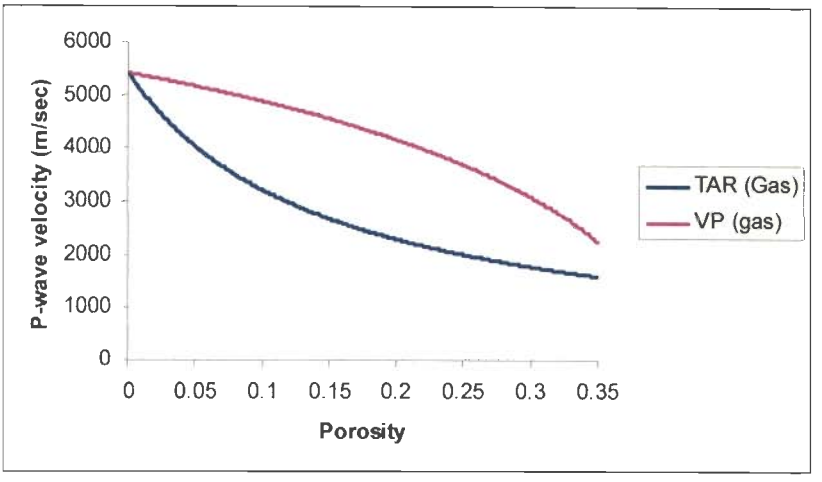

(a)

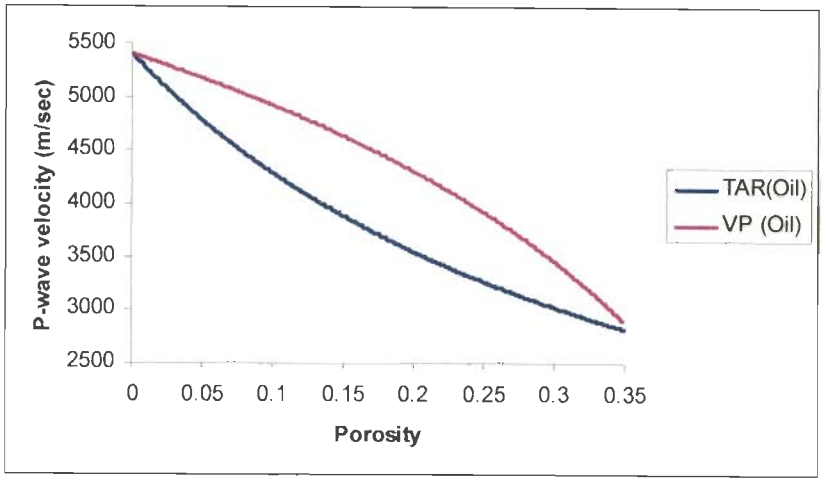

(b)

Figure 5.55: ***Comparison of the variation of P-wave velocity for VP and TAR with porosity when the second layer contains (a) gas and water (b) oil and water.***

It is evident from these figures that even for same type of fluid, the values of reflection coefficients are very much different. TAR values of reflection coefficients are higher for gas and water at both interfaces because of the greater reduction in the seismic wave velocities. However, in case of oil and water, VP reflection coefficients are higher.

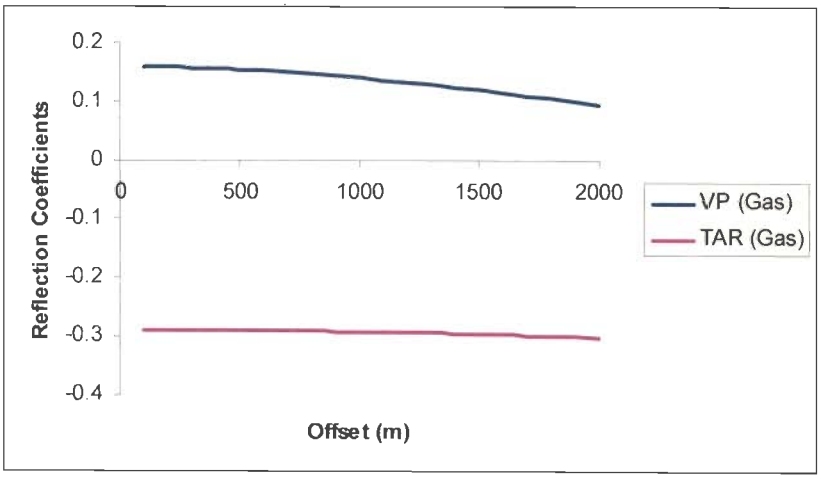

(a)

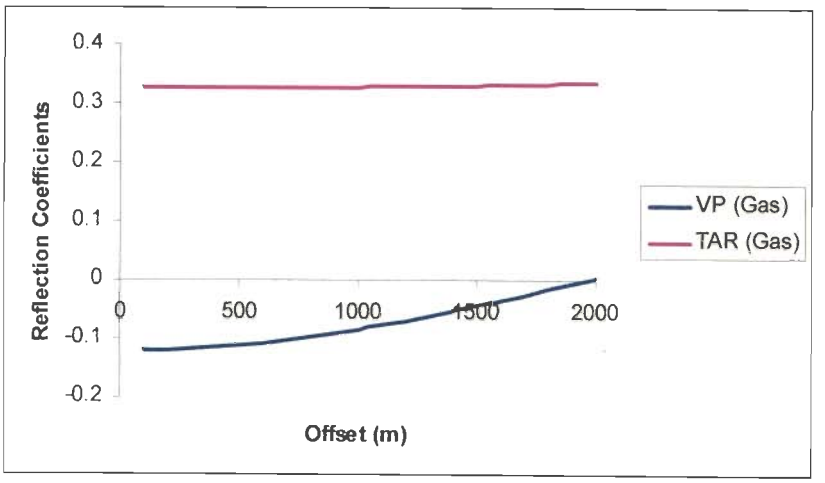

(b)

Figure 5.56: ***Comparison of the variation of reflection coefficients with angle of incidence at the (a) first interface and (b) second interface. Pore fluid is gas and water.***

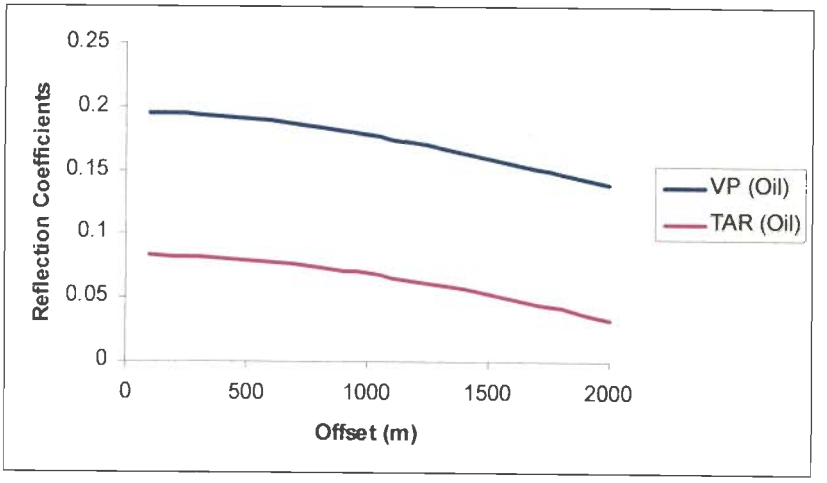

(a)

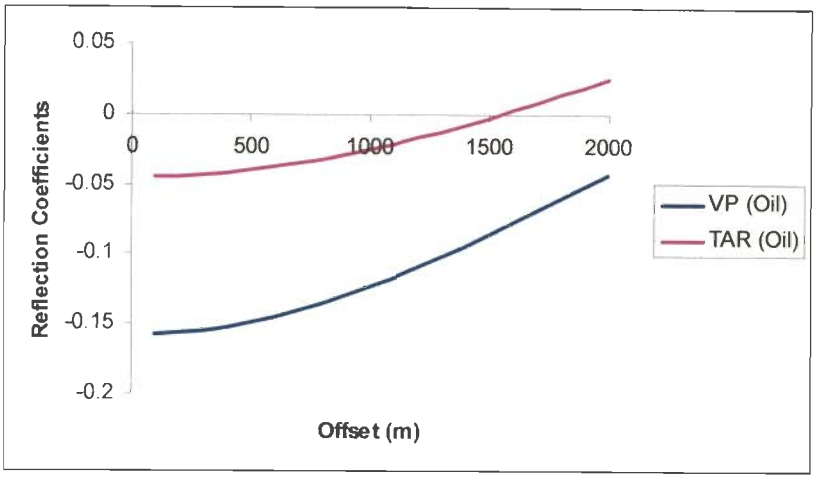

(b)

Figure 5.57: ***Comparison of the variation of reflection coefficients with angle of incidence at the (a) first interface and (b) second interface. Pore fluid is oil and water.***

5.4.3 Synthetic Seismograms

Figure 5.58 (a) and (b) show NMO corrected synthetic seismograms when viscoelastic layer is saturated with gas and water for TAR and VP cases respectively. It is observed that the TAR seismograms show increase of amplitude of wavelets with offset when porosity is 20%. On the other hand, at the same porosity value, the wavelets computed in present work, show decrease of amplitude with offset. The increase of amplitudes with offsets for VP case takes place at a porosity of 30% and above. Similarly, Figure 5.59 (a) and (b) show NMO corrected synthetic seismograms when the viscoelastic layer is saturated with oil and water for TAR and VP case respectively. When oil and water is present in the pore spaces, both TAR and VP synthetic seismograms show decrease of amplitude of wavelets with offset. The wavelets for TAR case show polarity reversal.

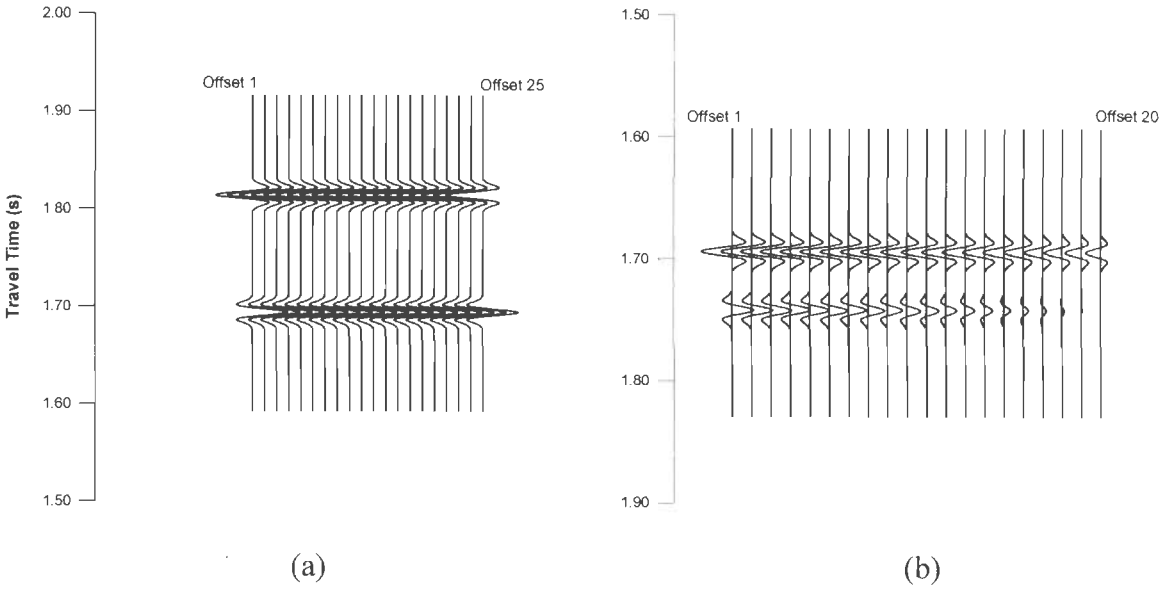

Figure 5.58: ***NMO corrected synthetic seismograms for 20 offsets simulating an AVO situation in case of (a) TAR and (b) VP. Pore fluid is gas and water.***

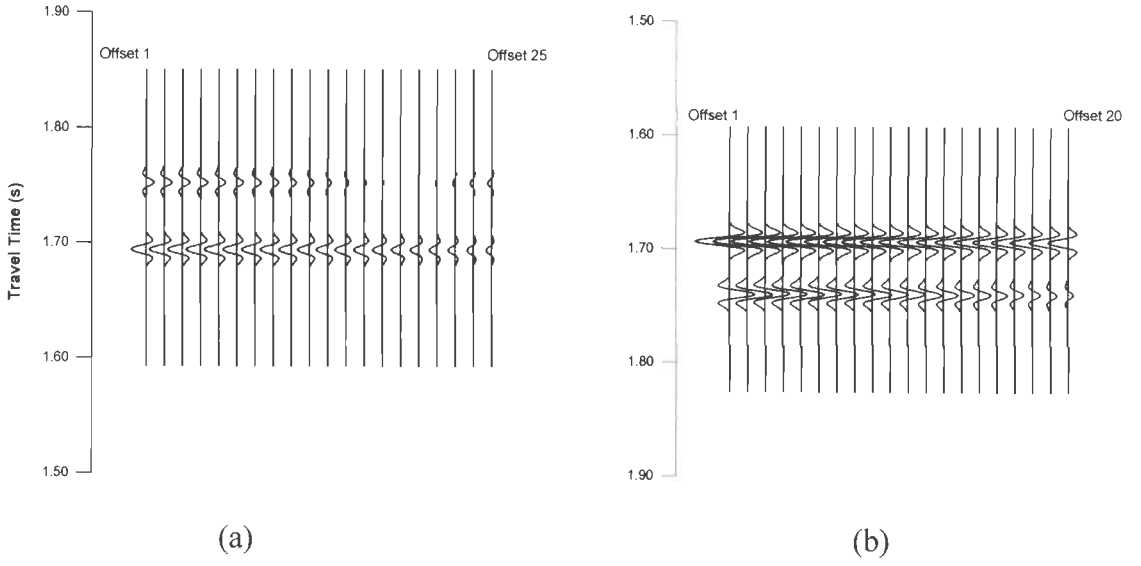

(a) (b)

Figure 5.59: ***NMO corrected synthetic seismograms for 20 offsets simulating an AVO situation in case of (a) TAR and (b) VP. Pore fluid is oil and water.***

5.4.4 Shapes of the Seismic Wavelets

A comparative study has been carried out of on the shapes of the reflected wavelets from second interface at the 2000 m offset for VP and TAR case. Figure 5.60 shows the wavelets when porous medium is saturated with gas and water when porosity is 30%. It is observed that the TAR wavelets show higher amplitude than those of VP. However, VP wavelets are delayed in time due to the effect of viscoelasticity. The VP wavelets also show asymmetry of shape. In Figure 5.61 the shape of the wavelets for the two cases are compared when oil and water is present in the pores when porosity is 30%. The TAR wavelets show higher amplitude. The differences in amplitudes of the VP and TAR wavelets are also the result of attenuation in the viscoelastic layer.

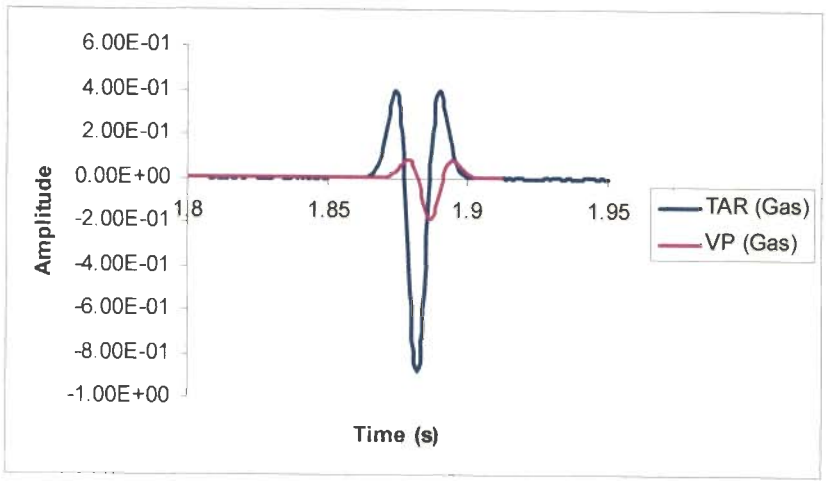

Figure 5.60: ***Comparison of seismic wavelets from second interface at 2000 m offset for VP and TAR. Pore fluid is gas and water and porosity is 30%.***

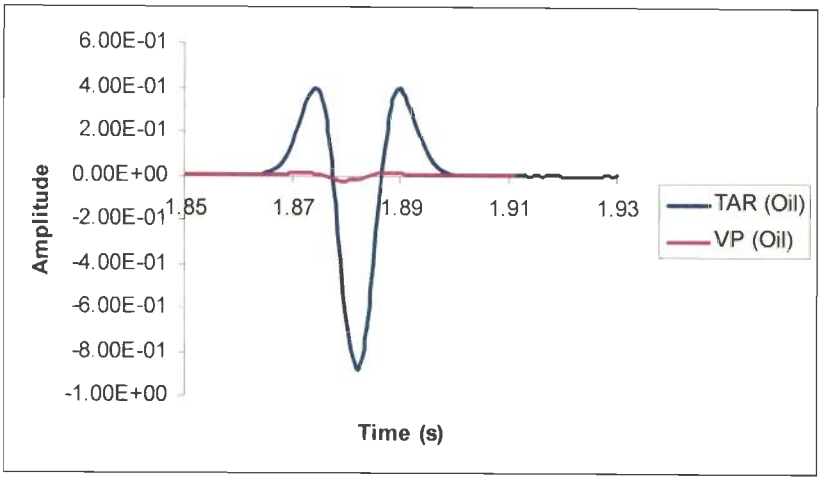

Figure 5.61: ***Comparison of seismic wavelets from second interface at 2000 m offset for VP and TAR. Pore fluid is oil and water and porosity is 30%.***

5.5 PART IV: QUANTIFICATION

A computation has been carried out to obtain normal incident reflected wavelets so that the effect of angle of incidence on the reflection coefficients for non-normal reflections can be avoided and the total effect of viscoelasticity and fluid interaction can be quantified.

5.5.1 Effect of Viscoelasticity

The effect of viscoelasticity on the reflected seismic wavelets has been quantified by comparing the wavelets obtained when P-waves are normally incident on both interfaces and second layer is (i) elastic and non-porous and (ii) viscoelastic and non-porous. The

thickness of the second layer has been taken to be 100 m for this study. The Figure 5.62 compares the amplitude of these reflected wavelets. It is observed that the amplitude of VNP wavelet is 0.2 dB lower than the EL wavelet. This attenuation will increase with the thickness of the second layer in VNP case. This has been clearly brought out in Figure 5.63 where the amplitude diminution factor, i.e., $exp(-\alpha x)$, where α is attenuation coefficient and x is the distance, has been plotted against the distance in the viscoelastic covered by waves. The amplitude diminution factor decreases with the increasing distance.

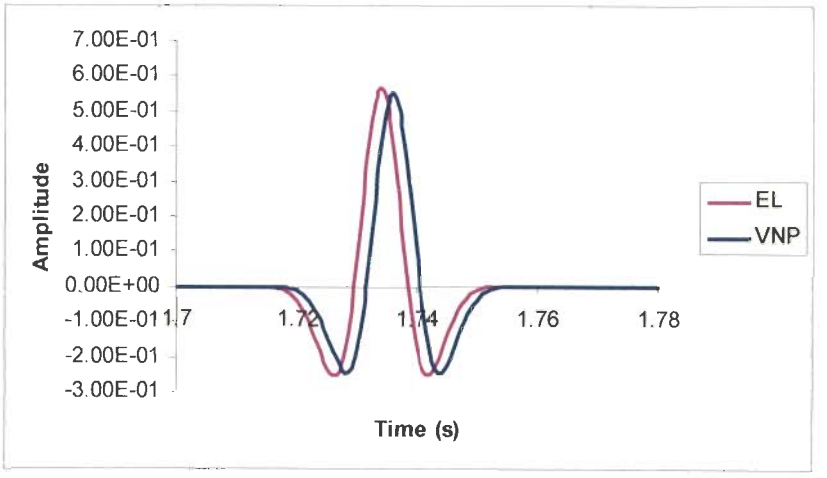

Figure 5.62: ***Comparison of reflected seismic wavelets for normal incidence, for EL and VNP, reflected from second interface depicting. The thickness of the second layer is 100m.***

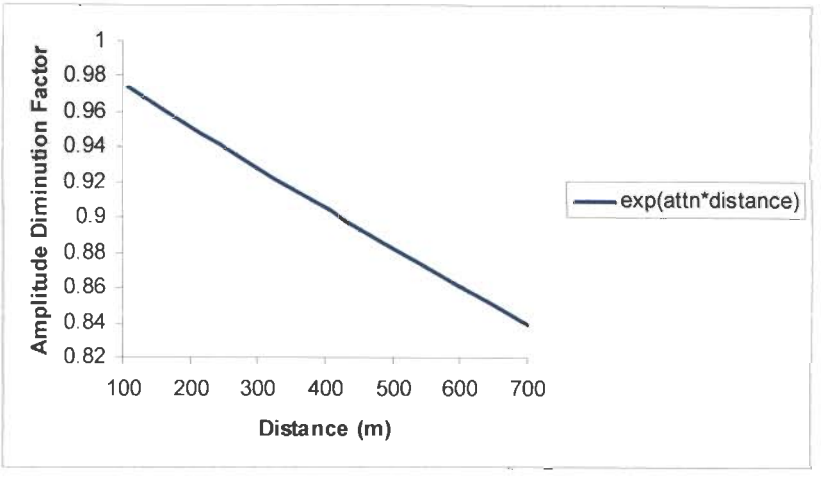

Figure 5.63: ***Variation of amplitude diminution factor, (exp(-αx),) with the distance traveled by the waves in viscoelastic non-porous layer. The term 'attn' stands for attenuation coefficient.***

5.5.2 Effects of Solid-Fluid Interaction and Viscoelasticity on Wavelets

A computation has been carried out wherein the seismic wavelets computed for normally incident P-waves for VNP and VP cases have been compared to quantify the effect of solid-fluid interaction and viscoelasticity. Figure 5.64 ((a) to (c)) compares wavelets when the 100 m thick viscoelastic layer contains gas (and water), oil (and water) and only water in the pore spaces when porosity is 20% and water saturation is 50% for oil and gas horizons. As expected, the wavelets show least amplitude in case of gas and water filled pores with a 3.82 dB loss of amplitude with respect to the VNP wavelet. The amplitude loss in case of oil and water and only water is 2.73 dB and 2.46 dB respectively. It is observed from Figure 5.50 to Figure 5.54 that the amplitude of the reflected wavelets varies with porosity. As a result the amplitude loss in dB for different porosities with respect to amplitude of the reflected wavelets obtained from VNP case has been given in Table 5.5.

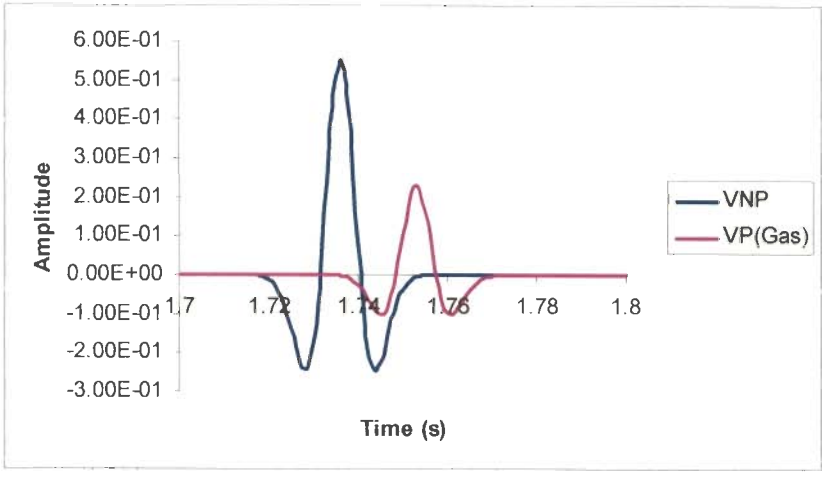

(a)

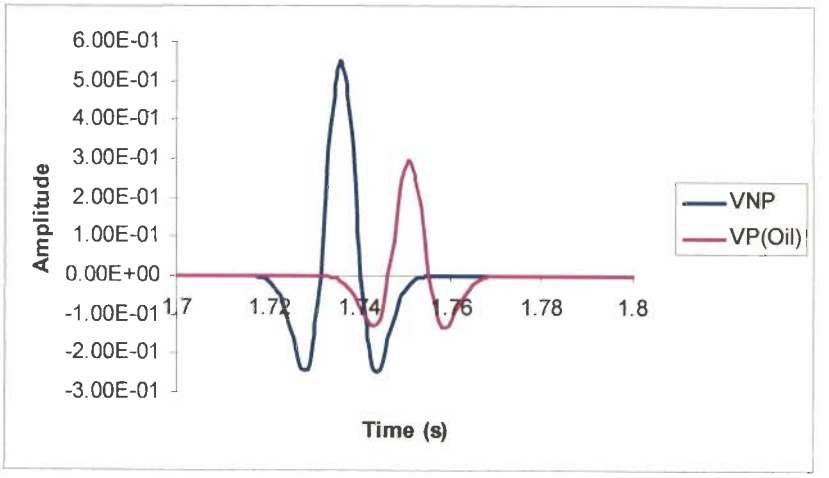

(b)

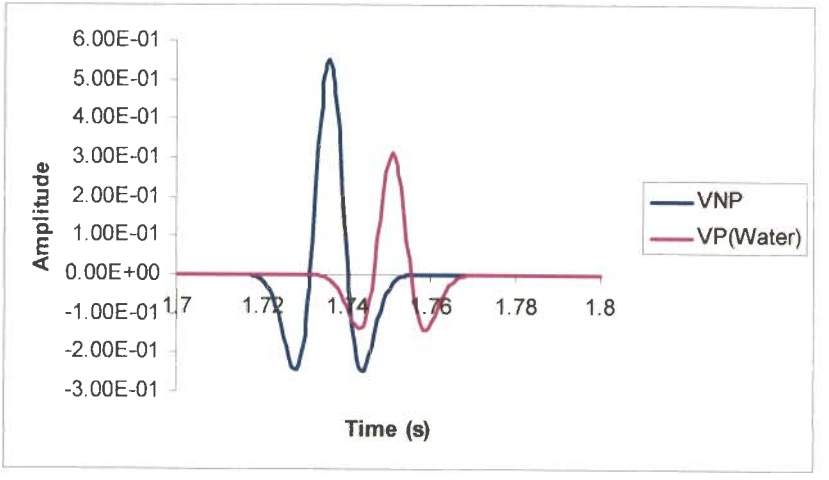

(c)

Figure 5.64: ***Comparison of reflected wavelet for normal incidence, for VNP and VP; (a) gas and water, (b) oil and water (c) only water.***

Table 5.5: ***Loss of Amplitude of Wavelets for Different Porosities***

Porosity	VNP	VP(Gas)	dB	VP (Oil)	dB	VP (Water)	dB
10%	0.551456	0.431	1.07	0.452	0.87	0.458	0.83
20%		0.229	3.82	0.294	2.73	0.313	2.46
30%		-0.143	5.88	0.028	12.9	0.074	8.70

5.5.3 Effect of Fluids on Amplitude Diminution Factor

As explained earlier, the attenuation of the amplitude increases with distance traveled by the wave in the viscoelastic porous layer. The type of pore fluid effects the total attenuation of the amplitude in a porous medium. Figure 5.65 shows the variation of the amplitude

diminution factor with the distance in the viscoelastic porous layer in the presence of gas and water or oil and water or only water. Overall, the magnitude of this factor decreases with the distance for each type of fluid. However, the amplitude diminution factor shows smallest value when gas and water is present in the pore spaces.

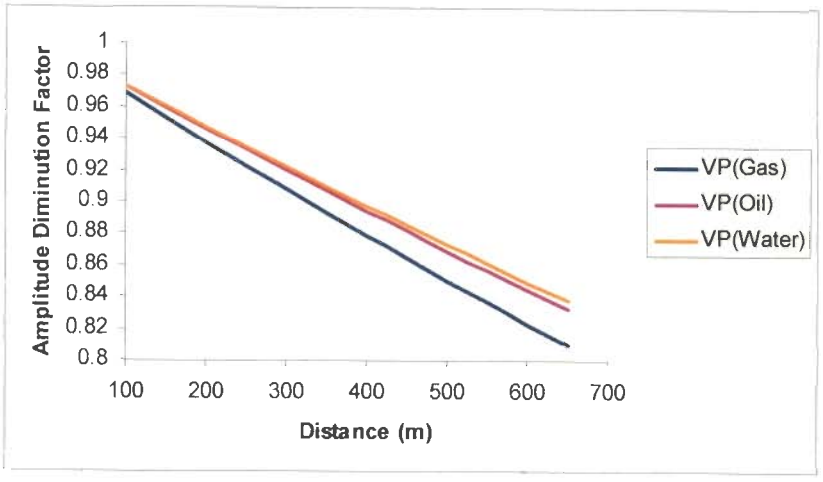

Figure 5.65: ***Variation of amplitude diminution factor, (exp(-αx)), with the distance traveled by the waves in viscoelastic porous layer for different fluids.***

5.5.4 Seismograms for Wedge Shaped Second Layer

The Figure 5.66 shows normally incident synthetic seismograms at the surface of three layered earth for a wedge shaped second layer. The wedge is viscoelastic porous having 20 % porosity and saturated with gas and water. The amplitudes of the reflected wavelets for VP and TAR cases for the wedge shaped second layer have been listed in Table 5.6.

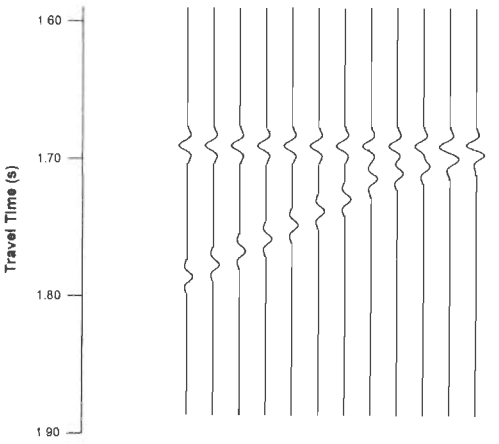

Figure 5.66: ***Normal incident synthetic seismograms at the surface of three-layered earth model where the porous viscoelastic layer is wedge shaped. Pore fluid is gas and water.***

Table 5.6: ***Thickness, amplitude of reflected pulses calculated using TAR and VP***

	TAR	VP
Thickness (m)	Amplitude	Amplitude
200	-0.595	0.223
180	-0.595	0.224
160	-0.595	0.225
140	-0.595	0.227
120	-0.595	0.228
100	-0.595	0.230
70	-0.595	0.231
50	-0.595	0.234
40	-0.595	0.234
30	-0.595	0.235
20	-0.595	0.236
10	-0.595	0.237

CHAPTER – 6
SUMMARY AND CONCLUSIONS

6.1 INTRODUCTION

In seismic prospecting, seismic waves propagate through the real earth during data acquisition. The recorded data has to undergo a number of processing processes before it is ready for interpretation. For interpretation purpose, simplified earth models are used. For example, earth is assumed to be composed of elastic, homogeneous and isotropic layers. However, none of the above conditions is met in the real earth, which is much more complex in its structure and physical properties. Real earth materials are commonly anelastic as illustrated by material dependent attenuation of seismic waves that leads to progressive loss of high frequency components from the wavefield. A part of energy of the seismic waves is converted into heat and the shape of seismic wavelets changes. It has been suggested that pore fluids like gas, oil and water present in the pore spaces of reservoir rocks also influence the attenuation and dispersion of seismic waves and a study of the changes of shape of seismic wavelets can lead to identification and characterization of pore fluids. One of the objectives of the work presented in this thesis is to study and quantify the effect of anelasticity of solid matrix and type and amount of pore fluids on the shape of reflected seismic wavelets. Some of the properties of fluid saturated anelastic porous media that are important in this work are following: viscoelastic properties of solid materials, porosity, water saturation, viscosity of pore fluids, and velocities and bulk densities of porous media.

6.2 SUMMARY

In order to achieve above objectives, synthetic seismograms have been generated at the surface of a three layered earth model at 20 offsets varying from 100 to 2000 m. The

porous and viscoelastic second layer of the earth model is assumed to be 100 m thick whereas first and third layers are elastic. A 50 Hz Ricker pulse has been used as the source wavelet. The upper interface of the viscoelastic layer lies at a depth of 2500 m. Standard Linear Solid (SLS) model of viscoelasticity has been used to represent the viscoelastic behavior of the second layer. Biot's theory has been used to compute the complex and frequency dependent seismic wave velocities in the porous viscoelastic layer. A boundary value problem has been solved for plane waves incident on the interface separating elastic and visoelastic media and equations similar to Zoeppritz equations have been derived to compute reflection coefficients of reflected P-waves from the top and bottom of the viscoelastic layer. The shapes of reflected seismic wavelets have been studied and analyzed. The porous viscoelastic medium is assumed to be saturated with gas and water, oil and water or only water. The results of present work have been compared with those that are obtained using conventional approach. An attempt has also been made to quantify the effect of viscoelasticity and pore fluids on the shapes of seismic wavelets.

6.2 CONCLUSIONS

The results of the present work lead to following conclusions:

- ✓ Viscoelasticity of the solid matrix of the propagating medium and interstitial fluids do produce measurable changes in the shapes of reflected seismic wavelets in the seismic frequency range (1-100 Hz).
- ✓ The variation of reflection coefficients with frequency is more significant at low frequencies than high frequencies. At the lowest velocity values at low frequencies (1 Hz.), the reflection coefficient is nearly 3% less than that at 50 Hz. At high frequencies the reflection coefficients virtually coincide with those obtained from the elastic layer.

- ✓ In a porous viscoelastic layer, the frequency dependence of seismic wave velocities is different for different fluids. In the presence of gas in pores, P-wave velocity is lowest but S-wave velocity is highest.
- ✓ Seismic wave velocities are more influenced by variations of porosity than variations in water saturation. The latter effect is more noticeable when the porosity is high and the pore fluid is gas.
- ✓ Frequency dependence of P-wave quality factor does not show any dependence on porosity in the presence of gas; however, when oil or water is present, dependence on porosity is noticeable.
- ✓ Frequency variation of attenuation coefficient shows more dependence on porosity in the presence of gas in pores. This dependence on porosity is noticeable only at higher frequencies.
- ✓ At 50 Hz, the influence of pore fluids on velocities – porosity variation of P-wave is more noticeable than on velocities – porosity variation of S-wave. The effect of water saturation on velocity – porosity variation is only slightly noticeable in the presence of gas.
- ✓ The variation of P-wave velocity with porosity in the viscoelastic layer obtained in the present work shows a trend that is quite different when this velocity is estimated using time average relationship. Time average relationship yields lower P-wave velocities than those obtained in the present work at all porosities.
- ✓ The variation of P-wave reflection coefficient with angle of incidence changes markedly with porosity in the presence of gas. This variation is dependent on the nature of overlying elastic layer, whether soft or hard.
- ✓ Variation of peak amplitude of seismic wavelets with offset is dominated by the type of pore fluid. For a given fluid, this variation dominated more by porosity than water saturation especially at near offsets.

- ✓ When a high porosity (porosity > 30%) viscoelastic layer is overlain by a soft layer, the wavelets reflected from the first interface show increase of amplitude with offset when gas is present in the pores whereas decrease of amplitude with offset when oil and water or only water present in the pores.
- ✓ When gas and water is present in the pores, the wavelets reflected from the second interface show increase of amplitude with offset. When oil and water is present in the pores, the wavelets reflected from the second interface show first decrease of amplitude with offset, change polarity and then increase of amplitude with offset. When only water is present, the amplitudes of wavelets from second interface decrease with offset.
- ✓ When the porous viscoelastic layer overlain by a hard layer, even at higher porosities (>30%), the wavelets reflected from the both interface show decrease of amplitude with offset when gas is present in the pores.
- ✓ The shapes of seismic wavelets from second interface of the viscoelastic layer show a marked variation with porosity, becoming broader at high porosity and also undergoing change of polarity when porosity is high. Variation with water saturation is not noticeable.
- ✓ The shapes of wavelets change with offset. Greater changes are observed with gas and water in the pores. Distinction between different fluids on the basis of wavelet shapes becomes more noticeable at larger offsets.
- ✓ When pore fluid is gas the amplitude of wavelet is small at low porosities but quite large at high porosities when compared with other fluid types.
- ✓ AVO analysis carried on synthetic data indicates that attributes A and B are also sensitive to porosity and water saturation.

- ✓ Due to viscoelasticity the seismic wavelets get attenuated and delayed; The Ricker wavelet that is symmetrical becomes asymmetric on propagating through the viscoelastic layer.
- ✓ The additional loss of amplitude takes place due to solid-fluid interaction when viscous fluid is present in the viscoelastic porous layer.
- ✓ The attenuating effects of viscoelasticity and pore fluids are dependent on the length of the path that waves take in the viscoelastic porous layer. This path will be longer for far offsets. Thus, amplitude decay as well as delay in phase will be more towards far offsets.

Thus, the effect of viscoelasticity and solid – fluid interaction not only to attenuate the reflected wavelets but also to causes some delay in their arrival and modify their shape. At the time of data processing, if this effect is taken into account, locating the interfaces can be more accurate. Thus, the processing of seismic reflection should include the effect of viscoelasticity and solid – fluid interaction.

References

Aki, K., Richard, P.C. (2002). Quantitative Seismology. *University Science Books, California*, ISBN 0-935702-96-2.

Batzle, M., Hofmann, R., Han, De-Hua., Castagna, J. (2001). Fluid and frequency-dependent seismic velocity of rocks. *The Leading Edge*, 20, 168-171.

Batzle, Michael L., Han, De-Hua., Hofmann, Ronny. (2006). Fluid mobility and frequency dependent seismic velocity-direct measurements. *Geophysics*, 71, N1- N9.

Ben-Menahem, A., Singh, S.J. (1981). Seismic Waves and Sources. *Springer-Verlag. New York*, ISBN 0-387-90506-5.

Berryman, James G. (1988). Seismic wave attenuation in fluid-saturated porous media. *PAGEOPH*, 128, 423-432.

Biot, M.A. (1956b). Theory of Propagation of elastic waves in a fluid-saturated porous solid, I. Low Frequency range. *Journal of Acoustic Society of America*, 28, 179-191.

Biot, M.A., Willies, D.G. (1957). The elastic coefficients of the theory of consolidation. *Journal of Applied Mechanics*, 24, 594-601.

Biot, M. A. (1962). Mechanics of deformation and acoustic propagation in porous media. *Journal of Applied Physics*, 33, 1482-1492.

Borcherdt, R. D. (1973). Energy and plane waves in linear viscoelastic media. *Journal of Geophysical Research*, 78, 2442-2453.

Borcherdt, R. D. (1982). Reflection-refraction of general P-and type-I S-waves in elastic and anelastic solids. *Geophysical Journal of Royal Astronomical Society*, 70, 621-638.

Borcherdt, R. D., Glassmoyer, G. (1989). An exact anelastic model for the free-surface reflection of P and S-I waves. *Bulletin of Seismological Society of America*, 79, 842-859.

Brie, A., Pampuro, F., Marsala, A.F., Meazza, O. (1995). Shear sonic interpretation in gas bearing sand. *SPE paper*, 30595, 701-710

Buchen, P. W. (1971). Plane waves in linear viscoelastic media. *Geophysical Journal of Royal Astronomical Society*, 23, 531-542.

Buchen, P. W. (1971). Reflection, transmission and diffraction of SH-waves in linear viscoelastic solids. *Geophysical Journal of Royal Astronomical Society*, 25, 97-113.

Carcione, J. M., Kosloff, D., Kosloff, R. (1988). Wave propagation simulation in a linear viscoelastic medium. *Geophysical Journal International*, 95, 597-611.

Carcione, J. M. (1993). Seismic modeling in viscoelastic media. *Geophysics*, 58, 110–120.

Carcione, J. M. (1997). Reflection and transmission of *qP-qS* plane waves at a plane boundary between viscoelastic transversely isotropic media. *Geophysical Journal International*, 129, 669–680.

Carcione, J. M., Helle, H.B., Pham, N.H. (2003). White's model for wave propagation in partially saturated rocks: Comparison with poroelastic numerical experiments. *Geophysics*, 68, 1389–1398.

Carcione, J. M., Picotti, S. (2006). P-wave seismic attenuation by slow-wave diffusion: effects of inhomogeneous rock properties. *Geophysics*, 71, O1–O8.

Carcione, J. M. (2006). Vector attenuation: elliptical polarization, raypaths and the Rayleigh-window effect. *Geophysical Prospecting*, 54, 399-407.

Cerveny, V. (2004). Reflection/transmission laws in viscoelastic anisotropic media. *Seismic waves in complex 3-D structure, Report 14,Department of Geophysics, Charles University, Praha,* 181-196.

Cole, K. S., Cole, R.H. (1941). Dispersion and absorption in dielectrics, I — Alternating current characteristics. *Journal of Chemical Physics*, 9, 342–351.

Deresiewicz, H. (1960). The effect of boundaries on wave propagation in a liquid filled porous solid, I, Reflection of plane waves at a free plane boundary (non-dissipative case). *Bulletin of Seismological Society of America*, 50, 599.

Deresiewicz, H. (1961). The effect of boundaries on wave propagation in a liquid filled porous solid, II, Love waves in a porous layer. *Bulletin of Seismological Society of America*, 51, 49-51.

Deresiewicz, H., Rice, J. T. (1962). The effect of boundaries on wave propagation in a liquid-filled porous solid: III. Reflection of plane waves at a free plane boundary (general case). *Bulletin of The Seismological Society of America*, 52, 595-625.

Dutta, N. C., Odé, H. (1979a). Attenuation and dispersion of compressional waves in fluid-filled porous rocks with partial gas saturation White model—Part I: Biot theory. *Geophysics*, 44, 1777–1788.

Dutta, N.C., Ode, H. (1979b). Attenuation and dispersion of compressional waves in fluid filled porous rocks with partial gas saturation (White model)-Part II: Results. *Geophysics*, 44, 1789-1805.

Dutta, N.C., Seriff, A.J. (1979). On white's model of attenuation in rocks with partial gas saturation. *Geophysics*, 44(11), 1806-1812.

Dutta, N.C., Ode, H. (1983). Seismic reflections from a gas-water contact, *Geophysics*, 48,148-162.

Dvorkin, J., Mavko, G., Nur, A. (1995). Squirt flow in fully saturated rocks. *Geophysics*, 60, 97-107.

Futterman, W. I. (1962). Dispersive body waves. *Journal of Geophysical Research*, 67, 5279–5291.

Gassmann, F. (1951). Elastic waves through packing of spheres. *Geophysics*, 16, 673-685.

Gregory, A.R. (1977). Aspects of rock physics from laboratory and log data that are important to seismic interpretation. 15-35, in C.E. Payton (ed.), "Seismic

Stratigraphy-Applications to Hydrocarbon Exploration," *Am. Assoc. Petrol. Geol. Mem. 26, Tulsa, Oklahoma.*

Hashin, Z., Shtrikman, S. (1963). A variational approach to the theory of the elastic behavior of multiphase materials. *J. Mech. Phy. Solid,* 11, 127-140.

Holtz, M.H., NúñezLópez, V., Breton, K.L. Moving Permian basin technology to the Gulf Coast: the geologic distribution of CO_2 EOR potential in Gulf Coast reservoirs. *Internet, Power Point Presentation, Gulf Coast Carbon Center, Bureau of Economic Geology.*

Linton, J.D. (2001). Theory of frequency dependent acoustics in patchy saturated porous media. *Journal of acoustic society of America,*110, 682-694.

Kjartansson, E. (1979). Constant Q-wave propagation and attenuation. *Journal of Geophysical Research,* 84, 4737-4748.

Knopoff, L. (1964). A matrix method for elastic wave problems. *Bulletin of the Seismological Society of America,* 54, 431-438.

Kolsky, H. (1956). The propagation of stress pulses in viscoelastic Solids. *Philosophical Magazine,* 1, 693–710.

Krebes, E.S., Hron, F. (1980). Ray-synthetic seismograms for SH waves in anelastic Media. *Bulletin of the Seismological Society of America,* 70, 29-46.

Krebes, E.S., Hron, F. (1980). Synthetic seismograms for SH waves in a layered anelastic medium by asymptotic ray theory. *Bulletin of the Seismological Society of America,* 70, 2005-2020.

Levorsen, A. I. (1967). Geology of petroleum. *W.H. Freeman and Company.*

Liu, H. P., Anderson, D.L., Kanamori, H. (1976). Velocity dispersion due to anelasticity; implications for seismology and mantle composition. *Geophysical Journal of Royal Astronomical Society,* 47, 41-58.

McDonal, F. J., Angona, F.A., Mills, R. L., Sengush, R.L., Nostrand, R.G.V., White, J.E. (1958). Attenuation of shear waves and compressional waves in Pierre shale. *Geophysics,* 23,421-439.

McQuillin, R., Bacon, M., Barclay, W. (1986). An introduction to seismic interpretation: Reflection seismics in petroleum exploration. *Graham & Trotman, Alden Press, Oxford.*

Nolen-Hoeksema, R.C. (2000). Modulus-porosity relations, Gassmann's equation, and the low frequency elastic-wave response to fluids. *Geophysics*, 65, 1355-1363.

Nur, A., Marion, D., Yin, H. (1991). Wave velocities in sediments, in Hoven, J.M., Richardson, M.D., and Stoll, R.D., Eds., Shear waves in marine sediments. *Kluwer Academic Publ.*, 131-140.

Postma, G.W. (1958). Changes of shape of seismic impulses in homogeneous viscoelastic meia. *Geophysical Prospecting*, 6, 438-455.

Quiroga-Goode, G. E., Krebes, E. S., Lawrence, H. T. Le. (1994). Modeling viscoelastic waves: a comparison of ray theory and finite-difference method. *Bulletin of Seismological Society of America*, 64, 1882-1888.

Raymer, L. L., Hunt, E. R., Gardner, J. S. (1980). An improved sonic transit time-to porosity transform. *SPWLA 21 Ann. Logging Symp.* 1–12.

Roden, R., Forrest, M., Holeywell, R. (2005). The impact of seismic amplitudes on prospect risk analysis. *The Leading Edge*, 24, 706 – 711.

Samec, P., Blangy, J.P. (1992). Viscoelastic attenuation, anisotropy, and AVO. *Geophysics,* 57, 441-450.

Schapery, R.A. (1969). A theory on non-linear thermoviscoelasticity based on irreversible thermodynamics. *Proceedings of the 5th U.S. National Congress of Applied mechanics, Minneapolis, USA, ASME, New York,* 511-530.

Sharma, M.D., Gogna, M.L. (1991). Seismic wave propagation in a viscoelastic porous solid saturated by viscous liquid. *Pure and Applied Geophysics*, 135, 384-400.

Sharma, M.D., Kaushik., V. P., Gogna, M.L. (1990). Reflection and refraction of plane waves at an interface between liquid-saturated porous solid and viscoelastic solid. *The Quarterly Journal of Mechanics and Applied Mathematics*, 43, 427-448.

Sheriff, R.E. (2002). Encyclopedic Dictionary of Applied Geophysic. *SEG Publication.*

Stine, J. A. (2004). Sensitivity of AVO reflectivity to fluid properties in porous media. *M.S. thesis, The University of Texas at Austin.*

Teverud, T., Ursin, B. (2005). Comparison of seismic attenuation models using zero-offset vertical seismic profiling (VSP) data. *Geophysics*, 70, F17-F25.

Ursin B., Teverud T. (2002). Comparison of seismic dispersion and attenuation models. *Stud. Geophys. Geod.* 46, 293-320.

Ursin B., Stovas, A. (2002). Reflection and transmission response of a layered isotropic viscoelastic medium. *Geophysics*, 67, 307-323.

White, J. E. (1965). Seismic waves. *New York, McGraw-Hill Book Co., Inc.*

White, J. E. (1975). Computed seismic speeds and attenuation in rocks with partial gas saturation. *Geophysics*, 40, 224–232.

Wyllie, M.R.J., Gregory, A. R., Gardner, L.W. (1956). Elastic wave velocities in heterogeneous and porous media. *Geophysics*, 21, 41–70.

Wyllie, M.R.J., Gregory, A. R., Gardner, L.W. (1958). An experimental investigation of factors affecting elastic wave velocities in porous media. *Geophysics*, 23, 459–493.

Zener, C. (1948). Elasticity and anelasticity of metals. *GUniversity of Chicago Press, Chicago, Illinois.*

APPENDIX A
WAVE PROPAGATION IN ELASTIC MEDIA

In the following, a model of the earth is considered that consists of two elastic half spaces. The interface coincides with $z = 0$. Plane P-waves, traveling in the first half space are incident on the interface at an angle i_1. Both the half spaces are assumed to be composed of materials that are homogeneous and isotropic and are characterized by P-wave velocity α_i, S-wave velocity β_i and density ρ_i, i= 1, 2.

The equation of motion for elastic media, written in terms of displacement vector, $\vec{u}$, are as follows:

$$\rho\left(\frac{\partial^2 u}{\partial t^2}\right) = (\lambda + \mu)\nabla(\nabla \cdot \vec{u}) + \mu\nabla^2\vec{u} \qquad \text{.....(A-1)}$$

where λ and μ are Lame' parameters and ρ is the density.

Following Aki and Richards (2002) the solution of equation (A-1) is written in term of displacements. The displacements are assumed to vary harmonically with time, i.e., have time dependence of the form $exp(-i\omega t)$. In the first layer the displacement components, u_x^1 in the x-direction and u_z^1 in the z-direction, are represented by

$$u_x^1 = P_1^d(\alpha_1 p)\exp\{i\omega(px+\xi_1 z-t)\} + P_1^u(\alpha_1 p)\exp\{i\omega(px-\xi_1 z-t)\} + S_1^u(\beta_1\eta_1)\exp\{i\omega(px-\eta_1 z-t)\}$$

.....(A-2)

$$u_z^1 = P_1^d(\alpha_1\xi_1)\exp\{i\omega(px+\xi_1 z-t)\} - P_1^u\alpha_1\xi_1\exp\{i\omega(px-\xi_1 z-t)\} + S_1^u(\beta_1 p)\exp\{i\omega(px-\eta_1 z-t)\}$$

.....(A-3)

where

p : ray parameter $(= sin\, i_1/\, \alpha_1)$

ω : angular frequency

j_1 : angle made by reflected S-ray with normal

ξ_1 : $cos\ i_1/\alpha_1 = (\alpha_1^{-2} - p^2)^{1/2}$

η_1 : $cos\ j_1/\beta_1 = (\beta_1^{-2} - p^2)^{1/2}$

P_1^d : displacement amplitude of downgoing incident P-wave

P_1^u : displacement amplitude of upgoing reflected P-wave

S_1^u : displacement amplitude of upgoing reflected S-wave

The stress components, p_{zx}^1, p_{zz}^1, are given by

$$P_{zx}^1 = \rho_1\beta_1^2\left(\frac{\partial u_x}{\partial z} + \frac{\partial u_z}{\partial x}\right)$$
$$= (i\omega)[P_1^d(2\rho_1\beta_1^2)p\alpha_1\xi_1 \exp\{i\omega(px + \xi_1 z - t) - P_1^u(2\rho_1\beta_1^2)p\alpha_1\xi_1 \exp\{i\omega(px - \xi_1 z - t)\}$$
$$- S_1^u(\rho_1\beta_1)(1 - 2\beta_1^2 p^2)\exp\{i\omega(px - \eta_1 z - t)\}]$$

.....(A-4)

$$P_{zz}^1 = \rho_1(\alpha_1^2 - 2\beta_1^2)\frac{\partial u_x}{\partial x} + \rho_1\alpha_1^2\frac{\partial u_z}{\partial z}$$
$$= (i\omega)[P_1^d(\rho_1\alpha_1)(1 - 2\beta_1^2 p^2)\exp\{i\omega(px + \xi_1 z - t) + P_1^u(\rho_1\alpha_1)(1 - 2\beta_1^2 p^2)\exp\{i\omega(px - \xi_1 z - t)\}$$
$$- S_1^u(2\rho_1\beta_1^2)p\beta_1\eta_1 \exp\{i\omega(px - \eta_1 z - t)\}]$$

.....(A-5)

In the second layer the displacement vectors are represented by

$$u_x^2 = P_2^d(\alpha_2 p)\exp\{i\omega(px + \xi_2 z - t)\} + S_2^d(\beta_2\eta_2)\exp\{i\omega(px + \eta_2 z - t)\}$$ .....(A-6)

$$u_z^2 = P_2^d(\alpha_2\xi_2)\exp\{i\omega(px + \xi_2 z - t)\} - S_2^d(\beta_2 p)\exp\{i\omega(px + \eta_2 z - t)\}$$ .....(A-7)

where

i_2 : angle made by downgoing transmitted P-ray with normal

j_2 : angle made by downgoing transmitted S-ray with normal

ξ_2 : $cos\ i_2/\alpha_2 = \left(\alpha_2^{-2} - p^2\right)^{1/2}$

η_2 : $cos\ j_2/\beta_2 = \left(\beta_2^{-2} - p^2\right)^{1/2}$

P_2^d: displacement amplitude of transmitted P-wave

S_u^2: displacement amplitude of reflected S-wave

The stress components are given by

$$P_{zx}^2 = (i\omega)\left[(2\rho_2\beta_2^2)p\alpha_2\xi_2 P_2^d - (\rho_2\beta_2)(1-2\beta_2^2 p^2)S_2^d\right]\exp\{i\omega(px-t)\} \quad \text{.....(A-8)}$$

$$P_{zz}^2 = (i\omega)\left[(\rho_2\alpha_2)(1-2\beta_2^2 p^2)P_2^d - (2\rho_2\beta_2^2)p\beta_2\eta_2 S_2^d\right]\exp\{i\omega(px-t)\} \quad \text{.....(A-9)}$$

Boundary conditions at the interface, require continuity of displacement and stress components, i.e.,

1) $u_x^1 = u_x^2$ .....(A-10)

2) $u_z^1 = u_z^2$ .....(A-11)

3) $P_{zx}^1 = P_{zx}^2$ .....(A-12)

4) $P_{zz}^1 = P_{zz}^2$ .....(A-13)

Applying the above boundary conditions yields the following four equations

$$(\alpha_1 p)P_1^d + (\alpha_1 p)P_1^u + (\beta_1\eta_1)S_1^u = (\alpha_2 p)P_2^d + (\beta_2\eta_2)S_2^u \quad \text{.....(A-14)}$$

$$(\alpha_1\xi_1)P_1^d - (\alpha_1\xi_1)P_1^u + (\beta_1 p)S_1^u = (\alpha_2\xi_2)P_2^d - (\beta_2 p)S_2^d \quad \text{.....(A-15)}$$

$$(2\rho_1\beta_1^2)p(\alpha_1\xi_1)P_1^d - (2\rho_1\beta_1^2)(\rho\alpha_1)P_1^u - (\rho_1\beta_1)(1-2\beta_1^2 p^2)S_1^u = 2\rho_2\beta_2^2 p(\alpha_2\xi_2)P_2^d + (\rho_2\beta_2)(1-2\beta_2^2 p^2)S_2^d$$

.....(A-16)

$$(\rho_1\alpha_1)(1-2\beta_1^2\rho^2)P_1^d + (\rho_1\alpha_1)(1-2\beta_1^2\rho^2)P_1^u - (2\rho_1\beta_1^2)p\beta_1^2\eta_1 S_1^u = \rho_2\alpha_2(1-2\beta_1^2\rho^2)P_2^d - 2\rho_2\beta_2^2 p(\beta_2\eta_2)S_2^d$$

.....(A-17)

The above equations can be rearranged in the following form

$$M\begin{bmatrix} P_1^u \\ S_1^u \\ P_2^d \\ S_2^d \end{bmatrix} = N\begin{bmatrix} P_1^d \\ 0 \\ 0 \\ 0 \end{bmatrix} \quad \text{.....(A-18)}$$

in which the M and N are defined as

$$M = \begin{pmatrix} -\alpha_1 p & -\cos j_1 & \alpha_2 p & \cos j_2 \\ \cos i_1 & -\beta_1 p & \cos i_2 & -\beta_2 p \\ 2\rho_1\beta_1^2 p\cos i_1 & \rho_1\beta_1\left(1-2\beta_1^2 p^2\right) & 2\rho_2\beta_2^2 p\cos i_2 & \rho_2\beta_2\left(1-2\beta_2^2 p^2\right) \\ -\rho_1\alpha_1\left(1-2\beta_1^2 p^2\right) & 2\rho_1\beta_1^2 p\cos j_1 & \rho_2\alpha_2\left(1-2\beta_2^2 p^2\right) & -2\rho_2\beta_2^2 p\cos j_2 \end{pmatrix}$$

.....(A-19)

and

$$N = \begin{bmatrix} \alpha_1 p \\ \alpha_1\xi_1 \\ (2\rho_1\beta_1^2)p(\alpha_1\xi_1) \\ \rho_1\alpha_1(1-2\beta_1^2 p^2) \end{bmatrix}$$

.....(A-20)

Substituting $P_1^d = 1$, the relation can be rewritten as

$$M\begin{bmatrix} R_{PP} \\ R_{PS} \\ T_{PP} \\ T_{PS} \end{bmatrix} = N\begin{bmatrix} 1 \\ 0 \\ 0 \\ 0 \end{bmatrix}$$

.....(A-21)

where R_{mn} and T_{mn}, (m = p, s and n = p , s) represent the reflection and transmission coefficients with first subscript indicating incident wave (P or S) and the second subscript indicating reflected or transmitted wave. The solution of (A-21) can be written as

$$\begin{bmatrix} R_{PP} \\ R_{PS} \\ T_{PP} \\ T_{PS} \end{bmatrix} = M^{-1}N$$

.....(A-22)

where yields the reflection and transmission coefficients. The above expressions apply when P-wave is incident from above. When P-wave is incident from below, the column vector N assumes the following form:

$$N = \begin{bmatrix} \alpha_2 p \\ \alpha_2\xi_2 \\ (2\rho_2\beta_2^2)p(\alpha_2\xi_2) \\ \rho_2\alpha_2(1-2\beta_2^2 p^2) \end{bmatrix}$$

.....(A-23)

APPENDIX B

PROPERTIES OF FLUID SATURATED MEDIA

Consider a pile of quartz sand. The sand particles have definite values of P and S-wave velocities through them; however, the sand pile has no strength since the particles are not cemented together. Once the particles are cemented, a porous rock is formed that has a definite strength and through which seismic waves can propagate. Initially, assume that this rock is devoid of any interstitial fluids; in other words, it is a dry rock. The bulk density, ρ_d, of such a rock is determined by the following relation:

$$\rho_d = (1-\varphi)\rho_m \qquad \text{.....(B-1)}$$

where φ is porosity and ρ_m is density of particles, also called matrix density. In case the rock is completely saturated with a fluid of density ρ_f, its bulk density, ρ_b, is determined by the following relation:

$$\rho_b = (1-\varphi)\rho_m + \varphi\rho_f \qquad \text{.....(B-2)}$$

For a porous rock totally saturated with fluid of density ρ_f, Gassmann (1951) proposed the following relations to calculate bulk modulus (K_b) and shear modulus (μ_b):

$$K_b = K_d + K_f \qquad \text{.....(B-3)}$$

$$\mu_b = \mu_d + \mu_f = \mu_d \qquad \text{.....(B-4)}$$

where K_d and μ_d are elastic moduli of dry rock (also called frame moduli), and K_f and μ_f denote elastic moduli of fluid filled pore space. K_f is the difference between the frame and saturated bulk moduli that results from the presence of fluid with a non-zero bulk modulus (Nolen-Hoeksema, 2000). The shear modulus is not affected by fluid saturation and so $\mu_f = 0$.

Let K_m and μ_m denote the bulk and shear moduli, respectively, of the solid constituents of a porous elastic medium (also called solid-grain moduli). Then K_d and μ_d are related to K_m and μ_m through the following relations:

$$K_d = K_m\left(1-\frac{\varphi}{\varphi_c}\right) \qquad \text{.....(B-5)}$$

$$\mu_d = \mu_m\left(1-\frac{\varphi}{\varphi_c}\right) \qquad \text{.....(B-6)}$$

where φ_c is critical porosity. Nur et al. (1991) introduced the concept of crotical porosity. There is a porosity φ_c above which K_d and μ_d are 0. Below the critical porosity, both the solid grains and pore fluids support the external load and frame modulii are greater than zero. Above the critical porosity, the entire load is supported by the fluid and the frame modulii become zero.

Nolen-Hoeksema, (2000) introduced α_K and α_μ, to relate frame moduli with solid grain moduli and gave the following definitions:

$$\alpha_k = \left(1-\frac{K_d}{K_m}\right) \qquad \text{.....(B-7)}$$

$$\alpha_\mu = \left(1-\frac{\mu_d}{\mu_m}\right) \qquad \text{.....(B-8)}$$

The following relation gives K_f

$$K_f = \frac{\alpha_k^2}{\left[\left(\frac{\varphi}{K_{fl}}\right)+\frac{(\alpha_k-\varphi)}{K_m}\right]} \qquad \text{.....(B-9)}$$

where K_{fl} is bulk modulus of the fluid filing the pores.

When the pores are filled with both water and hydrocarbons, the term φ/K_f in the definition of K_f given above has been modified to include bulk moduli of water and hydrocarbon and water saturation S_w. The modified definition of K_f is now given as

$$K_f = \frac{\alpha_k^2}{\left[\left(\frac{\varphi S_w}{K_w}\right) + \left\{\frac{\varphi(1-S_w)}{K_{fl}}\right\} + \left\{\frac{(\alpha_k - \varphi)}{K_m}\right\}\right]} \qquad \text{.....(B-10)}$$

where K_w is the bulk modulus of water and K_{fl}, that of the hydrocarbons.

Once K and μ_s are known, P and S wave velocities can be calculated in a saturated rock. Following relations are applicable where α and β stands for P and S wave velocities respectively:

For solid grains: $\alpha_m = \sqrt{\frac{K_m + (4/3)\mu_m}{\rho_m}}$, $\beta_m = \sqrt{\frac{\mu_m}{\rho_m}}$ .....(B-11)

For dry rocks: $\alpha_d = \sqrt{\frac{K_d + (4/3)\mu_d}{\rho_d}}$, $\beta_d = \sqrt{\frac{\mu_d}{\rho_d}}$ .....(B-12)

For saturated rocks: $\alpha_b = \sqrt{\frac{K_b + (4/3)\mu_b}{\rho_b}}$, $\beta_b = \sqrt{\frac{\mu_b}{\rho_b}}$ .....(B-13)

APPENDIX C

WAVE PROPAGATION IN POROUS ELASTIC MEDIA

Most of the real earth media through which the seismic waves propagate are porous, especially in the upper few kilometers of earth's crust. The reservoir rocks are essentially porous to store sufficient quantities of oil and gas. In a porous elastic medium, the solid constituents of such media are assumed to behave elastically.

The equations of motions in a porous elastic solid, as given by Biot (1956), are as follows:

$$\left(\frac{\partial^2}{\partial t^2}\right)\left(\rho_{11}\vec{u} + \rho_{12}\vec{U}\right) = \nabla\left[(\lambda + \mu)\nabla \cdot \vec{u} + Q\nabla \cdot \vec{U}\right] \qquad \text{.....(C-1)}$$

$$\left(\frac{\partial^2}{\partial t^2}\right)\left(\rho_{12}\vec{u} + \rho_{22}\vec{U}\right) = \nabla\left[Q\nabla \cdot \vec{u} + R\nabla \cdot \vec{U}\right] \qquad \text{.....(C-2)}$$

where $\vec{u}$ and $\vec{U}$ are displacement vectors in the solid and the fluid, respectively. The coefficient R is a measure of the pressure required on the fluid to force a certain volume of the fluid into the aggregate while the total volume remains constant. The coefficient Q is of the nature of a coupling between the volume change of the solid and that of the fluid. Both R and Q are positive. The quantities ρ_{11}, ρ_{22}, and ρ_{12} are mass coefficients which take into account the fact that the relative fluid flow through the pores is not uniform. The sum ρ_{11} $+2\,\rho_{12} + \rho_{22}$ equals the bulk density of the fluid-solid aggregate.

On applying divergence and curl to both sides of equations (C-1 & C-2) and simplifying, the equations governing the propagation of P and S waves in a porous elastic medium are obtained. The following equations govern the propagation of P-waves:

$$(P\theta + Q\varepsilon) = \left(\frac{\partial^2}{\partial t^2}\right)(\rho_{11}\theta + \rho_{12}\varepsilon) \qquad \text{.....(C-3)}$$

$$(Q\theta + R\varepsilon) = \left(\frac{\partial^2}{\partial t^2}\right)(\rho_{12}\theta + \rho_{22}\varepsilon) \qquad \text{.....(C-4)}$$

where $P = \lambda + 2\mu$, $\theta = \text{div } \vec{u}$ and $\varepsilon = \text{div } \vec{U}$. The equation governing the propagation of S waves is as follows:

$$\mu\xi = \rho_{11}\left[1 - \frac{\rho_{12}^2}{(\rho_{11}\rho_{12})}\right]\frac{\partial^2 \xi}{\partial t^2} \qquad \text{.....(C-5)}$$

where $\xi = \text{curl } \vec{u}$. In equation (C-5), the rotation of the fluid medium, curl $\vec{U}$, has been eliminated.

Biot (1956) has shown that there are two dilatational waves. For the first of these waves, the velocity is given by

$$V_1^2 = \frac{H}{z_1} \qquad \text{.....(C-6)}$$

where $H = P + R + 2Q$. For the second kind of dilatational wave, the slow P-wave, the velocity is given by

$$V_1^2 = \frac{H}{z_2} \qquad \text{.....(C-7)}$$

The values of z_1 and z_2 are roots of the following equation

$$(\sigma_{11}\sigma_{22} - \sigma_{12}^2)z^2 - (\sigma_{11}\sigma_{22} + \sigma_{22}\gamma_{11} - 2\sigma_{12}\gamma_{12})z + (\gamma_{11}\gamma_{22} - \gamma_{12}^2) = 0 \qquad \text{.....(C-8)}$$

where

$$\sigma_{11} = \frac{P}{H} \quad , \quad \sigma_{22} = \frac{R}{H} \quad , \quad \sigma_{12} = \frac{Q}{H} \qquad \text{.....(C-9)}$$

$$\gamma_{11} = \frac{\rho_{11}}{\rho} \quad , \quad \gamma_{22} = \frac{\rho_{22}}{\rho} \quad , \quad \gamma_{12} = \frac{\rho_{12}}{\rho} \qquad \text{.....(C-10)}$$

The velocity of transverse waves is given by

$$V_s = \sqrt{\frac{\mu}{\left\{\rho_{11}\left(1 - \frac{\rho_{12}^2}{\rho_{11}\rho_{22}}\right)\right\}}} \qquad \text{.....(C-11)}$$

APPENDIX D
MISCELLANEOUS

PART I: Stress-Strain Relation under Cyclic Load

In elastic materials, stress is proportional to strain. So, if such a material is subjected to cyclic stress, the resulting strain remains in phase with the stress as shown in Figure D-1. All the energy is recovered on unloading.

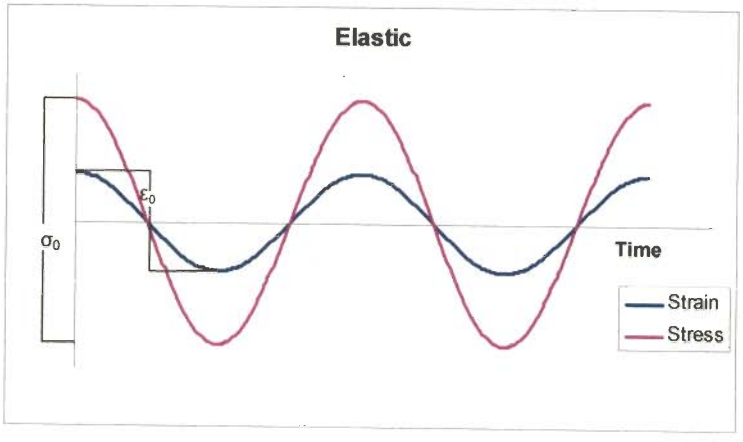

Figure D-1: ***Stress-strain relation for elastic material when subjected to cyclic load. The stress and strain remain in phase.***

In a Newtonian fluid that represents a viscous material, stress is proportional to rate of strain. Under cyclic stress, strain and stress are 90^0 out of phase, as shown in Figure D-2. In this kind of material, no energy is recovered on unloading.

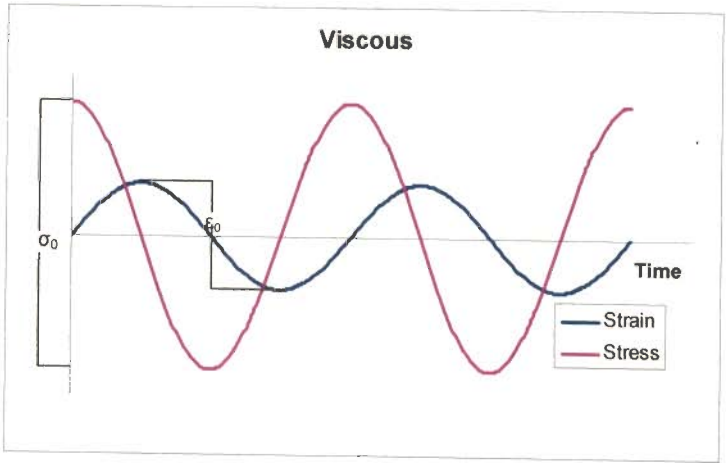

Figure D-2: ***Stress-strain relation for viscous material when subjected to cyclic load. The stress and strain remain 90^0 out of phase.***

In a viscoelastic material that combines the features of elastic and viscous substances, the strain lags behind the stress as shown in Figure D-3. In this case some energy may be recovered on unloading.

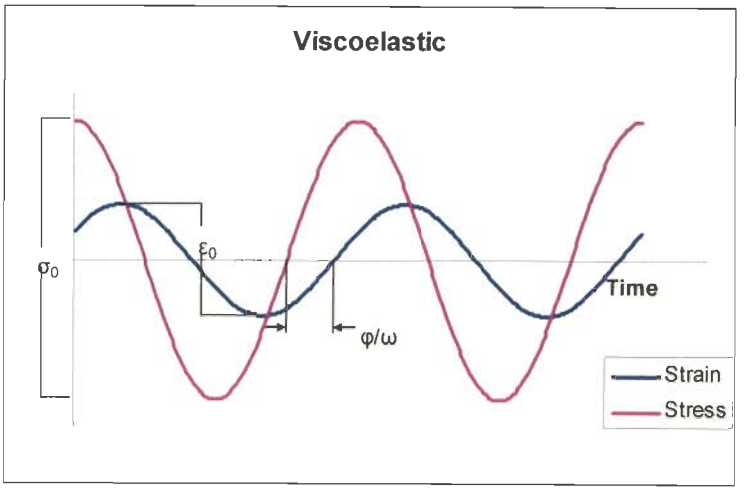

Figure D-3: ***Stress-strain relation for viscoelastic material when subjected to cyclic load.***

PART II: Relaxation Mechanism

Processes like thermo-elasticity, diffusion, motion of moving charged dislocations and point defects, and fluid flow in pores, phase changes will act to relieve an applied stress. During first stress cycle energy is absorbed, and during the next half cycle energy is given up. Usually a finite amount of time is required foe this energy exchange to take place; this is called the relaxation time and tends to make strain out of phase with the applied stress. Zener (1948) assumed that for all relaxation mechanisms, the rate of stress relief for constant strain is proportional to stress and showed that each of the above mechanisms contributes an internal friction of the form

$$Q^{-1} = \frac{M_u - M_R}{M_u} * \frac{f/f_p}{1 + f/f_p} \qquad \text{.....(D-1)}$$

Eq. (D-1) can be rewritten as

$$\left(\frac{Q^{-1}}{\frac{M_u - M_R}{M_u}} \right) = \frac{f/f_p}{1 + f/f_p} \qquad \text{.....(D-2)}$$

where M_u is unrelaxed elastic modulus, M_R is relaxed modulus, and f_p is the constant of proportionality between the stress and the rate of strain relaxation. A plot of left hand side of Eq. (D-2) against f/f_p is shown in Figure D-4. It can be seen that d that maximum internal friction occurs at $f=f_p$.

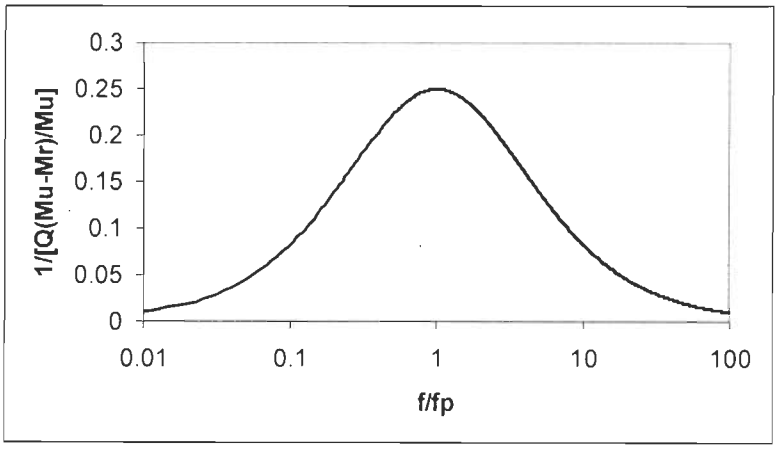

Figure D-4: ***The frequency dependence of Q^{-1} in a viscoelastic material.***

PART III: Nonlinear Viscoelasticity

In viscoelastic materials, if stress is held constant strains increases with time. This phenomenon is called creep. If the strain is held constant, the stress decreases with time. This phenomenon is called relaxation. The effective stiffness depends on the rate of application of the load. If cyclic loading is applied, hysteresis occurs wherein there is a phase lag between stress and strain, leading to a dissipation of mechanical energy.

All materials exhibit some viscoelastic response. In common metals such as steel or aluminum, as well as in quartz, at room temperature and at small strain, the behavior does not deviate much from linear elasticity. Synthetic polymers, wood, and human tissue as well as metals at high temperature display significant viscoelastic effects.

Creep is a slow, progressive deformation of a material under constant stress. In one dimension, suppose the history of stress σ as it depends on time t to be a step function beginning at time zero:

$$\sigma(t) = \sigma_O H(t) \qquad \text{.....(D-3)}$$

$H(t)$ is the unit Heaviside step function defined as follows:

$$H(t) = \begin{cases} 0, & t<0, \\ 0.5, & t = 0 \\ 1, & t>0 \end{cases} \qquad \text{.....(D-4)}$$

The strain $\varepsilon(t)$ in a viscoelastic material will increase with time. The ratio

$$J(t) = (\varepsilon(t) / \sigma_O \qquad \text{.....(D-5)}$$

is called the creep compliance. In linearly viscoelastic materials, the creep compliance is independent of stress level. If the load is released at a later time, the strain will exhibit recovery, or progressive decrease of deformation. Strain in recovery may or may not approach zero, depending on the material.

On the other hand, if the history of strain ε is a step function as defined above, the stress $\sigma(t)$ in a viscoelastic material will decrease with time. The ratio

$$E(t) = \sigma(t) / \varepsilon_O \qquad \text{.....(D-6)}$$

is called the relaxation modulus. In linearly viscoelastic materials, the relaxation modulus is independent of stress level.

If the compliance curves, i.e., plots of compliance $J(t)$ as a function of t, for difference stresses $\sigma_{0,}$ (or the relaxation modulus curves corresponding to different strains) overlap, the material is linearly viscoelastic. Creep compliance is independent of stress and relaxation modulus is independent of strain.

In a plot of log compliance vs. log time, if the curves are separate but have the same shape, then the behavior is consistent with quasilinear viscoelasticity (QLV). QLV

assumes the creep compliance can be written as a product of a function of time and a function of stress. If the compliance is in fact a product, then all the creep curves have the same shape.

If a stress-strain curve is generated at a constant strain rate, and the stress-strain curve has a concave up nonlinearity, then the material is nonlinear. If the creep or relaxation test reveals time dependence, then the material is viscoelastic.

If the curves for creep (or relaxation) at different stresses (or strains) have different shape, then neither linear viscoelasticity nor QLV describe the behavior, because creep compliance function depends on both time and stress (or the relaxation modulus function depends on both time and strain). The material may obey a more general nonlinear superposition law such as nonlinear superposition in which the creep compliance function is written explicitly as a general function of time and stress (or the relaxation modulus function is written explicitly as a general function of time and strain).

In a recovery experiment, the strain is set to zero after a period of relaxation or the stress is set to zero after a period of creep. In both a linearly viscoelastic solid and one which follows QLV, recovery must initially follow the same dependence as the creep or relaxation which preceded it. For nonlinear superposition or for a material describable by a Schapery model (Schapery, 1969) recovery can have a different time dependence.

PART IV: Electric Circuit Equivalent of a Kelvin – Voigt Solid

A Kelvin – Voigt solid can be represented by an electrical circuit consisting of a resistance and capacitance in parallel. The equation governing the growth of current in such a circuit is given by

$$RC\frac{dj(t)}{dt} + j(t) = J(t) \qquad \text{.....(D-7)}$$

where $j_0(t) \equiv J(t)$ is the driving current with the initial condition $J(t=0) = 0$

The solution of $j(t)$ can be written as

$$j(t) = \frac{1}{RC} e^{-t/RC} \int_0^t J(t) e^{-t/RC} \qquad \text{.....(D-8)}$$

Figure D-5 shows the growth of current in an RC circuit simulating the growth of strain in a Kelvin – Voigt solid.

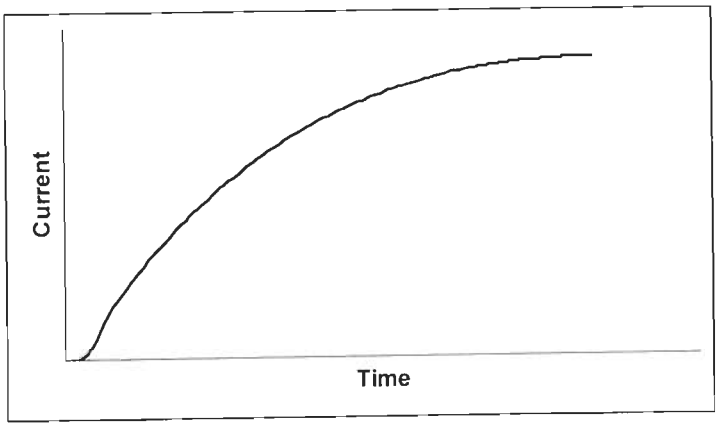

Figure D-5: ***Growth of current in a RC circuit. This growth resembles the build-up of strain in a Kelvin-Viogt Solid.***

PART V: Q^{-1} Variation with Frequency in Maxwell and Kelvin-Voigt Solids

The frequency dependence of Q^{-1} in Maxwell model and Kelvin-Voigt model, shown in Figure A-5 and Figure A-6, is derived using the following equation

Maxwell Model

$$\frac{1}{Q} = \frac{k}{f} \qquad \text{.....(D-9)}$$

Kelvin-Voigt model

$$\frac{1}{Q} = \frac{f}{k} \qquad \text{.....(D-10)}$$

where

$$k = \frac{E}{2\pi\eta} \qquad \text{.....(D-11)}$$

E is modulus of elasticity representing spring and η is viscosity representing the dashpot.

Figures D-6 and D-7 show the behavior of 1/Q for Maxwell and Kevin – Voigt solids respectively.

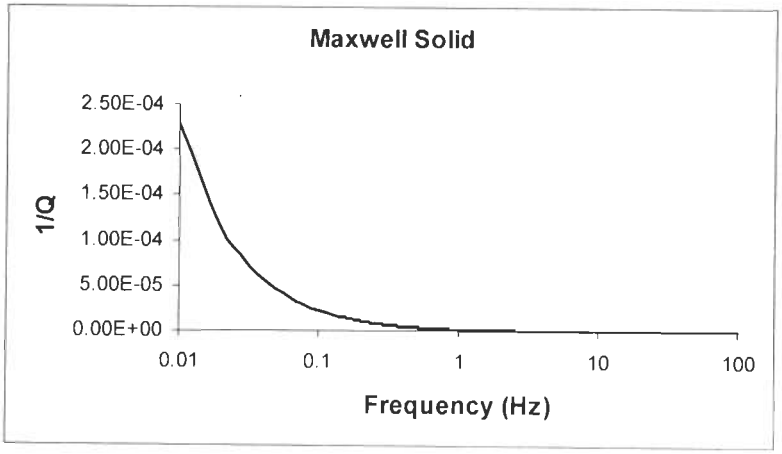

Figure D-6: *The frequency dependence of Q^{-1} in Maxwell Model.*

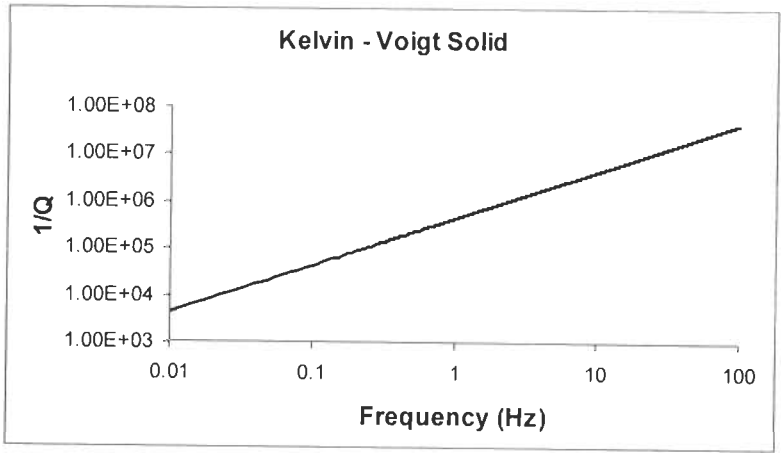

Figure D-7: *The frequency dependence of Q^{-1} in Kelvin-Voigt Model.*